INSTITUTO TECNOLÓGICO
Y DE ESTUDIOS SUPERIORES DE OCCIDENTE

Reconocimiento de validez oficial de estudios de nivel superior según acuerdo secretarial 15018, publicado en el Diario Oficial de la Federación el 29 de noviembre de 1976.

Departamento de Electrónica, Sistemas e Informática

DOCTORADO EN CIENCIAS DE LA INGENIERÍA

MÉTODO DE RASTREO DE ENVOLVENTE PARA LA LINEALIZACIÓN DE AMPLIFICADORES ÓPTICOS POR SEMICONDUCTOR USADOS EN SISTEMAS DE TRANSMISION ÓPTICA COHERENTE OFDM

Tesis que para obtener el grado de

DOCTOR EN CIENCIAS DE LA INGENIERÍA

presenta: Julio César Ortiz Cornejo

Director de tesis: Dr. Jorge Arturo Pardiñas Mir

Co-director de tesis: Dr. Stéphane Azou

Tlaquepaque, Jalisco. Diciembre de 2019

DOCTOR EN CIENCIAS DE LA INGENIERÍA (2019) ITESO, Tlaquepaque, Jal., México

TÍTULO: **Método de rastreo de envolvente para la linealización de amplificadores ópticos por semiconductor usados en sistemas de transmisión óptica coherente OFDM**

AUTOR: Julio César Ortiz Cornejo
Ingeniero en Comunicaciones y Electrónica (Universidad de Guadalajara, México)
Maestro en Energía Renovable (Universidad Autónoma de Guadalajara, México)

DIRECTOR DE TESIS: Jorge Arturo Pardiñas Mir
Departamento de Electrónica, Sistemas e Informática, ITESO
Ingeniero en Electrónica (ITESO, México)
Maestro en Electrónica Industrial (ITESO, México)
Doctor en Telecomunicaciones (*Telecom Sud/Paris/Université Pierre et Marie Curie*, Paris, Francia)

NÚMERO DE PÁGINAS: xxxi, 139

ITESO – The Jesuit University of Guadalajara

Department of Electronics, Systems, and Informatics

DOCTORAL PROGRAM IN ENGINEERING SCIENCES

ENVELOPE TRACKING FOR LINEARIZATION OF SEMICONDUCTOR OPTICAL AMPLIFIER IN COHERENT OPTICAL OFDM SYSTEMS

Thesis to obtain the degree of

DOCTOR IN ENGINEERING SCIENCES

Presents: Julio César Ortiz-Cornejo

Thesis Director: Dr. Jorge Arturo Pardiñas-Mir

Thesis Co-director: Dr. Stéphane Azou

Tlaquepaque, Jalisco, Mexico
December 2019

PHD IN ENGINEERING SCIENCES (2019) ITESO, Tlaquepaque, Jal., Mexico

TITLE: **Envelope tracking for linearization of semiconductor optical amplifier in coherent optical OFDM systems**

AUTHOR: Julio César Ortiz-Cornejo
Bachelor's degree in communications and electronics engineering (University of Guadalajara, Mexico)
Master's degree in renewable energy (Autonomous University of Guadalajara, Mexico)

THESIS DIRECTOR: Jorge Arturo Pardiñas Mir
Department of Electronics, Systems, and Informatics, ITESO
Bachelor's degree in electronics engineering (ITESO, Mexico)
Master's degree in industrial electronics (ITESO, Mexico)
Ph.D. degree in telecommunications engineering (*Telecom SudParis/Université Pierre et Marie Curie*, Paris, France)

NUMBER OF PAGES: xxxi, 139

To my Father

Resumen

Durante la última década, la sociedad ha elevado su interconexión, esto a su vez ha incrementado las expectativas sobre aumento en velocidad de datos, reducción en los costos de implementación, y flexibilidad de implementación de la siguiente generación de redes de comunicaciones. Por lo tanto, se ha propuesto la comunicación óptica coherente usando multiplexación por división de frecuencia ortogonal (CO-OFDM por sus siglas en inglés) como un método apto para cumplir estas expectativas. Esto, debido a que puede contar con una alta eficiencia espectral, robustez a la dispersión cromática y una conveniente flexibilidad de implementación y capacidades de compensar fácilmente los efectos no lineales usando técnicas de procesamiento digital de señales. Es por estas razones que se muestra conveniente investigar técnicas novedosas que mejoren el desempeño del sistema CO-OFDM, reduciendo las distorsiones no lineales a través del incremento del rango dinámico de trabajo de los componentes no lineales como los amplificadores ópticos por semiconductor (SOA por sus siglas en ingles).

En este trabajo, algunos métodos de compensación no lineal son estudiados y optimizados para obtener la menor magnitud del vector de error (EVM por sus siglas en ingles) en función de la potencia de entrada del SOA. También se presenta un análisis de cómo el SOA es afectado por el cambio de su fuente de alimentación (corriente de bias), dando una importante comprensión del comportamiento no lineal del SOA en términos del EVM, potencia de salida, y ganancia promedio. Estos efectos no lineales asociados con el SOA pueden provocar un bajo rendimiento para los sistemas de comunicación de modulación con envolvente no constante. Una variedad de métodos de linealización pueden ser adoptados para lidiar con los defectos de recepción y ofrecer un sistema efectivo.

En esta tesis de doctorado, un método de rastreo de envolvente (ET por sus siglas en inglés) es propuesto para la linealización de un sistema de transmisión CO-FDM amplificado por un SOA. Se estudia el desempeño de un diseño optimizado de ET para varios escenarios con el eventual uso de métodos de reducción de picos de potencia PAPR (PAPR por sus siglas en inglés) usando métodos de recorte o métodos de compensación no-lineal. También, se expone un minucioso análisis de la densidad de portadores para evaluar la efectividad del método propuesto. Además, se expone la robustez del sistema ET contra la variación de sus parámetros internos.

Summary

Since the last decade, the society has become more connected increasing the expectations about high data rates, low cost of implementation, and flexibility for the next generation of communication networks. Thus, to meet these requirements the coherent optical orthogonal frequency division multiplexing technique (CO-OFDM) has pointed out as a suitable technology. CO-OFDM can achieve high spectral efficiency, robustness to chromatic dispersion, and convenient implementation flexibility and capabilities of compensating nonlinear impairments with digital signal processing methods. Hence it is convenient to research novel techniques that improve performance, mitigating nonlinear distortions by increasing the dynamic range of nonlinear devices such as semiconductor optical amplifiers (SOA).

In this work, some nonlinear companding methods are studied and optimized to get the lower error vector magnitude (EVM) as a function of SOA input power. Also, a deep analysis of how the SOA behavior is affected by the change of its power supply (bias current) is presented, giving an important comprehension of the SOA nonlinear behavior in terms of EVM, output power, and gain. These inherent nonlinear effects associated with SOA may translate into a transmission performance loss for non-constant envelope modulation formats. However, a variety of linearization schemes may be adopted for coping with these impairments and offering an effective system design.

In this doctoral dissertation, an envelope tracking (ET) technique is proposed for linearizing an SOA-based CO-OFDM transmitter. Optimized design of the ET subsystem is performed under various scenarios, with the eventual joint use of peak to average power ratio (PAPR) reduction either via hard-clipping or nonlinear companding. A thorough SOA carrier density analysis is performed to assess the effectiveness of the proposed scheme. Moreover, the robustness of the proposed approach against some parameters variation both inside the ET path (DAC characteristics and bandwidth limited envelope generation) is exposed.

Acknowledgements

The author wishes to express his sincere appreciation to Dr. Jorge Arturo Pardiñas Mir, professor of the Department of Electronics, Systems, and Informatics at ITESO, for his encouragement, expert guidance and keen supervision as doctoral thesis director throughout the course of this work. The author offers his gratitude to Dr. Stéphane Azou, from Lab-SICC at National School of Engineers of Brest, his continuous support as co-director of this doctoral thesis, for his patience, motivation, and immense knowledge. The author could not have imagined having a better advisors and mentors for his Ph.D. study. He also thanks to Dr. Omar H. Longoria-Gándara, Dr. Luis Rizo-Domínguez, and Dr. Arturo Veloz-Guerrero, members of his Ph.D. Thesis Committee, for their interest, assessment, and suggestions.

The author has greatly benefited from working with Matlab developed by MathWorks, and with Advanced Design System (ADS) developed by Keysight. The author is grateful to Dr. Jack Little, President and Cofounder of MathWorks, for making the MATLAB packages available for this work. Also, the author is thankful to Ron Nersesian Chairman, President, and Chief executive officer of Keysight Technologies. for making the ADS packages available for this work.

Special thanks are due to Dr. Pascal Morel from ENIB Lab-STICC, and Dr. Ernesto Rayas-Sánchez, from ITESO, for their fruitful cooperation and helpful technical discussions.

It is the author's pleasure to acknowledge fruitful collaboration and stimulating discussions with his colleagues from ITESO : Jose M. Valencia-Velasco, Jesús G. Servín-Aguilar. And his colleagues from ENIB Lab-STICC, Mohamad Younes, Haidar Taki, and Ramez Hamie.

The author wants to express his special gratitude to Dr. Francisco de Leon, associate professor of the Department of Electrical and Computer Engineering at New York University for inspiring him to start his Ph.D. studies.

The author gratefully acknowledge the financial assistance through a scholarship granted by the *Consejo Nacional de Ciencia y Tecnología* (CONACYT), Mexican Government.

Finally, special thanks are due to my family: my wife Viridiana Mendoza Luna and my children Julio, Jesus and Akbar, for their understanding, patience, and continuous loving support.

Contenido

Contents

List of Figures

List of Tables

Introduction

The current society demands more capacity to exchange information and robust networks in terms of high-speed data transmission and bandwidth capacity. Optical networks are the predominant technology to achieve this objective [Reixats-12]. Recently, there has been interest in investigating optical communication systems using multicarrier modulation formats, such as orthogonal frequency division multiplexing (OFDM), in their various configurations [Shieh-10]. As stated before, multicarrier modulations [Shieh-10], [Zhao-14] have proved to be promising for satisfying the ever-increasing capacity demand in optical fiber networks [Agrell-16], with key features including high spectral efficiency, robustness to fiber chromatic dispersion and polarization mode dispersion, and powerful digital signal processing (DSP)-based implementation. However, multicarrier signals usually have the drawback of a nonconstant envelope with possible large peak to average power ratio (PAPR) [Rahmatallah-13], which makes them highly sensitive to nonlinear distortions. In this thesis, the robustness of an envelope tracking system with the eventual joint use of PAPR reduction methods as a crest reduction factor to linearize the semiconductor optical amplifier (SOA) as a power booster is studied.

PAPR reduction methods works reducing the peaks of power at the signal. In the latest years, a huge amount of PAPR methods have been published [Rahmatallah-13]. Among a considerable number of PAPR reduction techniques, there are companding transform methods (CT). CT techniques have been attracting attention because of their low computational complexity and relative effectivity to reduce the PAPR without increasing the input power [Y.Wang-13]. Companding methods works with the statistical redistribution of the signal applying a transforming function. Companding methods could be divided into linear companding and nonlinear companding. However, nonlinear companding methods exhibit more efficiency. These applications commonly use a piecewise function to transform the signal by selecting different inflection points. Performance improvement of an SOA-based CO-OFDM transmission system has been shown in [Azou-15] using some nonlinear companding methods. In this work performance improvement of 3 dB in bit error rate (BER) for SOA amplifier in saturation regime was achieved using optimal companding parameters, optimization was reached applying hybrid optimization schemes, combining genetic algorithms and local minima algorithms. These results

corroborate that companding methods reduce partially nonlinear behavior on SOA based CO-OFDM system. Although some companding methods have a relative difficulty to be optimized. This condition is due to the multiple parameters involved in the transforming functions. However, other classics companding methods are easy to implement such as μ-law [Wang-99] or hard clipping [Rahmatallah-13], which only have one parameter to optimize. In this thesis different optimization methods are applied for a nonlinear companding method [Wang-13], over a wide range of input powers to estimate in an adaptative way the optimal companding parameters as a function of input power signal.

On the other hand, the optoelectronics devices involved in fiber-optic communication systems may induce various specific nonlinear impairments, mainly at the transmitter side due to the sinusoidal characteristic of the optical modulator [Napoli-18], [Amiralizadeh-15] or in the fiber due to the Kerr-effect at high launch power [Amari-17], [Dar-17]. Further nonlinearities may be caused by optical amplifiers, especially if SOA are adopted [Bendimerad-17]. With the use of spectrally efficient modulation formats, these nonlinear impairments can translate into severe performance degradation, and their compensation via digital signal processing techniques is the subject of a growing literature. Popular methods encompass digital predistortion, digital back-propagation, Volterra series based nonlinear equalization, or machine learning.

In this doctoral dissertation, we focus on the nonlinear effects associated with SOA used as a booster amplifier. As pointed out in several recent studies [Bendimerad-17][Renaudier-19],[Koenig-14] SOA may be an alternative to the reference Erbium-Doped Fiber Amplifier (EDFA) technology in future WDM optical networks, due to their interesting key features including low-cost, wide optical bandwidth, compactness, and integrability. However, in some scenarios, compensation techniques appear to be of critical importance for combating the intrinsic nonlinear gain dynamics of the SOA and thus achieving favorable system performance. Different techniques have been reported so far, with various cases depending on the role of the SOA (booster, in-line amplifier or pre-amplifier, with possible cascade) and the number of channels involved. Some techniques alleviate the nonlinear distortions via digital signal processing like digital backpropagation [Li-10], [Ghazisaeidi-11] or digital predistortion [Lange-13], [Bejan-15], [Diouf-17], and non-DSP schemes have also been investigated, like feedforward linearization [Tabatabai-07], gain-clamped SOA [Tiemeijer-96] and non-uniform biasing [Ng-12], [Saleh-88]. Other efforts have focused on changing the device design, either with multi-contact SOA [Ó Dúill-17]

or Quantum-Dot structure [Akiyama-07].

Likewise, the design of an ET sub-system for coping with SOA nonlinear impairments is revealed. In this work this amplifier is used as a power booster in a CO-OFDM system. Also, some of our previous works are presented, including [Ortiz-Cornejo-17] in which we pointed out the effectiveness of ET-SOA for amplifying multicarrier signals and [Ortiz-Cornejo-18] devoted to the optimal tuning of some parameters of the ET block jointly with PAPR reduction, with the view to minimize the error vector magnitude (EVM) [Schmogrow-12]. A few other studies are identified in the literature regarding bias current control of SOAs for improving the transmission performance. These prior contributions share some similarities with [Ortiz-Cornejo-20], even if they have different objectives and system setups. Saleh et al. [Saleh-88] have shown for the first time that varying the bias current may theoretically lead to a constant average carrier density in the SOA while amplifying non-constant envelope signals. In [Saleh-88] the authors conducted an experiment for showing the linearization performance with a two-tone signal at the input of the SOA, which is used as an inline amplifier. Around 14 dB reduction in the intermodulation distortion over a wide range of input power has been reported in [Saleh-88] for a frequency separation going up to 1.25 GHz between the two tones. Later, Ng et al. [Ng-12] proposed an optimized non-uniform bias current so as to achieve SOA gain uniformity in the presence of high speed input pulses. In a recent work, Fujiwara and Koma [Fujiwara-07] proposed to vary the SOA bias current to cope with the near-far problem typical of PON upstream transmission. The approach relies on a cascade setup with the use of a fast feedforward control circuit applied to the first SOA and output burst frame powers being equalized in the second SOA. More recently, Dalla Santa et al. [Santa-19] have investigated an SOA bias current control strategy for optical equalization of the upstream in a passive optical network (PON) system with four 25 Gb/s channels and multilevel modulation format, the SOA being used as a pre-amplifier. Such adaptive biasing schemes actually shares some similarities with the popular envelope tracking (ET) technique [Wang-05], [Wang-15] used for increasing RF power amplifier efficiency, by modulating the supply voltage according to the input signal envelope fluctuation. Compared to digital baseband predistortion techniques, an ET scheme for linearizing SOA offers the advantage that it can be applied with a very similar approach whether SOA is used as a booster or as an inline amplifier, with no strict requirement regarding the linearizer tuning (no learning stage). In addition, ET may offer a more significant performance gain. Many extensions are proposed in this dissertation to corroborate the capability

of ET for achieving highly linear coherent optical transmitters, including an SOA. Also, the carrier density through the SOA active region is examined under an ET regime. Then, an optimization of the ET-subsystem is reported for various scenarios with an eventual joint use of hard clipping or soft clipping, considering numerous SOA target gains and QAM modulation orders. Likewise, the robustness of the optimized ET-SOA-based CO-OFDM transmitter is studied for changes of some parameters of the ET subsystem (low-pass filter bandwidth; DAC sampling rate and resolution) or in presence of some laser wavelength shift.

Even if we consider a conventional cyclic prefix OFDM (CP-OFDM) modulation format [Sahin-14] in this doctoral dissertation, our study is actually general, and we think that it may be of interest for other researchers interested in the use of SOAs with any other advanced non-constant envelope modulation format offering higher spectral efficiency, like OFDM/OQAM [Zhao-14].

Also, we consider PAPR reduction via nonlinear companding, but our intention is to reveal that combining ET with PAPR reduction translates into a significant transmission performance gain and this conclusion also holds if another PAPR reduction technique is used.

This doctoral dissertation is organized as follows:

In Chapter 1, the basic concepts about multicarrier modulation are presented. It explains the typical OFDM system and its unique features when it is applied to optical communications systems. Adding a brief review of the optical amplifier features and their characteristics is included. The peak to average power ratio (PAPR), and some methods to reduce this critical issue in OFDM systems are explained. Finally, the coherent optical orthogonal frequency division multiplexing (CO-OFDM) simulation system is described.

Chapter 2 shows a brief review of different companding transforms. Nonlinear companding transforms (NCT) are addressed, with the best performance reported in terms of BER and lower computational complexity. Furthermore, a comparative of optimization methods to identify which optimization method is more efficient to find Wang's nonlinear companding transform [Wang-13] optimal parameters that yield minimum EVM and low computational time is presented. Then, the optimization process using a hybrid scheme, a comparison of optimization methods, and the application of a gradient-free method over a wide range of input power on the CO-OFDM system is explained.

Chapter 3 is devoted to present the simulation results given by the bias current change on SOA based CO-OFDM system for a wide range of input power levels. An analysis of bias current

functions to control the EVM, output power, or optical gain , and also the benefits and disadvantages of these three approaches are presented.

Chapter 4 exposes a brief explanation of the envelope based methods for power management and linearization for radio frequency systems. Essential functions as envelope estimations and restoration and envelope tracking are illustrated. Also, this chapter is focused on the envelope shaping function as a critical operation element on an ET system to achieve power efficiency and linearity. The benefits of the ET technique adapted to a CO-OFDM system using an SOA as a power booster are evaluated

In Chapter 5, the SOA typical characteristics are summarized, and an ET scheme is presented for linearizing a CO-OFDM transmitter. Then, the ET block optimization via particle swarm optimization (PSO) is studied. Numerical results are developed to show the effectiveness of the proposed scheme.

Chapter 6 briefly reminds the relation between the SOA's optical gain and its bias current and describes our envelope tracking SOA system model. Then, the carrier density is analyzed under an envelope tracking regime. ET-SOA block is optimized under different conditions increasing the modulation schemes and PAPR reduction methods. Also, the robustness of the proposed ET-SOA based CO-OFDM transmitter to some parameter changes is outlined.

In the General Conclusions, the most significant contributions of this doctoral dissertation are digested, discussing the overall results of the proposed envelope tracking technique for semiconductor optical amplifier working as a booster in the CO-OFDM system and the optimization methods used to get the optimal tuned parameters to control de SOA bias current. Perspectives for future research are briefly summarized.

Finally, Appendix A shows the reference list of the nine internal research reports written during the doctoral research. In Appendix B, the reference to the academic production published in journals and conferences is shown.

1. Coherent Optical Orthogonal Frequency Division Multiplexing System

This chapter presents a brief description of nonlinearity issues produced in optical amplifiers applied to optical OFDM systems. It also analyzes the method to calculate the peak to average power ratio (PAPR) in OFDM signals. Additionally, this chapter presents a brief description of the most common methods to reduce PAPR, and thus, reduce nonlinearities in semiconductor optical amplifiers. Furthermore, this chapter presents an overview of the architecture of a simulation platform for semiconductor optical amplifiers (SOA) based on coherent optical OFDM (CO-OFDM) which I used all along my doctoral work. Some of my products contributed to enhance its original features, such as gain control and SOA input power control. The simulation platform also allows testing new methods for the linearization of SOA amplifiers, and to obtain data that allows controlling the SOA by monitoring the envelope of the OFDM signal.

1.1. Multicarrier Modulation

Multicarrier modulation (MCM) is a transmission scheme that uses several carriers to transmit data generated at the baseband by means of its translation in frequency to the passband of the channel [Proakis-02]. Fig. 1.1 shows the MCM fundamental frequency diagram. The most common MCM schemes are frequency division multiplexing (FDM) and orthogonal frequency division multiplexing (OFDM) [Armstrong-09].

1.1.1 Frequency Division Multiplexing (FDM)

FDM allows transmitting multiple signals in a single channel to various users. FDM assigns a different carrier frequency to each user for transmission [Proakis-02]. Fig. 1.2a illustrates the process to modulate a generic multicarrier FDM signal, where each signal x_n modulates a separate carrier $f_{c,}$ and each carrier is summed to be transmitted over the channel. Every single carrier is

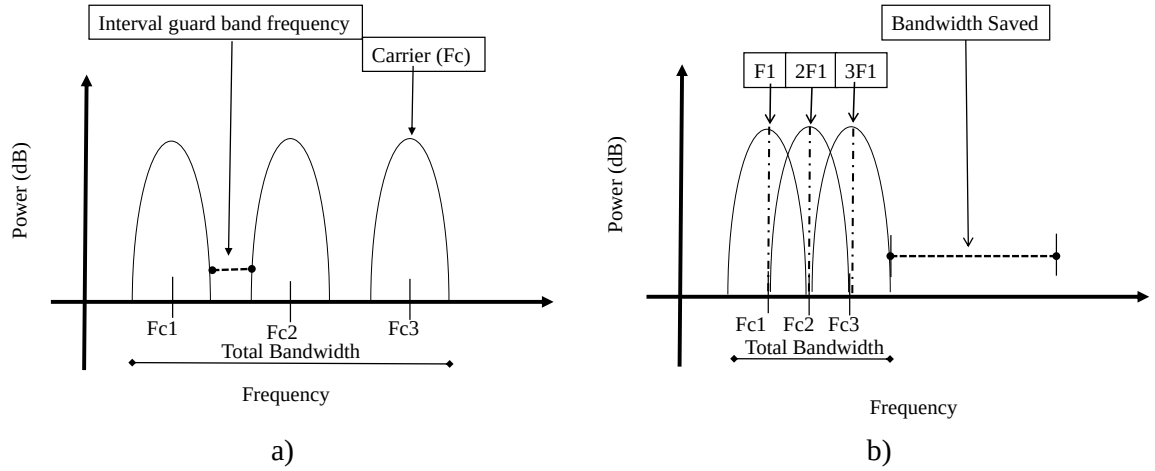

Fig. 1.1 Comparison of power spectrum between a) FDM and b) OFDM. The spectral efficiency of OFDM is better than FDM.

generated independently. However, the carrier frequency for each user is chosen so that the transmissions do not overlap in frequency. This results in significant use of bandwidth [Shieh-10], as shown in Fig. 1.1.

Equation (1-1) shows the basic principle of an MCM system, where the multicarriers are added for transmission and must be separated in the receiver before demodulation [Fitz-07].

$$s(t) = x_1 \sin(2\pi(f_1)\cdot t) + x_2 \sin(2\pi(f_2)\cdot t) + \cdots x_n \sin(2\pi(f_c)\cdot t) \qquad (1\text{-}1)$$

where $s(t)$ is the modulated signal and f_1, f_2, … f_c are the carriers frequencies, and x_1, x_2, … x_n are the information signals.

1.1.2 Orthogonal Frequency Division Multiplexing (OFDM)

An alternative to improve the FDM scheme is the OFDM. OFDM is a type of MCM and a particular case of FDM. The principal advantage of OFDM over FDM is the bandwidth saved. This is possible because the OFDM signal presents orthogonality between subcarriers. This is made thanks to the use of subcarrier frequencies that are multiples of the first frequency f_1 (harmonics), as shown in Fig. 1.2b. The spectra between subcarriers overlap, but each subcarrier is in the spectral nulls of all other subcarriers [Molisch-10]. Fig. 1.1b shows this principle in the

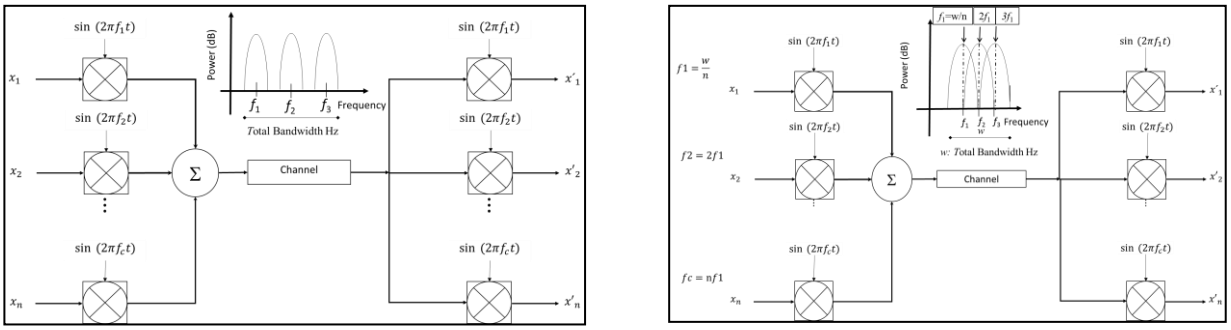

a) b)

Fig. 1.2 Multicarrier modulation system basic diagram: a) FDM and b) OFDM. RF interference are the major issues in the FDM technique while OFDM is immune to these problems.

frequency domain. A basic diagram of OFDM system is shown in Fig. 1.2b. Note that the main difference between FDM and OFDM is the way that the carrier frequencies are chosen, as seen in Fig. 1.2.

1.2. The OFDM System

OFDM has been widely deployed in wireless communications and recently studied for optical communications. Some of its main characteristics are the low level of intersymbol interference (ISI), and the high spectral efficiency compared with other techniques of multicarrier modulation like FDM [Shieh-10].

1.2.1 Elements of the OFDM System

Fig. 1.3 shows a basic block diagram of OFDM system. The first step is to convert the input data stream into a code-word, using coding and interleaving techniques to reduce the bit error rate (BER).

The second step consists of mapping each of the data words using an M-ary modulation technique like quadrature amplitude modulation QAM or phase-shift keying PSK; this is made at the lowpass equivalent signal level, so a complex signal is produced [Fitz-07]. The output of this functional block is a set of parallel data symbols, as shown in Fig. 1.3. Each output symbol is

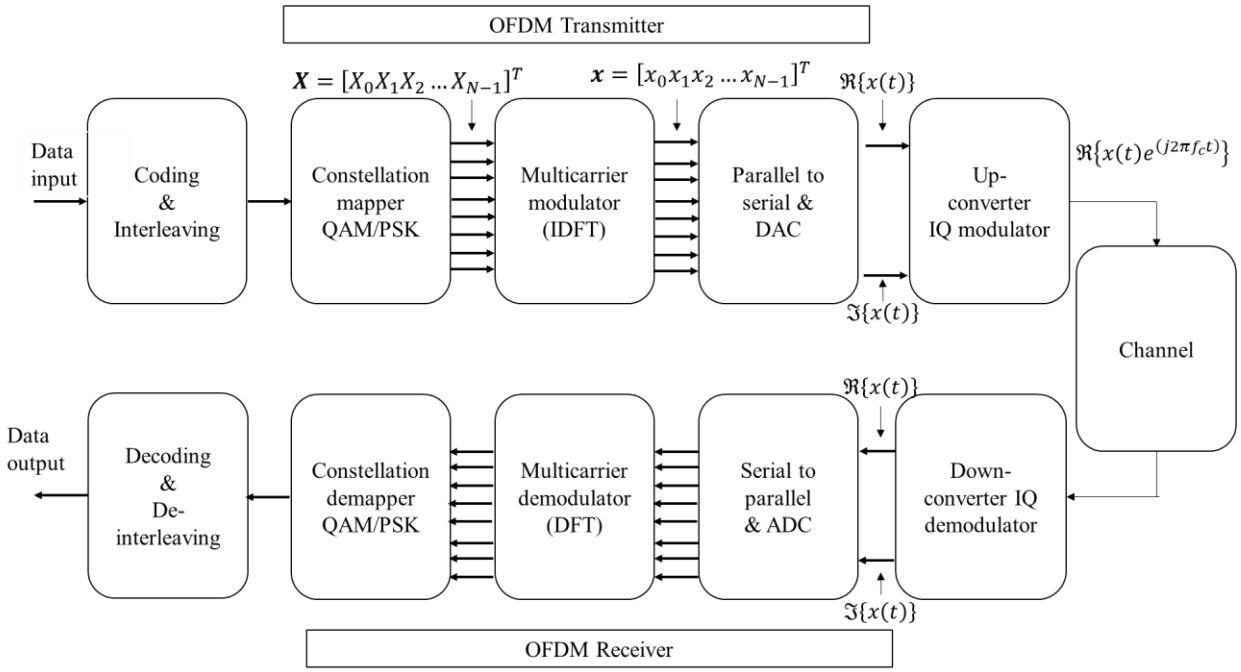

Fig. 1.3 Basic block diagram of an OFDM system. One of the key features in OFDM modulation is the use of IDFT to modulate the signal.

independently modulated on a separate subcarrier frequency.

The multicarrier modulator and demodulator in OFDM, can be implemented by the use of a parallel bank of filters based on the inverse discrete Fourier transform (IDFT). This functional block eliminates the necessity of using local oscillators and filters per each signal [Proakis-02]. The definition of the IDFT for the OFDM symbol sample is:

$$x_n = \frac{1}{\sqrt{N}} \sum_{k=0}^{N-1} X_k \cdot e\left(\frac{j2\pi kn}{N}\right) \quad for \quad 0 \le n \le (N-1) \tag{1-2}$$

where N is the total quantity of subcarriers, k is the subcarrier number, and X_k is the complex number (symbol) representing, for example, 4 bits if using 16-QAM mapping.

The input to the IDFT block is the complex vector $\boldsymbol{X} = [X_0\ X_1\ X_2\ \ldots\ X_{N-1}]^T$ where N is the size of the IDFT, and each of the array elements represents the data to be carried in the corresponding subcarrier. The resulting complex vector in the output of the IDFT is $\boldsymbol{x} = [x_0\ x_1\ x_2\ \ldots\ x_{N-1}]^T$ [Armstrong-09], as shown in Fig. 1.3.

OFDM modulation and demodulation based on IDFT/DFT can be performed efficiently by the use of inverse fast Fourier transform (IFFT) and fast Fourier transform respectively. This implementation reduces computation complexity [Proakis-02].

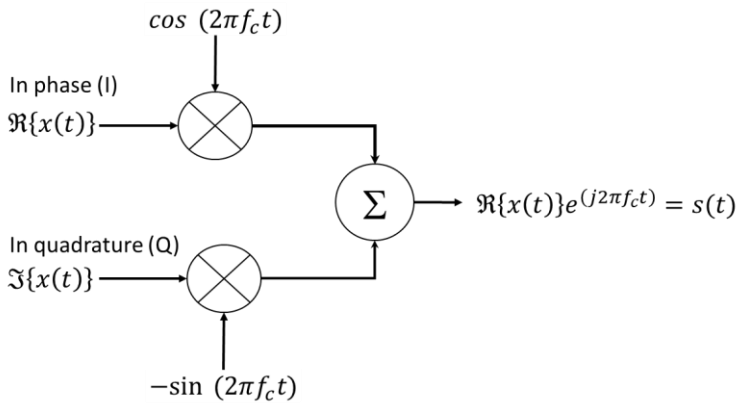

Fig. 1.4 Up-converter IQ Modulator block diagram, and the resulting OFDM signal $s(t)$, as showed in (1-4).

The complex vector $\boldsymbol{x}$ generated by computing the IFFT is passed through a parallel to serial converter (P/S), and then to a digital to analog converter (DAC), where the output is the OFDM signal waveform $x(t)$. This analog signal corresponds to the sum of the baseband subcarriers.

As said before, the modulation is made at the low pass equivalent signal level so $x(t)$ represents the baseband complex value signal having real $\Re\{x(t)\}$ and imaginary parts $\Im\{x(t)\}$ [Shieh-10].

$$x(t) = \Re\{x(t)\} + j\Im\{x(t)\} \tag{1-3}$$

Finally, the baseband complex value signal $x(t)$ is up-converted to passband signal $s(t)$ ready to be transmitted. Mathematically, this transformation involves a complex multiplier (mixer) that can be expressed as follow,

$$s(t) = \Re\{x(t)\}e^{(j2\pi(f_c)t)} = \Re\{x(t)\}\cos(2\pi(f_c)\cdot t) - \Im\{x(t)\}\sin(2\pi(f_c)\cdot t) \tag{1-4}$$

where the passband signal $s(t)$ is a real valued signal at the center frequency carrier of f_c.

This kind of modulation uses an "In phase (I)" and "In quadrature (Q)" modulator (IQ modulator). IQ data inputs represent the complex value signal, where $I = \Re\{x(t)\}$ is the real part of the signal and $Q = \Im\{x(t)\}$ is the imaginary part of the signal.

The I/Q modulator mixes the I part of the signal $s(t)$ with the f_c carrier, and mixes the Q part of the signal $s(t)$ with the same carrier at a 90-degree phase offset as shown in Fig. 1.4. The Q signal is subtracted from the output signal producing the final OFDM signal to be transmitted [Shieh-10].

TABLE 1.1. STANDARDS THAT USE OFDM

Application	Name of the Standard
Digital Audio Broadcasting	DAB Eureka 147
Digital television	DVB-T/T2 (terrestrial), DVB-H (handheld), DMB-T/H, DVB-C2 (cable)
Wireless LAN	LAN IEEE 802.11a, IEEE 802.11g, IEEE 802.11n, IEEE 802.11ac, and IEEE 802.11ad
Worldwide Interoperability for Microwave Access	WiMAX (30-40 Gbps)
Asymmetric digital subscriber line	ADSL High speed data communications ADSL (G.dmt/ITUG.992.1)
Long Term Evolution	LTE and LTE Advanced 4G mobile phone standards
Modern narrow and BROADBAND power line communications.	IEEE 1901, ITU-T G.hn standard

The second part of the OFDM system is the receiver that is shown in Fig. 1.3. It is composed by the same functional blocks as the transmitter but doing the inverse actions. The aim of the receiver is to transform the analog passband signal that comes from the channel to baseband signal using a down-converter IQ demodulator. After this step, the baseband signal is demodulated and converted to serial digital data, which is the nature of the transmitter data input, as shown in Fig. 1.3. Table 1.1 shows different communication standards where OFDM is used. OFDM is present in different areas of communication technology like audio, video, data, smart grid, and it has a promising future in high speed data rate systems [Rahmatallah-13]. In fact, OFDM has recently been applied to optical communications, in consequence, a diversity of optical OFDM systems have been proposed, like Coherent Optical OFDM (CO-OFDM) for their special modulation characteristic such as linear field modulation, which is explained in the following subsection.

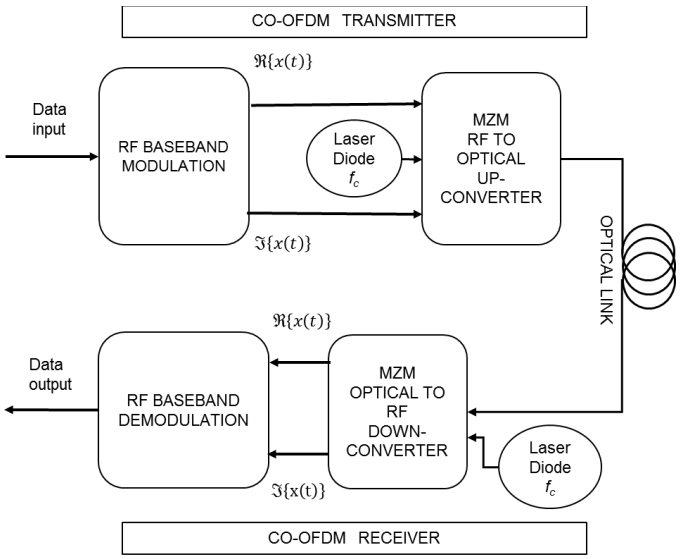

Fig. 1.5 Functional block diagram of a CO-OFDM system.

1.2.2 Coherent Optical OFDM

In the last few years, CO-OFDM has been one of the most studied OFDM schemes in theoretical research, as well as in practical performance [Shieh-10]. Fig. 1.5 shows the functional block diagram of a CO-OFDM system. As mentioned in the last sections CO-OFDM has been the subject to an intense research effort in recent years [Zhang-13], [Cvijetic-12]. This modulation technology offers several important advantages, including high spectral efficiency, inherent robustness against intersymbol interference (ISI) caused by chromatic dispersion (CD) and polarization mode dispersion (PMD), and flexible digital signal processing-based implementation.

CO-OFDM uses a linear field modulation from the output of the OFDM transmitter so that there is a linear relationship between the transmitter IFFT input and the receiver FFT output. Consequently, a linear transformation is the key goal for the CO-OFDM implementation. The challenges for CO-OFDM implementation are to obtain a linear radio frequency to optical (RTO) up-converter and linear optical to radiofrequency (OTR) down-converter. It has been proposed and analyzed that, by biasing the Mach–Zehnder modulators (MZMs) at the null point, a linear conversion between the RF signal and the optical field signal can be achieved [Shieh-10]. The IQ modulator uses a two Mach-Zehnder Modulator, as shown in Fig. 1.5.

An additional difference in CO-OFDM, as compared with other optical OFDM schemes,

TABLE 1.2. OPTICAL AMPLIFIER SEMICONDUCTOR FEATURES COMPARISON [Conelly-98]

Feature	OFA	SOA
Maximum internal gain (dB)	30-50	30
Insertion loss (dB)	0.1 – 2	6 – 10
Polarization sensitive	No	Weak (<2 dB)
Pump source	Optical	Electrical
3 dB gain bandwidth (nm)	30	30 – 50
Nonlinear effects	Negligible	Yes
Saturation output power (dBm)	10 – 15	5 – 20
Noise figure (dB)		
Integrated circuit compatible?	No	Yes
Functional device possibility?	No	Yes

is that CO-OFDM requires a laser at the receiver to generate the carrier locally to achieve linearity, and is more sensitive to phase noise [Shieh-10]. Fig. 1.5 shows the optical carrier generated by the Laser Diode LD1 on the IQ modulator and by Laser Diode LD2 on the demodulator.

In addition, CO-OFDM needs to use an optical power amplifier to enhance the power of transmission signal. Furthermore, optical amplifiers have some drawbacks like nonlinearities present at the output signal when they are operating near to the saturation region.

1.3. Optical Amplifiers

As mentioned in the last section, the optical amplifier is one of the key components in optical transmission systems. Optical amplifiers can be divided into optical fiber amplifiers (OFA) and semiconductor optical amplifiers (SOA). The four main parameters for characterizing the performance of optical amplifiers in a communication system are noise figure, signal gain, frequency bandwidth, and saturation output power [Keiser-91]. Table 1.2 shows a technical parameter comparison between OFA and SOA. Note that SOA can work with a larger optical gain bandwidth of 30 to 50 nm; moreover, SOA have good performance in terms of saturation output power even to 20 dBm [Khaleghi-12].

The main difference between OFA and SOA is that the OFA uses an optical pump source to amplify the optical signal, while SOA works with an electrical pump source to amplify the

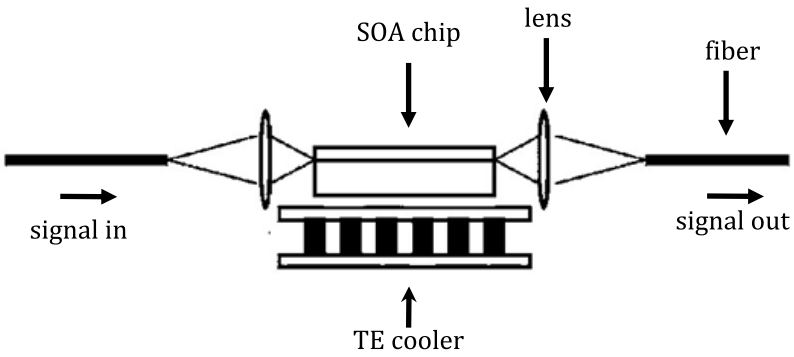

Fig. 1.6 Schematic diagram of SOA chip. Figure taken from [Shieh-10].

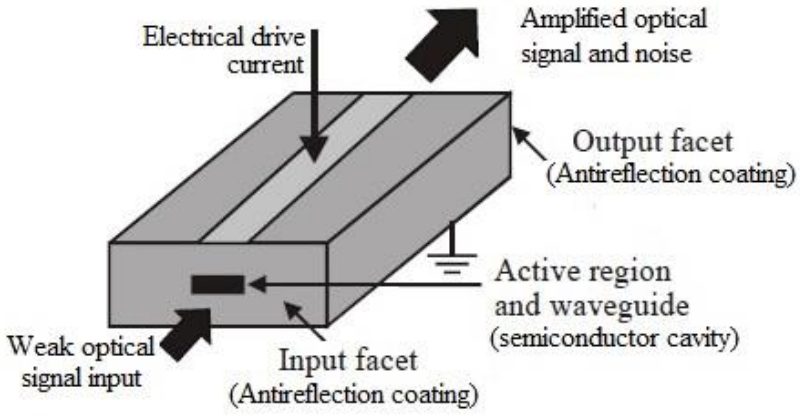

Fig. 1.7 SOA functional block diagram.

signal. Another advantage is that SOA have small physical dimensions, which makes it easy to assemble in an electronic circuit, as shown in Fig. 1.6 [Ware-11].

The SOA has three basic components: Electrical drive current (pump source), Active region (semiconductor cavity), and Facet input and output, (see Fig. 1.7). These are necessary to sustain the stimulated emission of photons and amplify the optical signal [Connelly-98].

The SOA is driven by an electrical current, also named as pump source or bias current. The active region stimulates the weak optical input signal to have a gain photon power at the Amplified optical signal output, as shown in Fig. 1.8.

The basic principle of operation is the same of the laser. Laser action is the result of three key processes. These are photon absorption, spontaneous emission, and stimulated emission. The three processes are represented by the simple two-energy-level diagram depicted in Fig. 1.9.

The gain saturation produces signal distortion, and additive noise. The additive noise is named amplified spontaneous emission (ASE), and it is generated by the amplification process

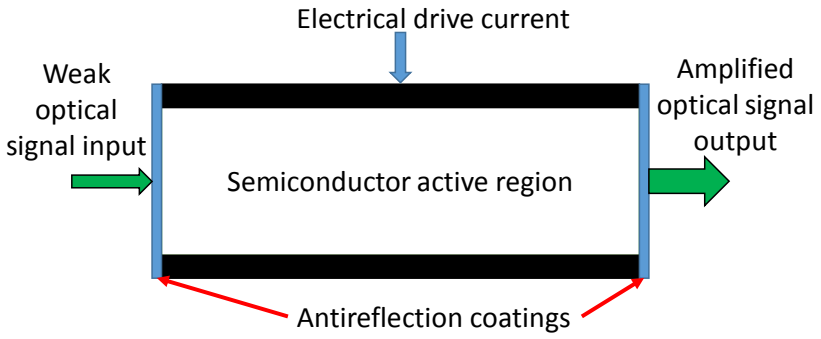

Fig. 1.8 SOA basic amplification process.

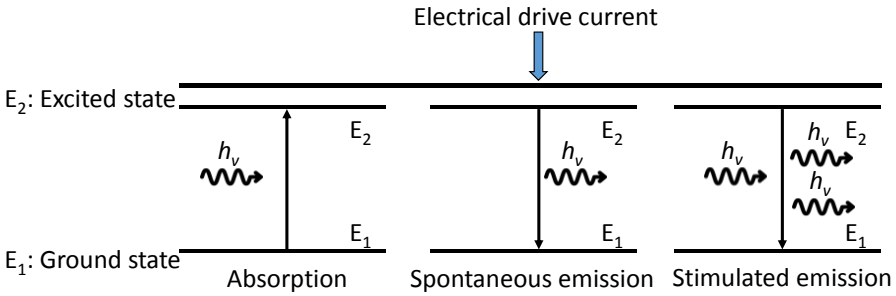

Fig. 1.9 Two energy level diagram.

into the active region [Connelly-98].

A major disadvantage of SOA is the nonlinear effects in the output signal and then the distortion of the output signal at the output power amplifier in the OFDM transmitter. This is the reason for the research interest in novel techniques to reduce the nonlinear effects and improve the performance of SOA in OFDM systems.

1.4. Peak to Average Power Ratio

A major disadvantage of the OFDM systems is the high peak-to-average power ratio (PAPR) that is inherent in the transmitted signal. Large signal peaks occur when the signals in the *N* subcarriers add constructively in phase. Such large signal peaks may saturate the power amplifier at the transmitter and, thus, cause intermodulation distortion in the transmitted signal. Fig. 1.10 shows how a high peak is obtained by adding four sinusoidal signals with different frequencies but with same phase shift. Then when the different subcarriers have high peaks aligned at the same time, this results in an instantaneous increment of energy that goes to the input of the SOA, driving

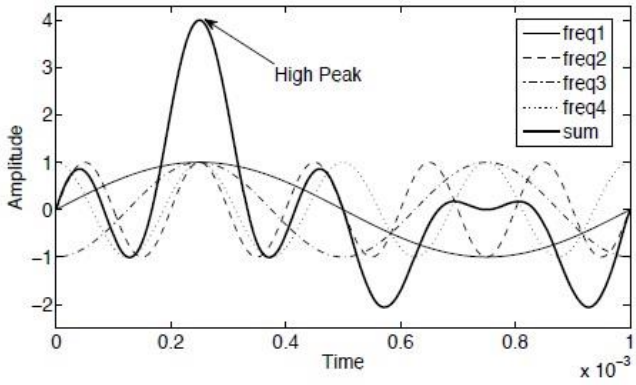

Fig. 1.10 High peak resulting from the sum of sinusoidal signals. Figure taken from [Ware-11].

it into the saturation region, as shown in Fig. 1.11.

The lowpass equivalent OFDM signal $x(t)$ has a PAPR defined as the ratio between the maximum instantaneous power and its average power,

$$PAPR[x(t)] = \frac{\max_{0 \le t \le NT} \left[|x(t)|^2 \right]}{P_{av}} \tag{1-5}$$

where P_{av} is the average power of $x(t)$ and it can be computed in the frequency domain because OFDM is modulated using IFFT, which is a scaled unitary transformation, N is the number of subcarriers and T is the symbol period in the single carrier system [Jiang-08].

1.5. Reduction Methods for PAPR

As mentioned earlier, a high PAPR drives into saturation the SOA in an OFDM transmitter producing nonlinearities in the output signal. One solution is to reduce the average power of the signal, but the performance of the amplification is also reduced. The most useful technique is to maintain the SOA working with a good performance, high output power, but reducing the power peaks of the signal [Rahmatallah-13].

The literature presents many PAPR reduction techniques published since the high PAPR problem was detected. These techniques can be classified in three main categories, as shown in Fig. 1.12: Signal Distortion techniques, with special emphasis in the companding techniques, which have good results in PAPR reduction with low BER and a low computational complexity; Multiple Signaling and Probabilistic techniques; and Coding techniques, which present a low

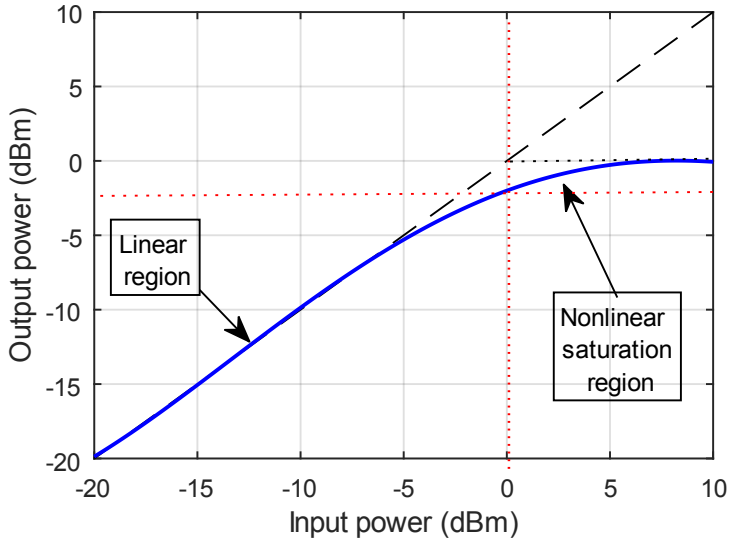

Fig. 1.11 Curve input/output power in dB for typical SOA.

performance in terms of BER and high computational complexity.

1.5.1 Coding Techniques

As mentioned in Section 1.2, coding is part of the first functional block in OFDM system, the main purpose being data protection and correction. The basic idea in a coding is to reduce the occurrence of the same phase of the signal, which is the main cause of high PAPR (see Fig. 1.10). Simple block coding techniques mapping the data and add bits to create a code work to reduce the probability to get high PAPR [Jiang-08]. In example, linear block coding techniques eliminates the code words with a high probability to present a high PAPR. And, other coding technique works with phase adjustment, multiplying the code words by a phase adjustment vector, and selecting the code words with the lowest PAPR to be transmitted [Rahmatallah-13].

1.5.2 Multiple Signaling and Probabilistic Techniques

These techniques work in one of two ways. The first one is the selective mapping, which generates multiple permutations of the OFDM signal and transmits the code word with minimum PAPR. The other way is to modify the OFDM signal by introducing phase shifts, adding peak reduction carriers, or changing constellation points. The modification parameters are optimized to

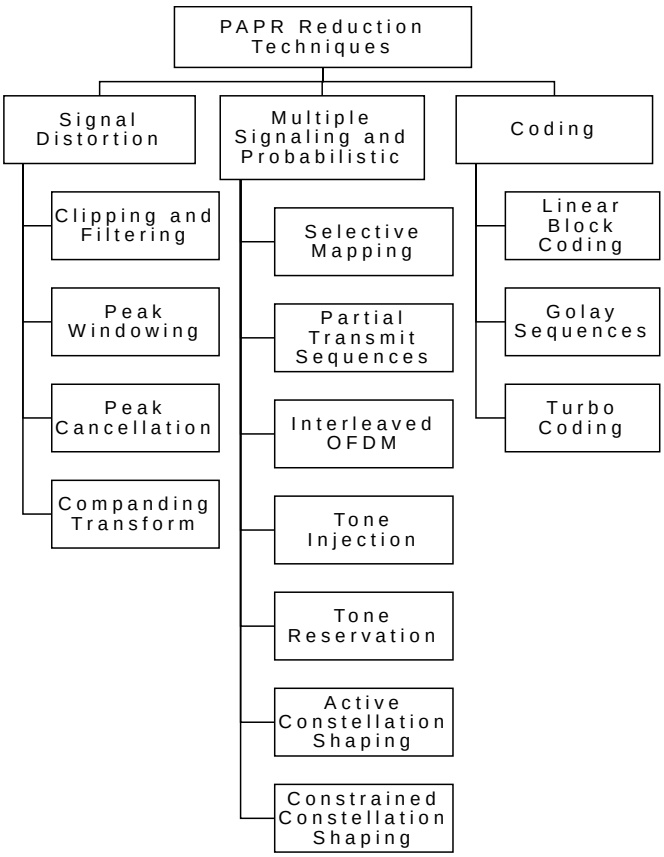

Fig. 1.12 Taxonomy of PAPR reduction techniques [Rahmatallah-13].

minimize PAPR.

a) Selective Mapping: Selective mapping (SLM) is a relatively simple approach to reduce PAPR. It generates a set of sufficiently different OFDM symbols, each of length *N*, all representing the same information as the original OFDM symbol *x*, then it transmits the one with the least PAPR. Information about the selected phase sequence should be transmitted to the receiver as side information to allow the recovery of the original symbol sequence at the receiver, which reduces the data transmission rate [Jiang-08].

b) Partial Transmit Sequence: In partial transmit sequence (PTS), an input data block of length *N* is partitioned into a number of disjoint sub-blocks. The IDFT for each of these sub-blocks is computed separately and then weighted by a phase factor. The phase factors are selected in such a way as to minimize the PAPR of the combined signal of all the sub-blocks. The process of selecting the optimum phase factors is usually limited to a finite number of elements to reduce search complexity

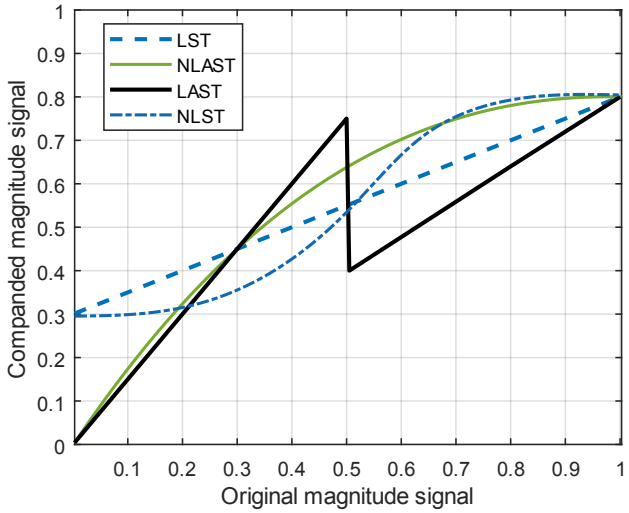

Fig. 1.13 Companding techniques and their curves response [Rahmatallah-13].

[Louët-08].

1.5.3 Signal Distortions Techniques

These techniques introduce a distortion into the transmission signal before the amplification process. In addition, they can be classified in clipping and filtering, peak windowing, and peak cancellation. One of their characteristics is that the peaks are removed from the signal, but the drawback is an increase in the BER. A brief description about the most common signal distortion techniques follows.

a) Clipping and filtering: This method uses a clipper that limits the high peaks of the OFDM signal envelope to a predetermined clipping level (CL) if the signal exceeds that level; otherwise, the clipper passes the signal to the High Power Amplifier without change. This introduces in-band distortion and out-band distortion. Filtering the clipped OFDM signal can preserve the spectral efficiency by eliminating the out-of band distortion and, hence, improving the BER performance, but it can lead to peak power regrowth.

b) Peak windowing: The peak windowing limits such high peaks by multiplying them by a weighting function called a window function. Many window functions can be used in this process as long as they have good spectral properties, and they reduce the distortion

as compared with clipping and filtering.

c) Peak cancellation: A peak cancellation waveform is appropriately generated, scaled, shifted and subtracted from the OFDM signal at those segments that exhibit high peaks. Peak cancellation can be carried out after the IFFT block of the OFDM transmitter. While performing the peak cancellation process, care should be taken to not create new peaks.

d) Companding Transforms: Companding transforms are typically applied to speech signals to optimize the required number of bits per sample. OFDM and speech signals behave similarly, and these techniques have a relatively low computational complexity as compared to other PAPR reduction techniques. In this case companding complexity is not affected by the number of subcarriers. Companding transforms can be generally classified into four classes: linear symmetrical transform (LST), linear asymmetrical transform (LAST), nonlinear symmetrical transform (NLST), and nonlinear asymmetrical transform (NLAST). Fig. 1.13 depicts the profiles of these four classes [Jiang-08]. The NLAST increases the mean power and reduces the peak power, and, consequently, reduces PAPR.

1.6. SOA based CO-OFDM Simulation Platform

In this section, we present a coherent optical orthogonal frequency division multiplexing (CO-OFDM) simulation system, aiming to analyze the main steps of the proposed simulation method. CO-OFDM is a well-established multicarrier modulation format capable of transmitting at high data rates. CO-OFDM has been positioned as an excellent option for the next generation of long-haul optical networks [Agrell-16].

While it is true that there are several commercially available software tools that allow the simulation of optical networks, such as OptiSystem[1], we considered that it would be more convenient to develop a low-cost, fully customizable tool focused on the SOA amplification.

[1] OptiSystem14.2.0, Optiwave System Inc., 7 Capella Court Suite 300 Ottawa, ON, Canada K2E 8A7.

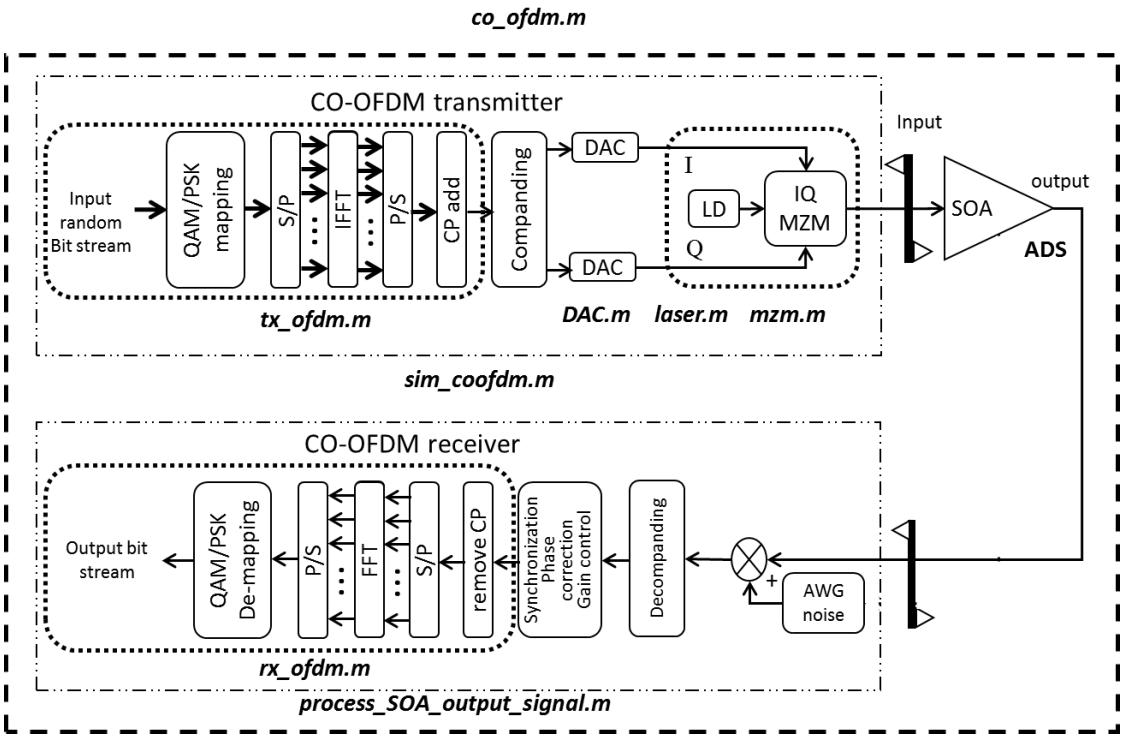

Fig. 1.14 SOA-based CO-OFDM co-simulation system. Digital signal processing has been implemented in MATLAB, and the SOA simulator is developed in ADS. Ideal coherent detection has been considered.

We explain in this work the CO-OFDM simulation execution process through flowcharts and numerical simulations. This simulation platform was initially developed to test the CO-OFDM system performance when it is amplified by a semiconductor optical amplifier (SOA) [Khaleghi-13]. This included the testing of companding methods [Azou-15], and digital predistortion to alleviate the nonlinear effects due to the SOA saturation [Bejan-15], [Younes-17].

The proposed simulation platform has been built in Matlab[2] software. Although Matlab offers excellent flexibility to perform digital signal processing (DSP), it has limited features for simulating the amplification process by an SOA. To cope with these limitations, our simulation platform uses an interface with the specialized electronic design software Advanced Design System (ADS)[3]. Then, a co-simulation in ADS was implemented. Fig. 1.14 shows the SOA based CO-OFDM system block diagram, remarking the corresponding Matlab functions (with bold italics and dotted sub-blocks) to relate these functions with the CO-OFDM signal processing block.

It is important to remark that, in the current research work, we are evaluating the CO-

[2] MATLAB, Version 9.5.0.944444, The Math Works, Inc., 3 Apple Hill Drive, Natick MA 01760-2098, 2018.
[3] Advanced Design System 2016, Keysight Technologies, Santa Rosa, CA, United States, 2016.

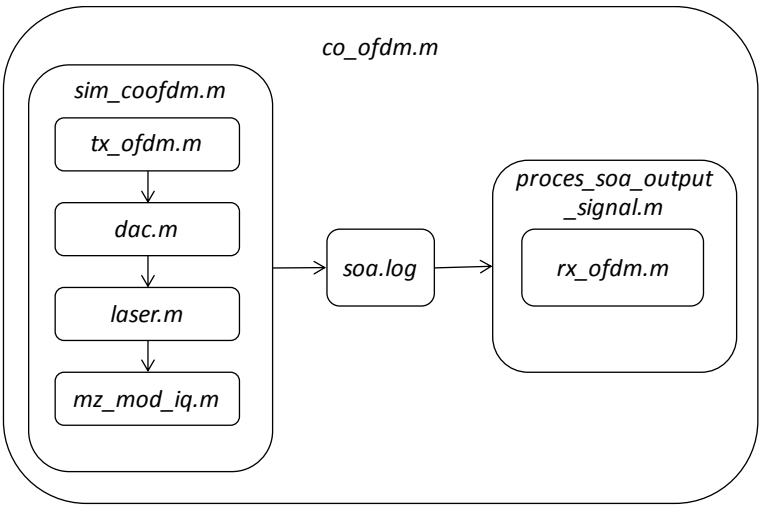

Fig. 1.15 CO-OFDM simulation execution structure in Matlab. The simulation platform is composed by eight main Matlab functions and one SOA log file to interact with ADS software where the SOA amplification is simulated.

OFDM link as a back to back transmission, discarding channel impairments, and considering an ideal receiver. Also, this simulation system works with a self-developed SOA model [Morel-09], which has been fitted to simulate a commercially available bulk 750 μm long SOA (INPHENIX-IPSAD1501). For the purposes of system simulation, the SOA model acts as a black box, that is, it is a device that is not modified in the process.

1.6.1 SOA based CO-OFDM Simulation Platform Functionality

The aim of this section is to show how the simulation platform works in terms of its functional structure. The execution structure of the Matlab function files is shown in Fig. 1.15, where the Matlab function named as co-ofdm.m is the main function. Thus, it should be run first and the other Matlab functions are invoked accordingly to assess the transmission and reception link performance. As mentioned before, the SOA based CO-OFDM simulator works as a co-simulation system. The CO-OFDM transmitter and receiver are processed in Matlab, while ADS computes the amplification response of the SOA. Each Matlab function and their most important subsections are described in the following subsections.

1.6.1.1 Main CO-OFDM Function co_ofdm.m

CO-OFDM main function performs the entire simulation process. The flowchart that describes co-ofdm.m execution task is depicted in Fig. 1.16.

First of all, the user sets up the principal modulation parameters, such as data subcarrier number (*Nsc*), SOA bias current (I_{dc}), baseband modulator QAM or PSK, modulation order (can be set up at 4, 16, 32, or even 64 states), electrical bandwidth, oversampling factor, amplified spontaneous emission (ASE) noise. Those parameters feed the inputs of CO-OFDM transmitter function named as sim_coofdm.m. When the number of desired runs is achieved, the simulator stops. In the following subsections, each subprogram is described.

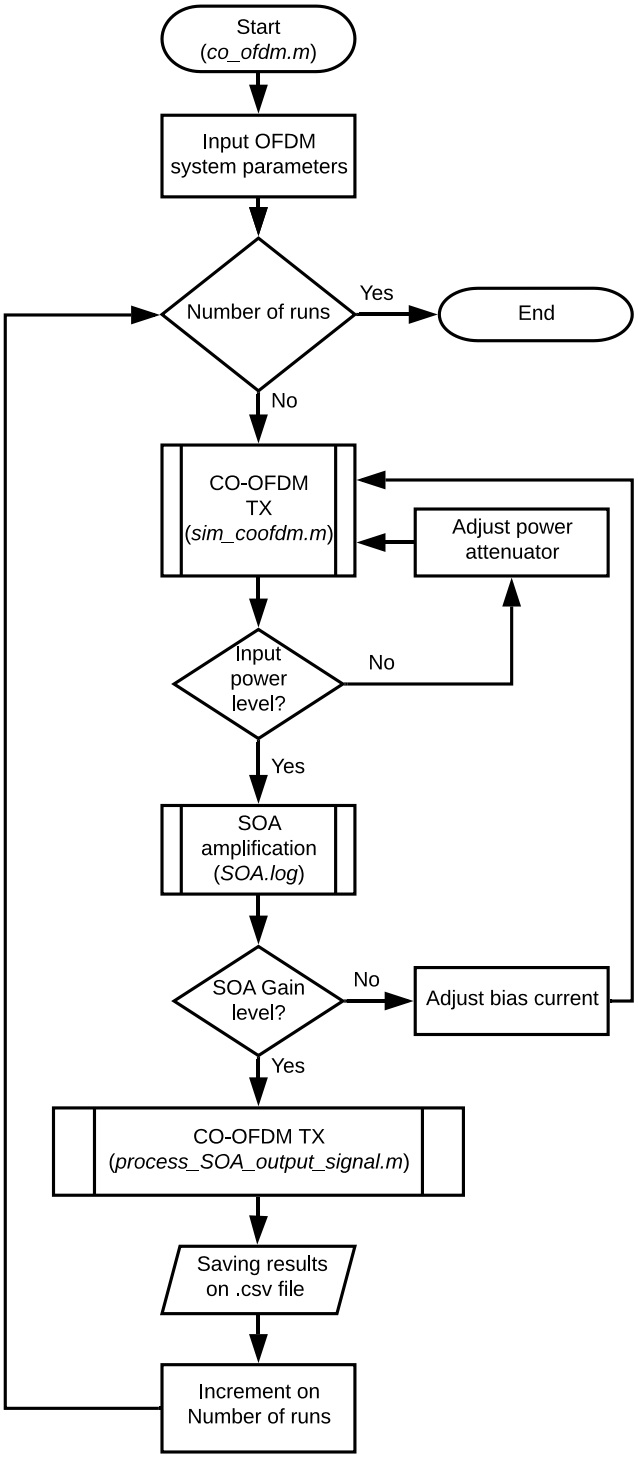

Fig. 1.16 Flowchart of the main CO-OFDM simulation Matlab function co-ofdm.m file. It includes input power control by changing the attenuator adjust loop and gain control loop by bias current adjustment.

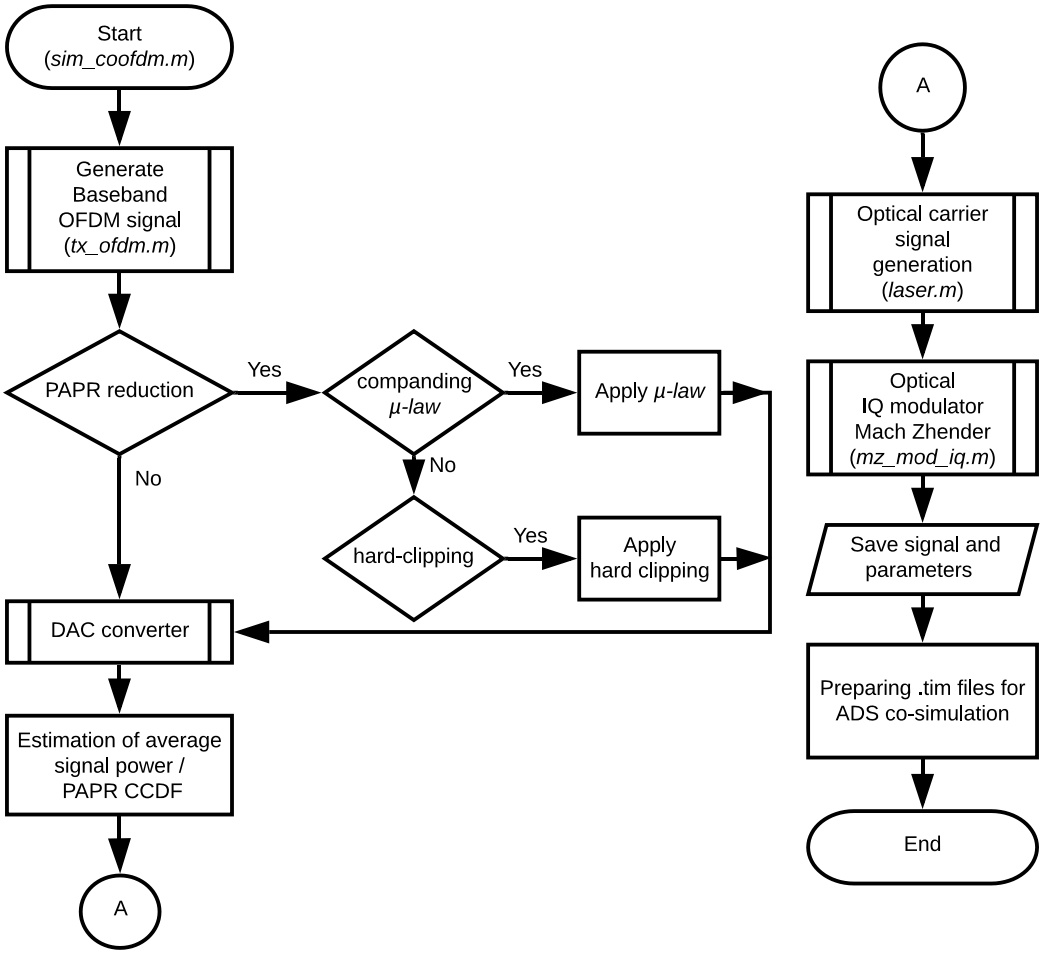

Fig. 1.17 The sim_coofdm.m function emulates the CO-OFDM signal generation and modulation before amplification process.

1.6.1.2 CO-OFDM Transmitter sim_coofdm.m

In this subprogram, the CO-OFDM transmission is processed according to the flowchart depicted in Fig. 1.17. First, the process tx_ofdm.m generates the OFDM signal. According to Fig. 1.14, it is possible to apply a peak to average power ratio (PAPR) reduction method to the OFDM signal. If this feature is enabled, a companding μ-law [Wang-99] technique or hard clipping [Rahmatallah-13], or any other PAPR reduction method is processed. After this, a digital to analog conversion (DAC) is applied to each part of the OFDM complex baseband signal. The modulation

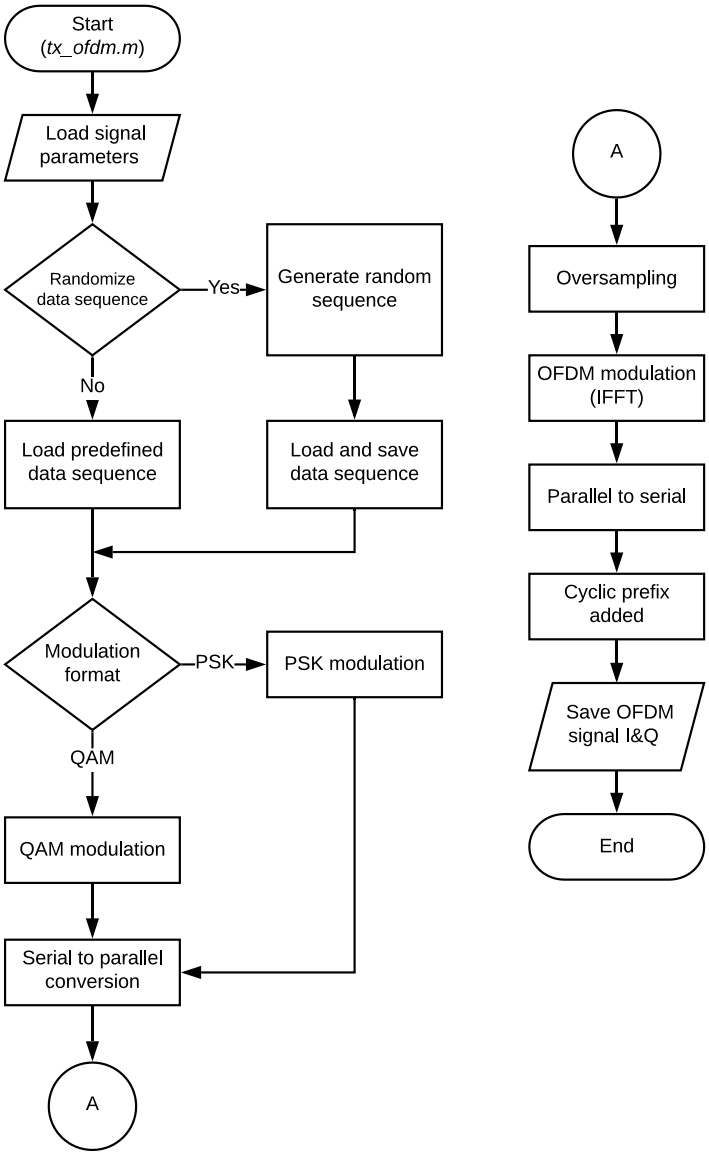

Fig. 1.18 Transmitted OFDM signal generation flowchart. Digital baseband modulation can be selected QAM or PSK at different order modulation level (4, 16, 32, 64).

process is then performed according to the I/Q Mach-Zehnder modulator (see Section 1.2.2).

The operating details of each block within this subprogram are explained, following the flow shown in Fig. 1.17 :

a) OFDM Modulator tx_ofdm.m. This function generates the electrical OFDM baseband signal. The input bit stream sequence can be generated randomly, or it can be loaded from a previously selected file. Digital baseband modulation format QAM or PSK at different constellation sizes, 4, 16, 32, or 64, is executed here. After this, the OFDM modulation is

implemented through IFFT operation, as shown in Fig. 1.18.

b) Digital to analog converter, dac.m. The DAC execution process is depicted in Fig. 1.19. This process is applied for each part of the OFDM complex baseband signal, as shown in Fig. 1.14. The DAC function uses a uniform quantization method. After that, up-sampling and low-pass filter is processed to emulate the analog signal conversion. This DAC function also computes quantization error mean and standard deviation; these features are useful to assess the DAC performance when other quantization methods or different sampling rates are tested.

c) Mach Zehnder modulator, mz_mod_iq.m. This process implements an electro-optical conversion function based on the IQ Mach Zehnder modulator (IQ-MZM) model [Shieh-10]. IQ-MZM is a planar waveguide used as a radiofrequency to optical (RTO) passband modulator (see Fig. 1.5).

d) Carrier laser, laser.m. This function provides a laser lightwave signal used as a local laser, since the IQ-MZM (see Fig. 1.14) requires a laser to generate the optical carrier [Shieh-10]. Here, the laser lightwave simulation is carried out by using:

$$s = \sqrt{P_s}\,\exp\left(j\omega_0 t\right) \tag{1-6}$$

where P_s is the laser power and $\omega_0 = 2\pi\nu$ is the angular frequency, and ν is the frequency of light in Hertz [Barry-90].

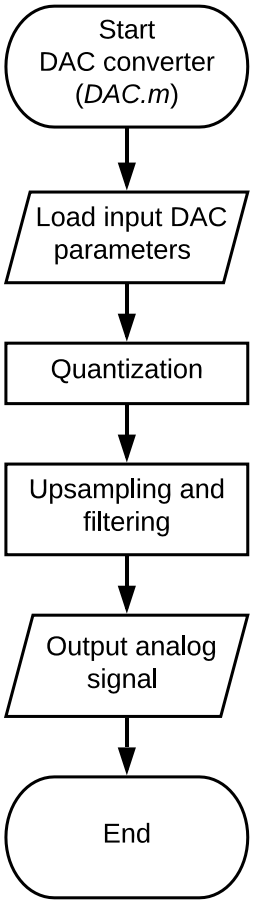

Fig. 1.19 Digital to analog converter (DAC) diagram. Uniform quantization, upsampling and filtering is used to emulate the analog signal conversion process.

1.6.1.3 SOA Model

The ADS-SOA model relies on the carrier density rate and propagation equations of the optical signal field and the intensity of the amplified spontaneous emissions (ASE) noise. SOA model is based on Bulk 750 μm long SOA. This model uses a generalized time domain transfer matrix model (TDTMM). It was originally developed in [Morel-09], and it has been proved to be highly effective in various problems, including all optical RF mixer design based on cross-gain modulation in a SOA [Bohémond-11], coherent optical OFDM signal amplification via SOA [Khaleghi-13] or RSOA based IM/DD OFDM transmission [Hamze-15]. More specifically, in the latter work, the intensity modulation of the CW optical signal from the laser source is achieved by varying the amplifier current with the OFDM signal to be transmitted (an adaptive format being

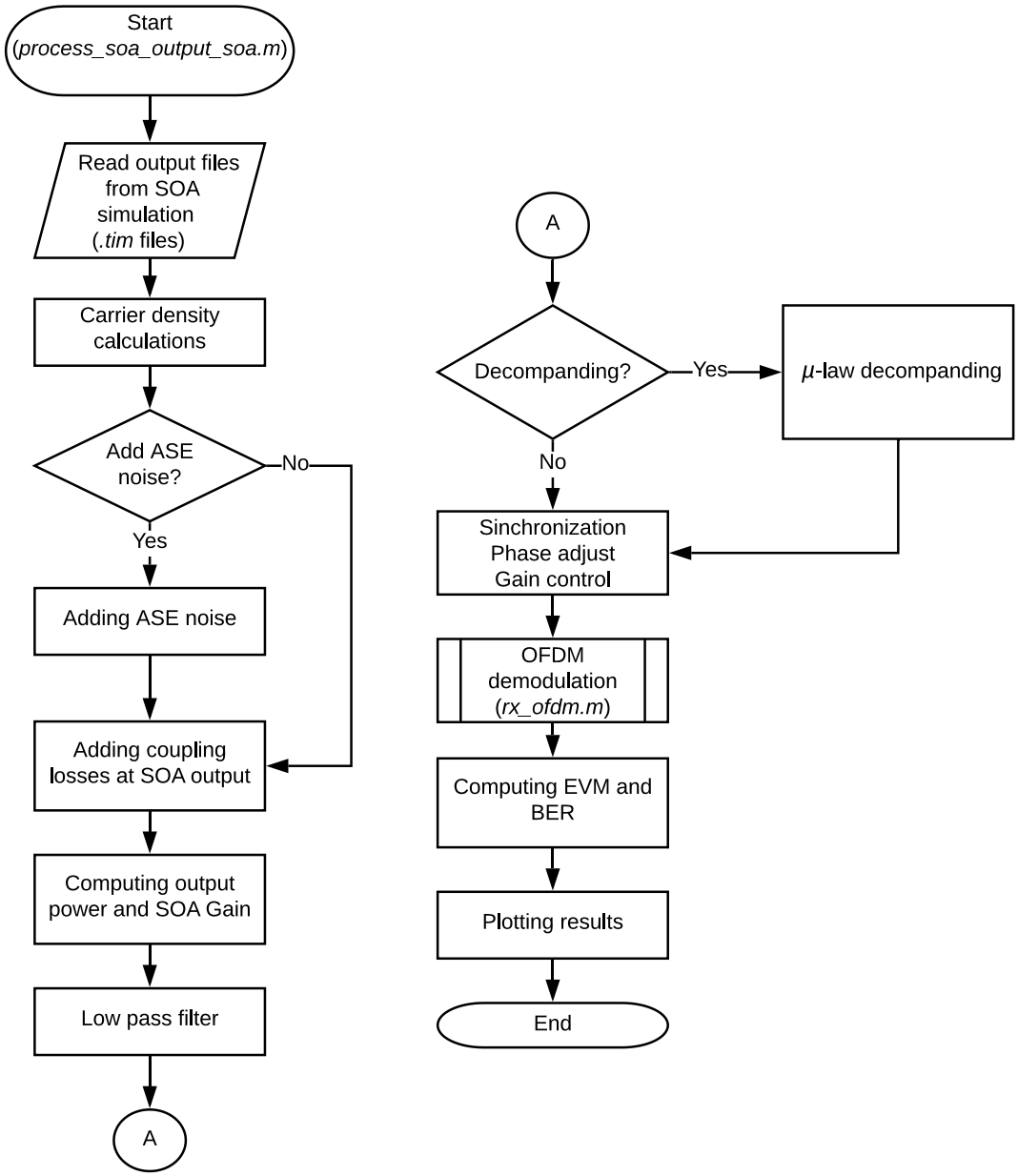

Fig. 1.20 CO-OFDM receiver function named as process_soa_output_signal.m. It processes the SOA simulation file from Keysight ADS.

eventually used depending on the transmission quality observed on the various subcarriers). Also, the XGM effect in the SOA is used for achieving a wavelength conversion for the IM-OFDM signal. A comparison between numerical results and measurements is also conducted. Overall, a good agreement is noticed which reveals that our SOA model can realistically reflect the amplifier behavior under high speed bias current variation. Furthermore, the implementation of this SOA model is done under an equivalent circuit, which permits to perform several types of calculations

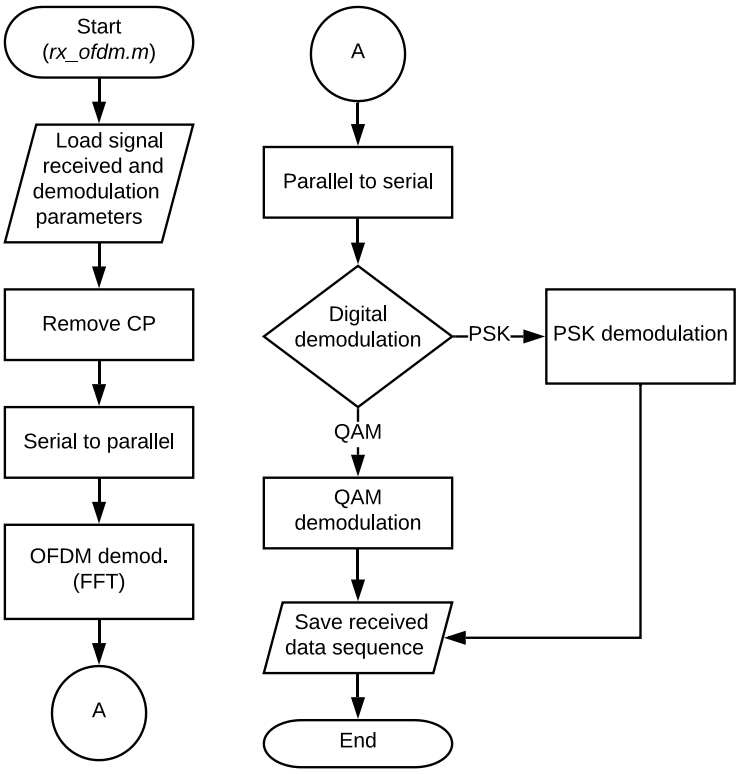

Fig. 1.21 OFDM demodulation process rx_ofdm.m runs into the process_soa_output_signal.m function. Transmission inverse actions are computed to recover the original signal.

(DC, AC, transient). SOA model has been tested, showing similar simulated results versus experimental results [Khaleghi-13].

1.6.1.4 CO-OFDM Receiver process_SOA_output_signal.m

In the receiver simulation, shown in Fig. 1.20, inverse actions of the transmitter have been configured in such a way that the transmitted signal is recovered and analyzed, calculating the system performance. Specifically, amplification losses have been added at the SOA input and output as well as ASE noise at the received signal. Likewise, it is considered an ideal coherent detection and a perfect compensation of the laser phase noise. Power control and phase shift correction due to amplification in SOA are adjusted at the SOA output. Synchronization is performed by a cross-correlation, using the pilot symbol added in the transmitted frame.

A customized function, rx_ofdm.m, is used to develop OFDM demodulation and digital demodulation. Its process flowchart is shown in Fig. 1.21.

TABLE 1.3. CO-OFDM SIMULATOR SETUP

Simulator feature	Configuration
baseband modulation format	4-QAM
electrical baseband bandwidth	5 GHz
number of symbols (QAM/PSK)	2^{11}
data subcarriers	128
null subcarriers	384
oversampling factor	4
cyclic prefix length ratio	1/8
data rate	8.88 Gbps
time symbol	25.6 ns
sampling time	50 ps
SOA bias current	150 mA
SOA gain	15 dB

1.6.2 CO-OFDM Simulation Process

In this section, we explain the simulation process and show a numerical assessment for one CO-OFDM signal across the whole optical link. Table 1.3 shows the setup parameters for the CO-OFDM simulation system.

The first step in creating the OFDM signal, is to generate randomly the 2^{11} 4-QAM data which was defined by the modulation order. This is a sub-block of the tx_ofdm.m function shown in Fig. 1.14. After that, the serial 4-QAM data symbols are distributed among the 128 data subcarriers in parallel. Then, an oversampling factor (os) of 4 multiplies the number of data subcarriers to determine the total *Nsc*. In that case, 384 null subcarriers are inserted in the middle of each array of 4-QAM symbols to complete 512 total subcarriers, as shown in Fig. 1.22 at the left side of the OFDM baseband modulator.

The OFDM baseband modulator uses IFFT operations to modulate each 4-QAM data symbol. Its output is the low-pass signal, in a matrix of complex symbols per subcarrier. Fig. 1.22 shows that 4 OFDM symbols have been generated.

Now, the electrical bandwidth (BW) value (5 GHz, in our example) is used to estimate the

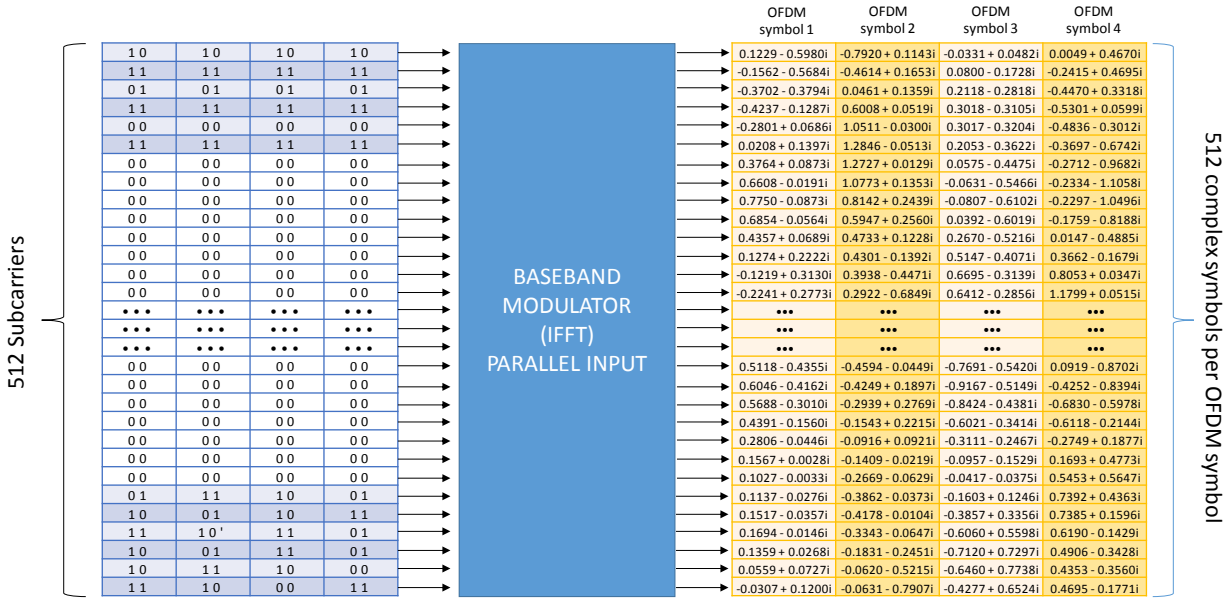

Fig. 1.22 OFDM symbol arrangement for 512 subcarriers input and output for orthogonal baseband modulation. Each OFDM symbol arrangement contains 128 data subcarriers and 384 null subcarriers added with centered zero padding.

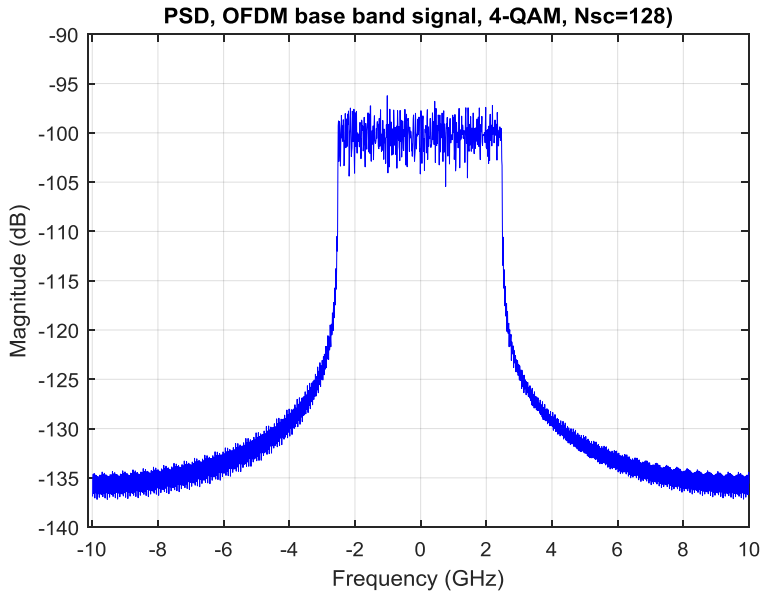

Fig. 1.23 Power spectrum density (PSD) of baseband modulated OFDM signal. The OFDM electrical bandwidth has been increased by oversampling to prevent spectral spreading, from 5 GHz to 20 GHz.

useful time duration of an OFDM symbol (Tu) where $Tu = (1/BW)(Nsc) = 22.5$ ns before oversampling and guard interval. The sampling period (Tc) per each 4-QAM data symbol is defined by $Tc = Tu/((os)(Nsc)) = 50$ ps, after the null subcarriers have been inserted. We can notice

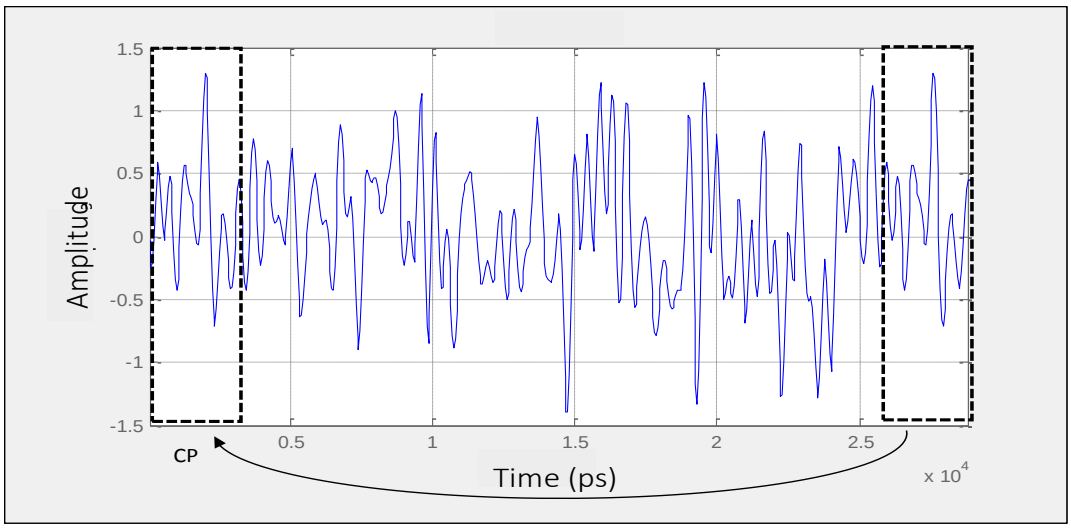

Fig. 1.24 One CO-OFDM symbol with guard interval (square dot dash section) in time domain. Guard interval is a portion of the OFDM symbol end placed at the beginning to prevent ISI. Guard interval method used is cyclic prefix.

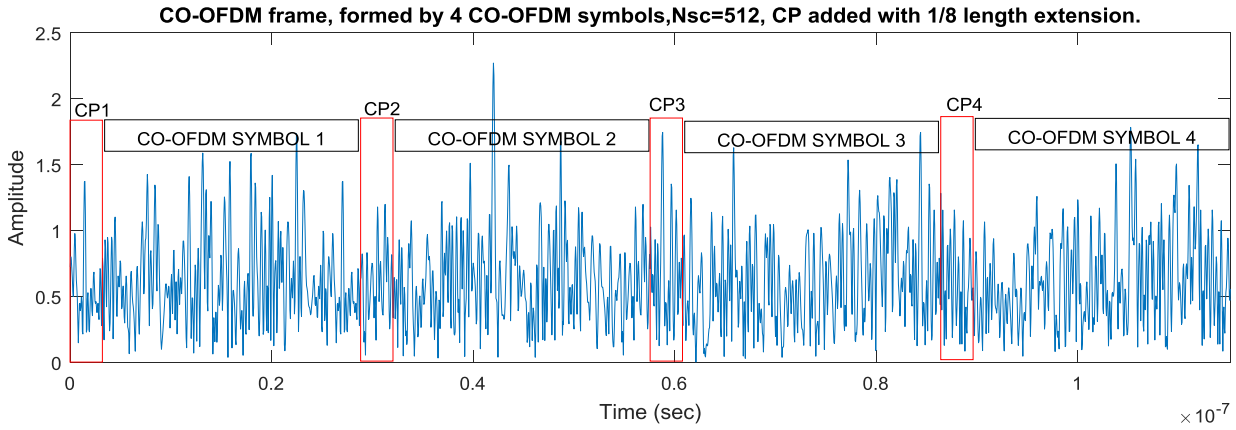

Fig. 1.25 One CO-OFDM frame with 2304 data symbols, allocated in 4 CO-OFDM symbols. The sampling period is 50 ps per data symbols. Original BW 5GHz with an oversampling factor of 4.

that oversampling increases proportionally to the original electrical bandwidth BW from 5 GHz to 20 GHz to avoid spectral spreading, as confirmed in Fig. 1.23.

Once the IFFT baseband modulation is done, guard interval is inserted to prevent intersymbol interference (ISI). The guard interval method used is cyclic prefix (CP). In Fig. 1.24, CP is one eight of the IFFT size, and we finally have 576 complex symbols after CP insertion per each OFDM symbol. CP increases the useful OFDM symbol duration in $Tsymb = Tu + Tg =$ 576*50 ps = 28,800 ps, where Tg is the guard interval time defined as $Tg = Tc*CP*Nsc$ (see Fig. 1.24.

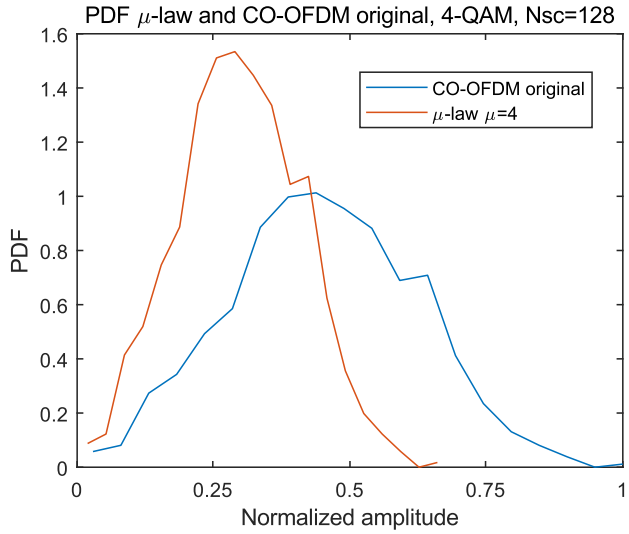

Fig. 1.26 PDF μ-law and CO-OFDM original signal. μ-law works compressing large amplitudes signal and enlarging small ones.

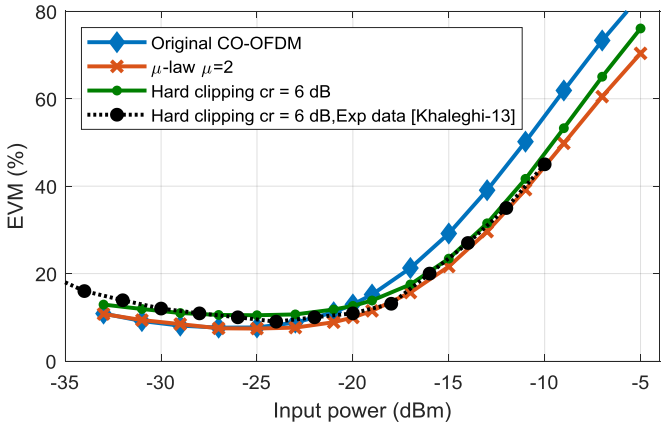

Fig. 1.27 EVM versus input power for different simulations; PAPR reduction methods has been simulated. Simulations shows good agreement with experimental data obtained in [Khaleghi-13].

Once the OFDM symbol is produced, it is converted from parallel to serial, forming a CO-OFDM frame as shown in Fig. 1.25. This corresponds to the output of the `tx_ofdm.m` function. The first CO-OFDM symbol is used as a pilot symbol for synchronization at the receiver.

The CO-OFDM signal is processed in our simulation platform by a PAPR reduction technique, named as companding, as shown in Fig. 1.14. This operation applies a transforming function to the baseband signal, changing the statistical amplitude distribution to mitigate any harmful nonlinear effects at the received signal, due to the presence of high peaks of amplitude at

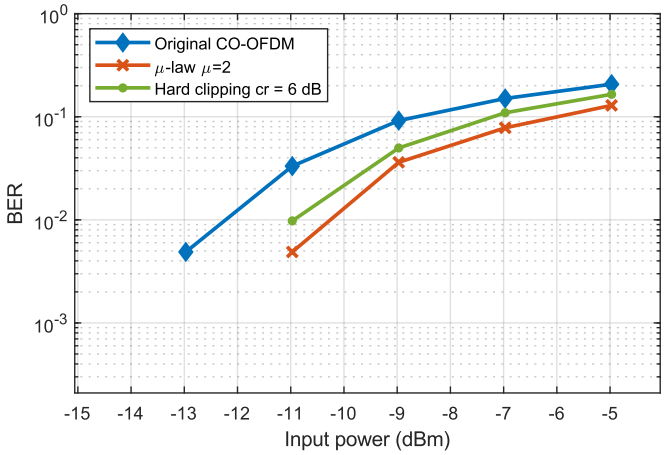

Fig. 1.28 BER versus input power. Nonlinear companding μ-law shows slight improvement with respect to simulated hard clipping method.

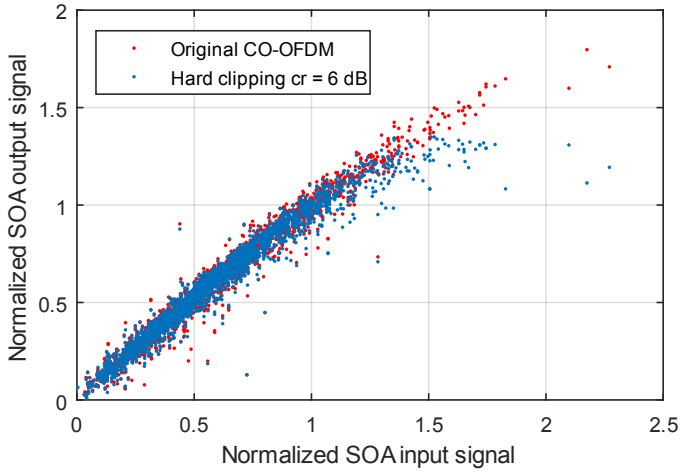

Fig. 1.29 AM/AM for a CO-OFDM with a 5 GHz of electrical baseband bandwidth. Input power of −15 dBm and SOA gain at 15 dB.

the SOA input. Fig. 1.26 shows the probability density function (PDF) of a CO-OFDM signal and its companded form by using μ-law. In Chapter 2 it is briefly explained the theory of some companding methods.

After companding, the IQ-MZM generates the complex optical passband signal [Shieh-10] (see Fig. 1.14 and Fig. 1.17). This signal is fed to the ADS co-simulator for the SOA amplification process through a time domain waveform data file.

As mentioned before, amplification process simulation is made in Keysight ADS software. ADS provides two files as output, corresponding to the real and the imaginary amplified complex

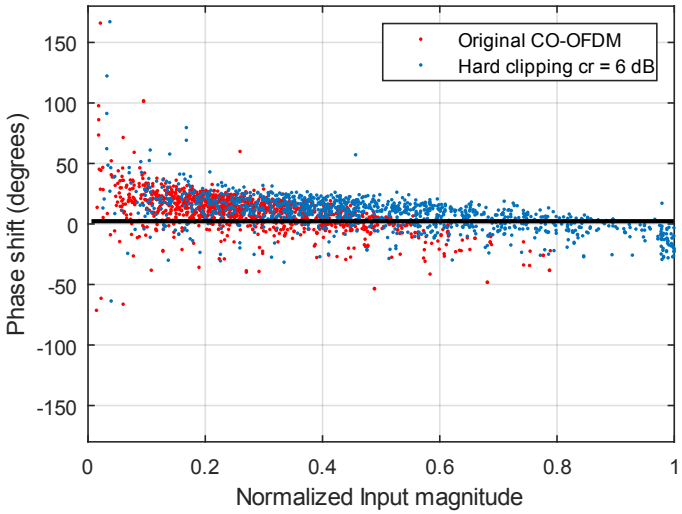

Fig. 1.30 Phase shift as a function of normalized input magnitude hard clipping 6 dB. CO-OFDM system input power −15dBm. SOA gain at 15 dB.

optical signal. As we consider perfect coherent detection, it is not necessary to simulate a particular kind of receiver. Nevertheless, we consider the addition of ASE noise.

The performance assessment of the process is computed by the EVM [Schmogrow-12], which is a measure of how accurately the digital modulated (QAM/PSK) symbols are transmitted within its constellation. Fig. 1.27 shows an example of EVM results for three different companding methods. On the other hand, the bit error rate (BER), the number of bit errors that occur for a given number of bits transmitted, is also provided as a measure of performance, an example is shown in Fig. 1.28.

Also, our simulation platform computes the nonlinear behavior and the memory effects on SOA by plotting the input amplitude to output amplitude (AM/AM) and input amplitude to output phase (AM/PM) on SOA. As an example, Fig. 1.29 shows that, for a SOA input power of −15 dBm, the AM/AM characteristics are not linear when the input amplitude is increased. Likewise, AM/PM measures the amount of undesired phase deviation that is caused by amplitude variations of the system (see Fig. 1.30). In both Fig. 1.29 and Fig. 1.30, it is shown the results comparing a companded signal (hard clipping) versus the original signal. It is clear that, for the hard clipping case, as more scattered points appear, more memory effects are present, due to the companding distortion. Finally, at the end of the simulation process a csv file is saved with key results data, such as output power, SOA gain, EVM, BER, output power, and more variables which can be enabled by the user.

1.7. Conclusions

OFDM has a promising future in optical communications systems, hence it is attractive to search for novel techniques that increase performance, reduce PAPR, and thus prevent nonlinearities in optical power amplifiers OFA and SOA. Because of the low manufacturing cost of SOA compared to other technologies, they are in good position to grow up in the optical networks systems.

Related to PAPR reduction, the nonlinear companding methods exhibit a good performance in terms of low BER with a low computational complexity to be implemented. This opens up new possibilities for research in novel techniques based on improving the properties of nonlinear companding techniques.

A SOA based CO-OFDM simulation platform functionality has been explained in this chapter. Our simulation results show a good fit with experimental data obtained in [Khaleghi-13]. In addition, the proposed simulation platform has flexible features due to its functional blocks structure. These features allow setting up by the user of the transmission characteristics of the signal: modulation type (QAM or PSK), modulation order (4, 16 and more), number of subcarriers, cyclic prefix length, even high BW. The proposed simulation platform also allows to enable or disable different companding and linearization methods, and the user can even add more features to the flexibility given by Matlab coding. A general performance evaluation is included, measuring EVM and BER, as well as other figures of merit such as AM/AM and AM/PM.

The proposed simulation platform has become into an essential tool for our research on the effects of the amplification of CO-OFDM signals through an SOA and for the evaluation of different techniques to improve system's performance.

2. Companding Techniques to Reduce Nonlinearities in Orthogonal Frequency Division Multiplexing Systems

As mentioned in section 1.4, the relative high peak to average power ratio (PAPR) is the cause of signal distortion and nonlinearities in OFDM transmission. Within the whole range of PAPR reduction techniques presented in [Jiang-08], nonlinear companding transform (NCT) techniques are the most effective and easy to implement in terms of computational complexity. The compress OFDM signals at the transmitter and expand them at the receiver [Jiang-08]. In this chapter, a brief review of different companding transforms is illustrated. Also the Wang's NCT (WNCT) [Wang-13] is presented with the advantage of reducing PAPR without increasing the power average in a CO-OFDM signal. Different optimization methods are applied for WNCT, over a wide range of input powers on a SOA based CO-OFDM system. Subsequently, a nonlinear regression function is computed to estimate the optimal companding parameter values depending on the power input average of SOA used as a booster in CO-OFDM system.

2.1. Companding Techniques

Within the whole range of PAPR reduction techniques presented in Chapter 1, companding transform (CT) techniques are the most effective and easy to implement in terms of computational complexity. Basically, CT techniques compresses OFDM signals at the transmitter and expands

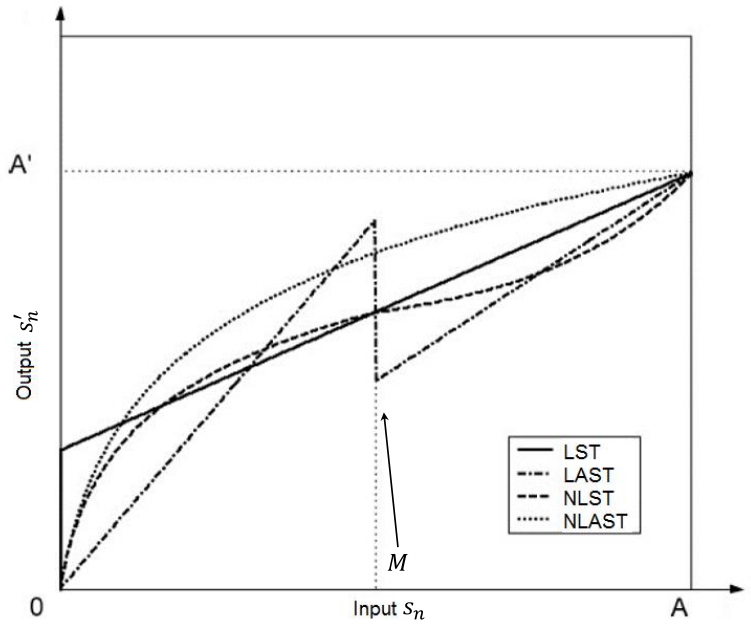

Fig. 2.1 Transform profiles of the four general companding transform classes. Figure taken from [Huang-04].

them at the receiver [Wang-12]. These techniques use the statistical amplitude distribution of OFDM signals to choose the transformation parameters. The companding transform is an extra operation after the modulation of OFDM signals, thus CT schemes reduce PAPR at the expense of generating companding distortion. Hence, it is important for the design of a CT technique to minimize the impact of companding distortion on the bit error rate (BER) performance. By properly choosing transform parameters, CT techniques can achieve a good trade-off between BER performance and PAPR reduction [Hu-14].

Companders can be divided in four types of transforms: linear symmetrical transform (LST), linear asymmetrical transform (LAST), nonlinear symmetrical transform (NLST), and nonlinear asymmetrical transform (NLAST). Fig. 2.1 shows the companding transform profiles of these categories as a graphical relation between the amplitudes of the original input signal s_n and the companded output signal s'_n. Each CT method will be described in the next subsections, with emphasis in nonlinear companding transform (NCT), which have been recently studied for deployment in optical systems, based on Coherent OFDM modulation [Azou-15]. Basically, the optimization method estimates the optimal companding parameter values *c* and k_2, in terms of the minimum EVM when the power input (Pin) is −16dBm.

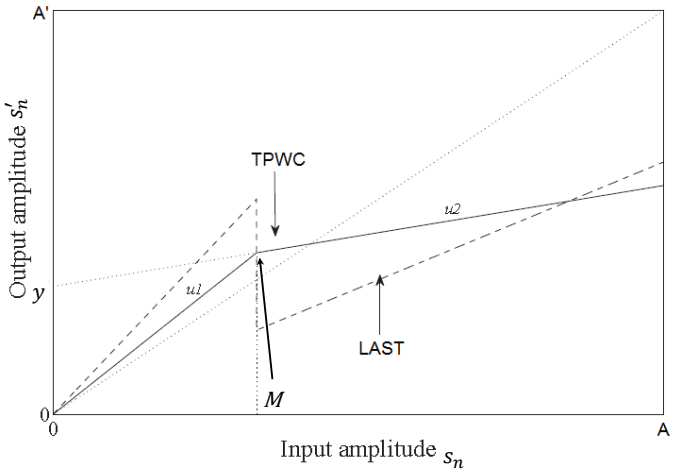

Fig. 2.2 Transform profile of amplitude input and output in TPWC compared with LAST. TPWC has two different slopes defined by u1 for low amplitudes and u2 for high amplitudes. Figure taken from [Yang-11].

2.1.1 Linear Symmetrical Transform

The linear symmetrical transform (LST) is the most basic CT. LST is a simple scaling of the input signal by using a slope equation, as shown below by

$$s'_n = a \cdot s_n + b \cdot \mathrm{sgn}(s_n) \tag{2-1}$$

where s_n is the original signal, s'_n is the companded signal, $0 \le a \le 1$ is the slope parameter, $0 \le b \le A$ is the offset parameter, and A is the maximum peak amplitude value as shown in Fig. 2.1 [Huang-04]. The drawback in LST is the low power efficiency by increasing power average.

2.1.2 Linear Asymmetrical Transform

The opposite method to LST is the linear asymmetrical transform (LAST); it works with large and small amplitudes divided by a cutoff point M. Usually M takes the average amplitude signal value, but it can be greater, in order to control the compression level. The companding transform is defined by a linear piecewise function with two different slopes given by

$$s'_n = \begin{cases} \frac{1}{u} \cdot s_n & |s_n| \le M \\ u \cdot s_n & |s_n| > M \end{cases} \tag{2-2}$$

where the amplitude signal s_n is compressed by using different scales u and 1/u [Huang-04]. Therefore, the transform profile has a linear asymmetrical shape, as shown in Fig. 2.1.

An additional LAST scheme is presented in [Yang-11], named as two piecewise companding transform (TPWC). The TPWC has two different scale factors, $u1$, $u2$, the cutoff point is M, and w is a shift value defined as $w = (u1\text{-}u2)M$. TPWC function is given by

$$s'_n = \begin{cases} u1 \cdot |s_n| \cdot \mathrm{sgn}(s_n) & |s_n| \le M \\ (u2 \cdot |s_n| + w) \cdot \mathrm{sgn}(s_n) & |s_n| > M \end{cases} \tag{2-3}$$

In TPWC the amplitude values below $|s_n| \le M$ are multiplied by $u1$ and the amplitude values greater than $|s_n| > M$ are multiplied by $u1$ but also shifted by w. The cutoff point is selected as $M = y/(u1 - u2)$, with $y > 0$. The resulting transform profile is shown in Fig. 2.2 [Yang-11].

2.1.3 Nonlinear Symmetrical Transform

The nonlinear symmetrical transform (NLST) is another companding scheme that changes the OFDM signal by increasing the low amplitude values and reducing the high amplitude values [Sen-11], as shown in Fig. 2.1. The NLST function consists in two curves defined by a nonlinear piecewise function

$$s'_n = \begin{cases} \mathrm{sgn}(s_n) \cdot \frac{M}{\ln(1+u)} \ln\left(1 + \frac{u}{M} \cdot |s_n|\right) & |s_n| \le M \\ \mathrm{sgn}(s_n) \cdot \frac{u}{v} \left\{ \exp\left[\frac{\ln(1+u)}{v}\right] \cdot |s_n + M \cdot \mathrm{sgn}(s_n)| - 1 \right\} + M \cdot \mathrm{sgn}(s_n) & |s_n| > M \end{cases} \tag{2-4}$$

where the signal is amplified when $|s_n| \le M$ and it is compressed when $|s_n| > M$. The companding parameters are $u > 0$ and $0 < v \le A - M$, where M is the inflexion point and A is the peak amplitude of s_n. NLST transform profile has a symmetrical distribution with respect to the inflexion point M, as shown in Fig. 2.1.

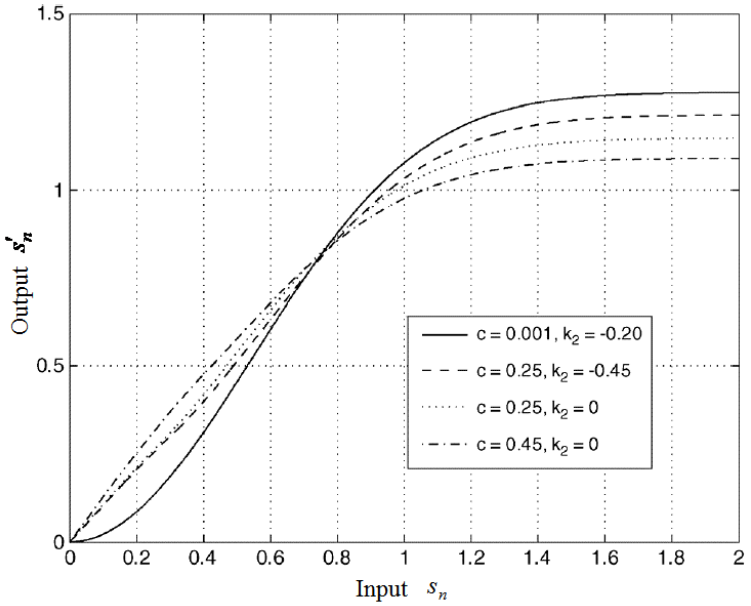

Fig. 2.3 Wang NLAST transform profiles with different values of companding parameters c and k_2, for controlling the PAPR reduction. Figure taken from [Wang-13].

2.1.4 Nonlinear Asymmetrical Transforms

The nonlinear companding approaches can be presented also as a nonlinear asymmetrical transform (NLAST), where the transform profile has an asymmetrical shape, as showed in [Huang-04]. The first nonlinear companding transform is the μ-law. The μ-law belongs to the NLAST. It works compressing large signals and enlarging small ones, with the drawback of increasing the average power of the transmitted signal [Huang-04]. The μ-law is given by

$$s'_n = \operatorname{sgn}(s_n) \cdot \frac{A}{\ln(1+\mu)} \ln\left(1 + \frac{\mu}{A}|s_n|\right) \tag{2-5}$$

where μ is the companding parameter and A is the maximum absolute value of the amplitude signal s_n.

Also, several NLAST methods have been proposed, e.g., exponential companding (EC). EC works by keeping the same average power as that one of the original signal, and significantly less impact on the original power spectrum comparing to the μ-law. Large and small signals can keep the average power at the same level [Jiang-05]. The EC is given by

$$s'_n = \mathrm{sgn}(s_n) \cdot \sqrt[d]{\alpha\left(1+\exp\left(-\frac{|s_n|^2}{\sigma^2}\right)\right)} \tag{2-6}$$

where α is a positive value to keep constant the average power, σ^2 is the average signal power, and d is the nonlinear companding parameter.

Another NLAST is presented in [Wang-13] and it is expressed as a piecewise function. The Wang nonlinear companding transform (WNCT) proposes to modify the statistics of the amplitude, defined by using its PDF, as a reference to select the companding parameter values. The companding function is given by

$$s'_n = \begin{cases} \mathrm{sgn}(s_n)\sqrt{\dfrac{2}{k_1}\left(1-\exp\left(-\dfrac{|s_n|^2}{\sigma^2}\right)\right)} & |s_n| \le M \\ \mathrm{sgn}(s_n)\dfrac{1}{k_2}\left((k_2-k_1)c\cdot D+\sqrt{(k_2-k_1)k_1c^2D^2+2k_2\left(1-\exp\left(-\dfrac{|s_n|^2}{\sigma^2}\right)\right)}\right) & |s_n| > M \end{cases} \tag{2-7}$$

where k_1, k_2 and c ($0 < c < 1$) are the companding parameters, $M = \sigma\left(-\ln\left(1-(k_1/2)\cdot c^2\cdot D^2\right)\right)^{1/2}$ is the inflexion point, and D ($D > 0$) is the cutoff point on the transforming profile. Different transforming profiles are illustrated in Fig. 2.3.

The correct choice of the companding parameters values is very important in order to avoid companding distortion at the output signal. Because of this, an efficient design of Wang NLAST has been proposed in [Azou-15] by using global optimization and a genetic algorithm, in order to find the optimal companding parameters.

2.2. Techniques in Non-Linear Asymmetrical Transforms

Recently, effective companders have been designed by modification of the signal amplitude distribution with nonlinear asymmetrical transform profiles [del Marco-14], [Hu-14], [Jeng-11]. Compared to other CT techniques, these NLAST approaches provide less companding distortion, more degrees of freedom to choose the optimal companding parameters, and good tradeoff between BER and PAPR reduction. This Section presents some new CT techniques with focus on the nonlinear asymmetrical transform and a brief explanation of their companding parameters.

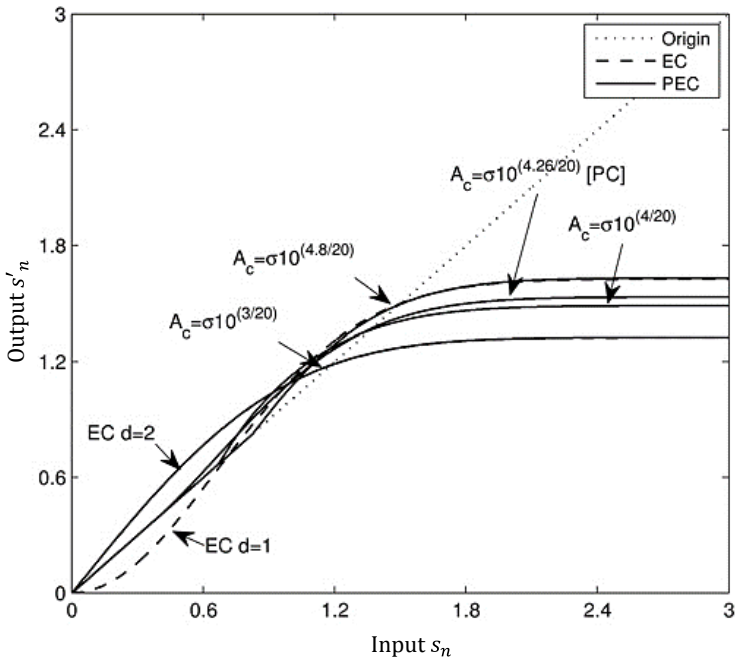

Fig. 2.4 PEC transform profiles with different values of companding parameters and EC technique. Figure taken from [Hu-14].

2.2.1 Piecewise Exponential Companding

The Piecewise Exponential Companding (PEC) is a NLAST scheme based on the EC and TPWC schemes. PEC transforms the small and large signals differently, changing the distribution of the large signals into an exponential distribution, by using.

$$s'_n = \begin{cases} s_n & |s_n| \le M \\ \mathrm{sgn}(s_n)\left(\left(M^d - A_c^d\right)\exp^{-\left(|s_n|^2 - M^2\right)/\sigma^2} + A_c^d\right)^{(1/d)} & |s_n| > M \end{cases} \quad (2\text{-}8)$$

where σ^2 is the variance of s_n, M is the cutoff point, the linear and nonlinear companding parameters A_c and d, respectively, give more flexibility to achieve a higher PAPR reduction level than Wang NLAST [Hu-14]. Some transform profiles of the PEC with different values of companding parameters are shown in Fig. 2.4.

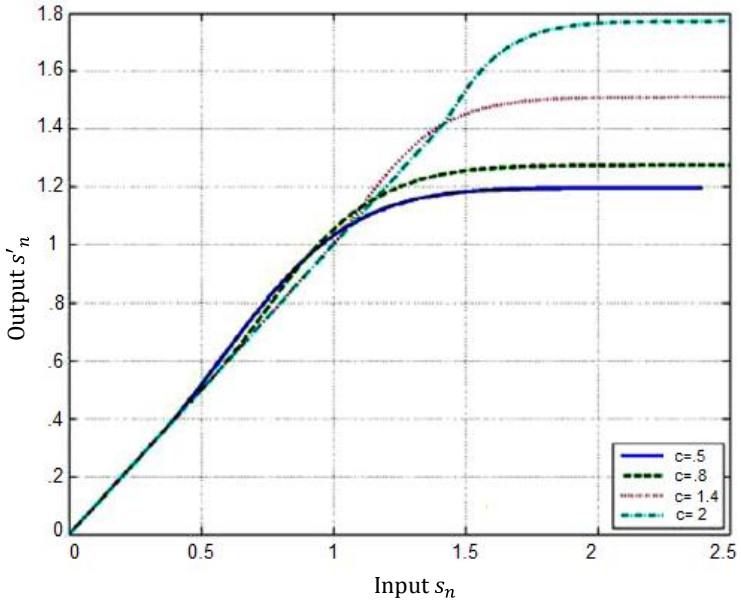

Fig. 2.5 Del Marco NLAST transform profile. The companding parameter c controls the grade of signal compression. Figure taken from [del Marco-14].

2.2.2 Del Marco Family of Companders

A different NLAST is presented in [del Marco-14]. This transform function generalizes the piecewise amplitude distribution modification approach to a compander design by defining a family of closed form companders. This technique is also named inverse square root (ISQR). The companding function uses the appropriate values for α, e, and δ, given the initial point $M = c\sigma$,

$$s'_n = \operatorname{sgn}(s_n)\begin{cases} s_n & |s_n| \le M \\ \left(\dfrac{\sqrt{1-e^{-\frac{|s_n|^2}{\sigma^2}}}-\delta-e}{\alpha}\right)^2 & |s_n| > M \end{cases} \tag{2-9}$$

where α, β, e, and δ denote, respectively, argument scaling, argument translation, and ordinate translation parameters. In addition, c is the companding parameter and σ is the expectation value of s_n. The transform profile is shown in Fig. 2.5.

This companding transform provides solutions over regions of the operating conditions space where other modern companders fail to exist. In fact, by tolerating more PAPR it provides lower demodulation errors and better out-of-band power rejection.

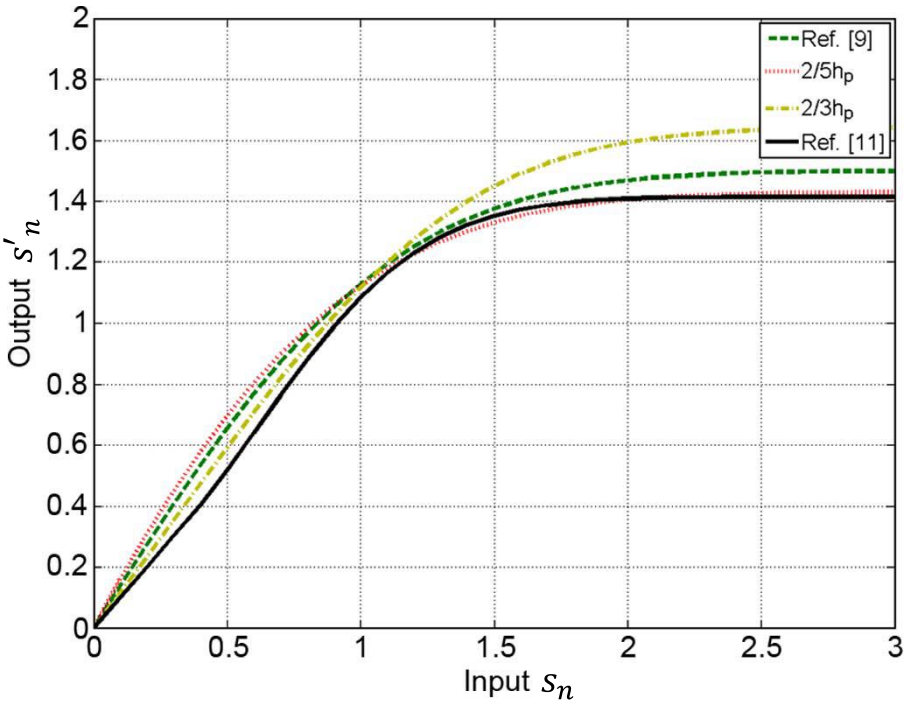

Fig. 2.6 Transform profiles of the Trapezium CT adjusted to 2/5 h_p, 2/3 h_p and compared to other references. Figure taken from [Jeng-11].

2.2.3 Trapezium Distribution

In [Jeng-11] it is proposed a NLAST to convert the original OFDM signal into the trapezium distribution by regulating a governing parameter. The companding function is a continuous function. This scheme can achieve a good trade-off between the BER performance and PAPR reduction by adjusting the value of q, i.e. $a = q/h_p$. Its mathematical expression is

$$s'_n = \frac{\sqrt{6}}{1-2q}\left(\sqrt{\frac{\sigma^2}{3-2q}\left(q^2 + \left(1-2q^2\right)\cdot \mathrm{erf}\left(\frac{y}{2\sigma^2}\right)\right)} - q\sqrt{\frac{\sigma^2}{3-2q}}\right)\cdot \exp\left(j\cdot \arg(s_n)\right) \quad (2\text{-}10)$$

where a is used to specify the forms of the trapezium distribution, $0 \le a \le 1/h_p$, and h_p is the upper-bound of the proposed scheme. The transforming profile of the proposed scheme is varied by adjusting a, as shown in Fig. 2.6.

The proposed scheme may offer a more efficient PAPR reduction or a lower BER than the uniformly-distributed EC and piecewise schemes TPWC by varying the parameter a.

2.3. On Nonlinear Companding Optimization over a SOA-Based CO-OFDM System

In this section, a comparative of optimization methods, is presented, to identify which optimization method is more efficient to find the WNCT optimal parameters that yield minimum EVM and low computational time. Then, a nonlinear regression model is applied, which describes the optimal WNCT parameters behavior when changing input power P_{in}. Additionally, these nonlinear regression functions are used to compare the EVM performance of SOA based CO-OFDM system using optimal WNCT parameters against other optimization algorithms.

2.3.1 WNCT Optimization Process

As mentioned before, a first approach to optimize the WNCT parameters is presented in [Azou-15] using a hybrid function in the optimization method. The hybrid function works with a genetic algorithm (GA) to allocate a global minimum and then a gradient-based method (Matlab command fmincon) to find local minima. The resulting optimal values are c = 0.43 k_2 = –0.25. That study was done with our simulator platform (see Section 1.6). EVM is used to evaluate the reduction of nonlinearities using the optimal values in the SOA-based CO-OFDM system, among a wide input power range.

2.3.1.1 Hybrid Optimization Over a Wide Range of Input Power

Here, we use the same hybrid approach (GA-fmincon) and co-simulation system as stated in [Azou-14]. The main idea is to obtain a set of optimal WNCT parameter values of c and k_2 over a wide operation range of P_{in} in a SOA-based CO-OFDM system, and not only for one P_{in} value as it was the case. In a first experiment, we set up the optimization algorithm at larger P_{in} values, from –29 dBm to –6 dBm using 24 trial points with 1 dBm per trial interval. The range of P_{in} values covers the linear and nonlinear work region of SOA. We use this set of optimal values, in the co-simulation system to evaluate the reduction of nonlinearities in the CO-OFDM system.

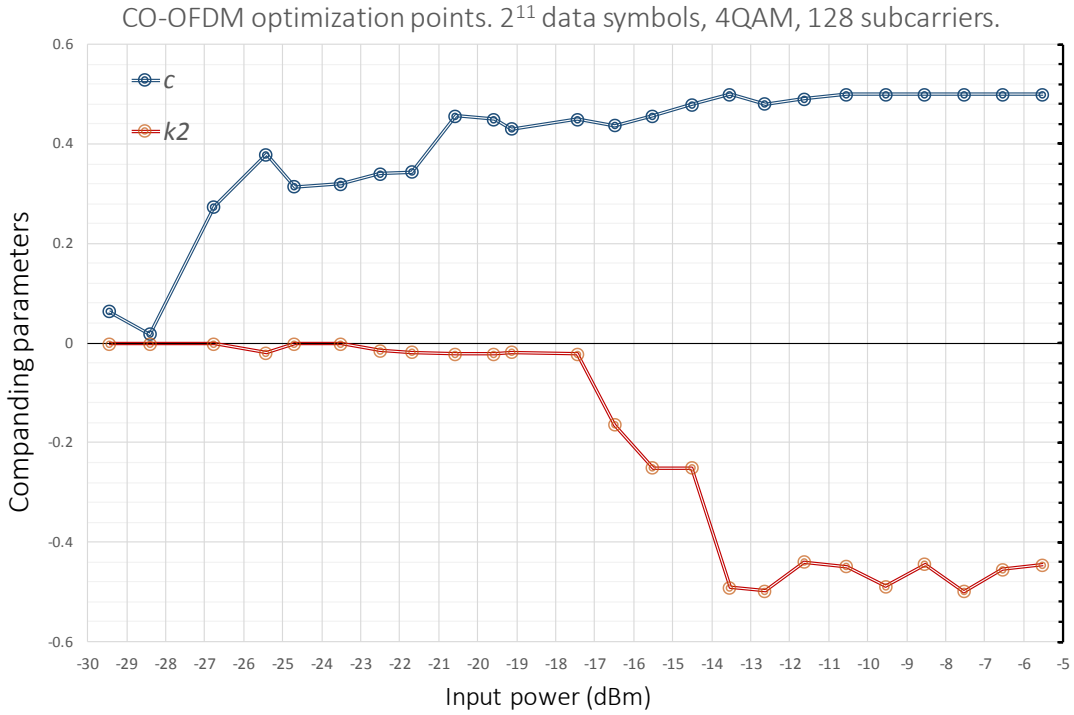

Fig. 2.7 Optimal WNCT parameters c and k_2 by the GA-fmincon approach. The elapsed time for all the optimization process was 192 hrs.

2.3.1.2 Comparison of Optimization Methods

In the aforementioned experiment we use a gradient based method (fmincon) which is not efficient in discontinuous problems such as stochastic process [Deb-01], as it is the case for the CO-OFDM signals. For this reason, we explore other optimization algorithms. In a second experiment, we tried some gradient-free global optimization algorithms included in a typical global optimization software in order to find the most consistent result between the computational time and minimum optimal EVM. The experiment used the same P_{in} as in [Azou-14].

2.3.1.3 Pattern Search Over a Wide Range of Input Power

In a third experiment, we configure a pattern search (PS) optimization algorithm to work in parallel computing to save computational time in the optimization process. Thus, we set up the search of optimal WNCT parameter for several power input values using 97 trial points, from –32 dBm to –7.5 dBm. Hence, we apply a nonlinear regression model to obtain a function which will

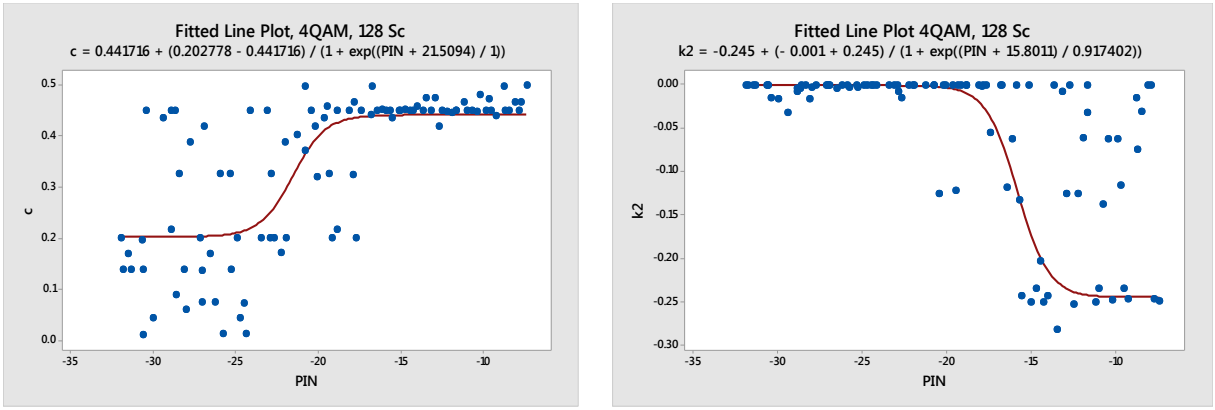

a) b)

Fig. 2.8 Optimized values of WNCT parameters c and k_2 by using pattern search algorithm and nonlinear regression curves. WNCT parameters c and k_2 have inverse behavior, c is affected for noisy signal at lower input power, and k_2 shows variability to find the optimal values at high input power.

be used to estimate the optimal companding parameters c and k_2 as a function of P_{in}. In the following section we will draw the results of each experiment.

2.3.2 Numerical Results

As a result of the application of the hybrid approach GA-fmincon, we obtained a set of optimal WNCT parameter values of c and k_2 over an operational work-range of SOA (shown in Fig. 2.7). The elapsed time for all the optimization process consumed a lot of computational time (around 192 hours). At the final experiment we tested the effectiveness of this optimal values by comparing with those obtained by the third experiment using PS algorithm. Regarding the second experiment, the optimization results are shown in Table 2.1, where the PS algorithm has the best relation between elapsed time and minimal EVM found.

In addition, according to the results on the third experiment, shown in Fig. 2.8, the behavior of c parameter attempts to reach its upper bound when P_{in} increases and presents non-stable results due to the high presence of noise in the low P_{in} CO-OFDM signal. The behavior corresponding to k_2 (shown Fig. 2.8 b)) is stable in the linear region and it tends to decrease in the saturation regime. The optimal data for c and k_2 have an exponential response similar to the logistic growth function. For this reason, we used that function for obtaining a nonlinear regression model. The nonlinear regression functions for c and k_2 are:

TABLE 2.1. OPTIMIZATION METHODS COMPARATIVE

128 Subcarriers, 4 QAM, 2^{11} QAM Symbols, $P_{\text{in}} \cong 16$ dBm

Optimization Methods	c	k_2	EVM %	Number of generations	Total evaluated functions	Elapsed time (hrs.)
Hybrid GA & Pattern Search	0.3792	–0.025	10.62	10	320	8.6
Pattern Search	0.3250	–0.001	10.3	NA	63	1.7
Fminsearch	0.4725	–0.001	10.25	NA	201	5.4
Hybrid GA & Fminsearch	0.3121	–0.120	10.42	10	320	8.7
Hybrid GA & FminCon	0.4075	–0.212	10.61	10	281	7.5

$$c = \frac{0.4417 + (0.2027 - 0.4417)}{1 + e^{(P_{\text{in}} + 21.5)}} \tag{2-11}$$

and

$$k_2 = \frac{0.245 + (-0.001 + 0.245)}{1 + e^{\left(\frac{P_{\text{in}} + 15.8}{0.917}\right)}} \tag{2-12}$$

where P_{in} is the average SOA input power.

Both (2-11) and (2-12) are used to estimate in an adaptive way the optimal values of c and k_2 parameters for different P_{in}. This adaptive approach allows to reduce the EVM by adjusting the WNCT parameters according to the estimated P_{in}.

Finally, we evaluate the presence of nonlinear distortions in the SOA-based CO-OFDM system. EVM degradation is used as a measurement of nonlinear distortion. Fig. 2.9 shows the EVM curves using WNCT with optimized values by using hybrid approach GA-fmincon, nonlinear regression model PS, constant optimal WNCT parameter, and the OFDM signal with no companding. From that figure, it is seen that WNCT using (2-11) and (2-12) shows better performance to reduce EVM in the range from –20dBm to –16dBm. However, the main advantage of using PS optimization method is the lower computational time.

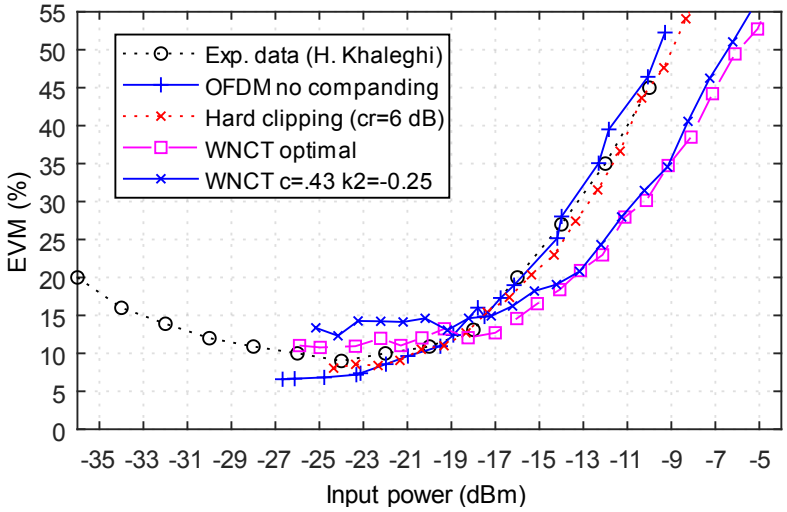

Fig. 2.9 Comparative of WNCT optimization by using Pattern Search, GA-fmincon and constant values $c = 0.43$ and $k_2 = -0.25$. Here we can see a slight improvement when using the nonlinear regression function obtained from pattern search optimal values.

2.4. Conclusions

Nonlinear companding is an extra operation in an OFDM system that introduces pre-distortion to the transmitted signal. This is a disadvantage as compared to other techniques. Hence, companding parameters calculation is a very important task in order to reduce the impact of companding distortion. Additionally, being OFDM an appropriate modulation technique for optical communication, it is necessary to look for new companding schemes, adapted to optical OFDM, to afford the reduction of nonlinear effects in optical components, such as optical amplifiers, optical modulators, and optical fibers.

The optimization process over WNCT has been done comparing different optimization methods. As shown in Table 2.1, pattern search algorithm, based on a gradient-free search method, was faster to find the optimal WNCT parameters than the hybrid algorithms based on genetic algorithms and gradient search method. A nonlinear regression function for each WNCT parameter was presented and used to estimate the value parameters according to the input power. Finally, the EVM curves obtained show slight improvements in the SOA-based CO-OFDM system when the nonlinear regression functions were used.

3. Characterization of the Bias Current Behavior in a SOA for Linearizing Amplification in a CO-OFDM System

As stated in Section 1.3, SOA is driven by its bias current injection, which controls the amplification level. It is well known that SOA is prone to nonlinear distortion when high input power is used at high gain level, due to the gain saturation. These nonlinearities can cause problems, such as frequency chirping and generation of inter-modulation products. One way to avoid these undesirable effects, is to regulate the bias current (I_{bias}) to control de SOA amplification, in order to avoid SOA gain saturation. This chapter presents an analysis of a SOA based CO-OFDM system, when it is used as a booster power amplifier, mapping the system response as a function of the bias current and input power. In addition, three operation scenarios have been presented, so as to characterize the performance of the system and obtain a way to optimize the SOA performance, under each scenario, controlling the bias current. To achieve our goal, we use a simulation system based presented in Section 1.6. The transmission quality link is evaluated by computing the EVM [Schmogrow-12].

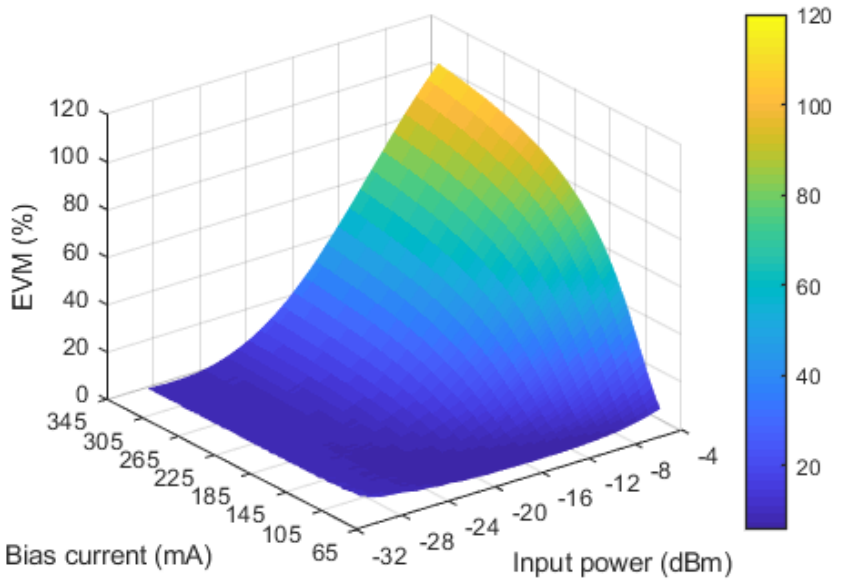

Fig. 3.1 EVM as a function of input power and bias current in CO-OFDM system with SOA as booster amplifier. EVM increases exponentially when SOA amplification is biasing with high current at high input power level.

3.1. Bias Current Change on SOA

As mentioned before , we simulate a back-to-back CO-OFDM transmission, using the SOA as a booster amplifier, as seen in Section 1.6, Fig. 1.14. The system was simulated with 128 subcarriers, 4 QAM baseband modulation, electrical bandwidth of 5 GHz, and an oversampling factor $os = 4$, adding 1/8 cyclic prefix, and an optional companding block to reduce peak to average power ratio (and their decompanding block). The objective of the simulation is to characterize the impact of the bias current on three main aspects of SOA behavior as a power booster within a CO-OFDM system: EVM, P_{out}, and SOA gain. All of this under different conditions of the input power. To achieve this goal, we measured the aforementioned variables for a range of different input powers, from –31 dBm to –6 dBm, in steps of 1 dBm. For each test point, we vary the bias current from 65 mA to 315 mA in intervals of 1 mA. This gives a total of 6,526 tests. These values have been chosen in order to include the linear and nonlinear SOA operation work region.

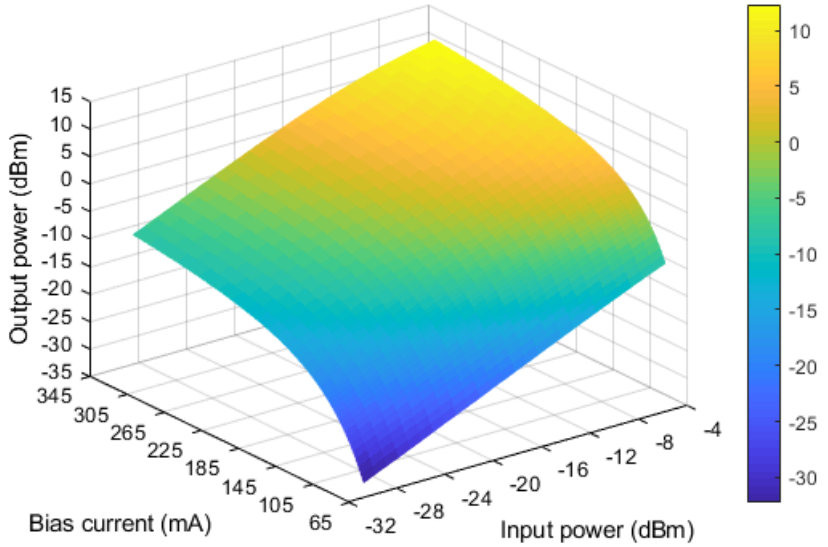

Fig. 3.2 SOA output power versus bias current and input power. Given this results we could find the bias current set up to get certain output power.

3.1.1 EVM as a Function of P_{in} and I_{bias}

First, we run simulations to obtain the behavior of the EVM for variations of the bias current and the input power. Fig. 3.2 shows graphically the results, where we can observe the EVM variation with respect to input power and bias current. It is seen that EVM rises rapidly for high values of I_{bias} and P_{in}. For instance, the system can get up to 40% EVM for a P_{in} equal to −16 dBm aimed at I_{bias} of 345 mA.

3.1.2 P_{out} as a Function of P_{in} and I_{bias}

The simulations for obtaining the behavior of the output power, P_{out}, in terms of the bias current and the input power, produced the results shown in Fig. 3.2. As it is known [Saleh-88], the amplifier output power level, for a specific input power value, can be controlled by selecting the right bias current. As a reference in our study, for an input power of −16 dBm, the amplifier produces around 0 dBm at its output for an EVM of 40% when using an I_{bias} of 345 mA. Fig. 3.1 and Fig. 3.2 provide a useful broad view of the SOA behavior.

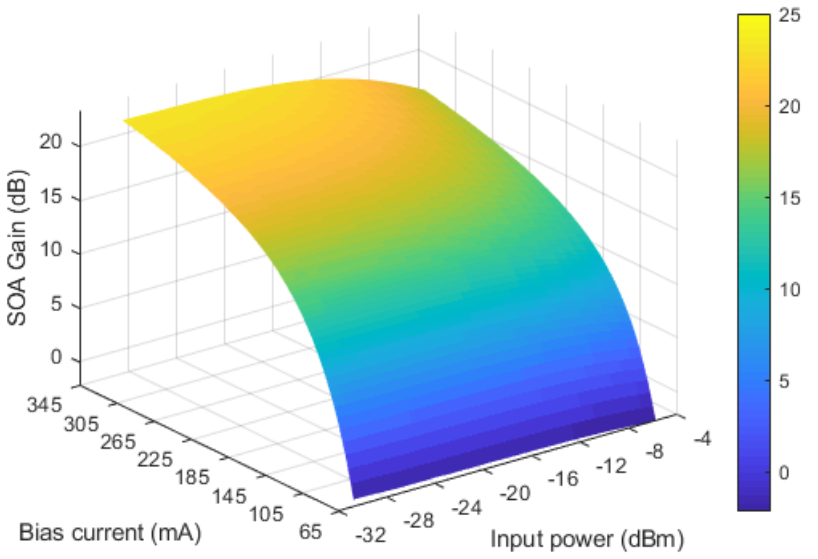

Fig. 3.3 SOA gain as a function of bias current and input power. A gain attenuation is observed at high input power, even if bias current slightly increases.

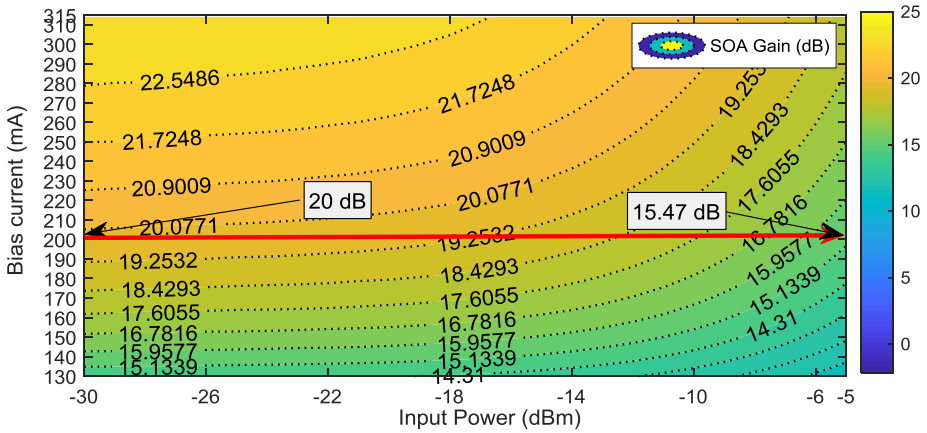

Fig. 3.4 SOA gain curves as a function of bias current and input power. Red line shows 4.5 dB of attenuation gain, if the SOA is biased by 200 mA.

3.1.3 Gain as a Function of P_{in} and I_{bias}

The Fig. 3.3 illustrates the behavior of the SOA gain with respect to input power and bias current. We can clearly see the direct dependence of SOA gain with respect to the bias current. Here, the maximum gain is obtained for low input powers. For example, the amplifier's gain is 22 dB for an input power of −28 dBm using an I_{bias} of 345 mA. On the contrary, there is a reduction

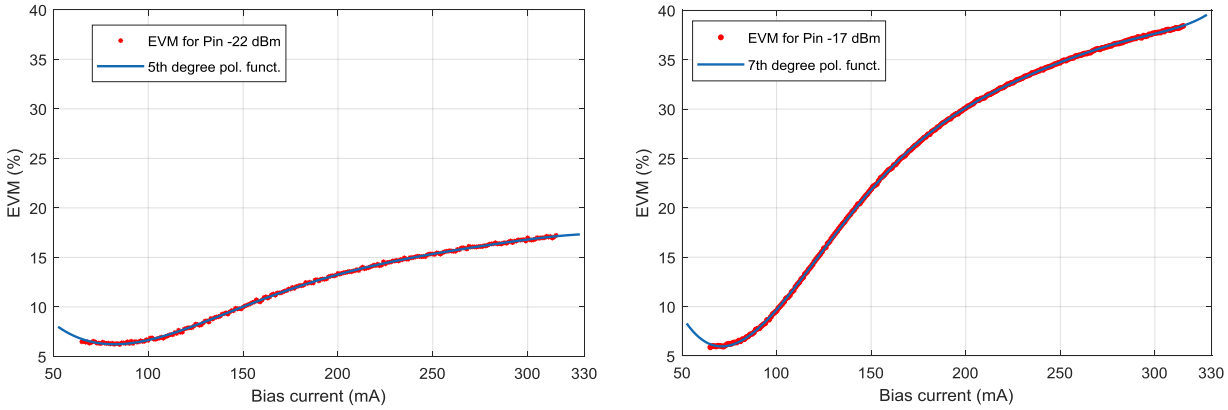

a) b)

Fig. 3.5 EVM values (red dots) as a function of SOA bias current and their polynomial approximation for two different input powers: a) –22 dBm, b) –17 dBm.

of the gain for high input powers even if the bias current slightly increases.

Gain contour plots or level curves as a function of bias current and input power are shown in Fig. 3.4. It is clearer the gain reduction as the input power increases for a constant bias current. For instance, the red line in Fig. 3.4 shows the gain attenuation when SOA is biased by 206 mA: at $P_{in} = -31$ dBm gain is 20.1 dB; at $P_{in} = -5$ dBm gain is 15.47 dB.

3.1.4 Bias Current for Minimum EVM

We are interested in characterizing the behavior of the SOA under certain conditions. One condition is to obtain the minimum possible EVM regardless of the value of the input power. We want to know what bias current to use to achieve this.

We can get a model from the EVM behavior obtained in Section 3.1.1, for each input power value. As an example, Fig. 3.5 shows the curves of the EVM as a function of bias current for two different input powers: –22 dBm (Fig. 3.5a) and –17 dBm (Fig. 3.5b). Using a MATLAB fitting function, we obtain the following two polynomials for –22 dBm and –17 dBm, respectively:

$$EVM(I_{bias}) = -0.13{I_{bias}}^5 + 0.4{I_{bias}}^4 + 1.3\times10^{-4}{I_{bias}}^3 - 1.4{I_{bias}}^2 + 4.2I_{bias} + 18.5 \qquad (3\text{-}1)$$

and

$$EVM(I_{bias}) = -0.7{I_{bias}}^7 + 0.14{I_{bias}}^6 - 0.9{I_{bias}}^5 + 0.4{I_{bias}}^4 + 2{I_{bias}}^3 - 4.7{I_{bias}}^2 + 9.7I_{bias} + 28.6 \qquad (3\text{-}2)$$

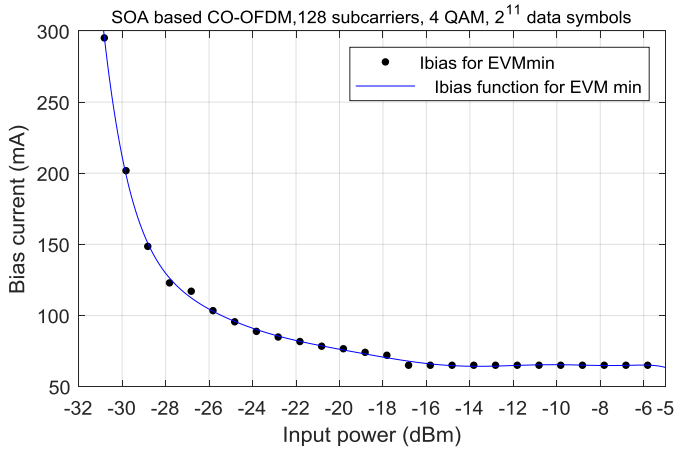

Fig. 3.6 Model to estimate the bias current I_{bias} to obtain the minimum EVM as a function of P_{in} (blue curve). This model results from a linear regression of EVM minimum values (black dots) obtained from (3-3).

The next step to obtain a model for all input powers (-31 dBm $< P_{in} < -6$ dBm), is to search for the minimum EVM of each single-variable polynomial function in a constrained region for I_{bias}, as follows:

$$\arg\min_{I_{bias}} EVM(I_{bias}) \qquad 65\,mA \le I_{bias} \le 315\,mA \tag{3-3}$$

Next, we apply linear regression to obtain the following model:

$$\begin{aligned} I_{bias} = \; & -2.6P_{in}{}^{9} + 4.9P_{in}{}^{8} + 9.5P_{in}{}^{7} - 15P_{in}{}^{6} - 18P_{in}{}^{5} \\ & + 18.5P_{in}{}^{4} + 12.2P_{in}{}^{3} + 4.7P_{in}{}^{2} - 20.5P_{in} + 71.59 \end{aligned} \tag{3-4}$$

Model (3-4) allows estimating the bias current needed to obtain the minimum EVM for a given P_{in}, where P_{in} is normalized by a mean value of -18.32, a standard deviation of 7.649, and coefficients with 95% of confidence bounds. The curve of such a model is shown in Fig. 3.6.

We run a test in the simulator of the CO-OFDM system using model (3-4). We introduced a signal with different input powers; for each input power we used a different bias current, obtained from (3-4), and we computed the EVM of the received signal. Fig. 3.8 shows the results for two cases: variable I_{bias} and fixed I_{bias} at 150 mA. It is confirmed that the second case makes the SOA based CO-OFDM system to exhibit a high EVM degradation.

The observation of our simulation results shown in Fig. 3.8, Fig. 3.7 and Fig. 3.9 allows us find that the cost of minimizing the EVM consists of forcing a decrease in output power, originated by reducing the SOA gain. This is expected, since the decrease in current reduces the gain of the amplifier. Both behaviors are shown in Fig. 3.7 and Fig. 3.9. This model allows us to know exactly

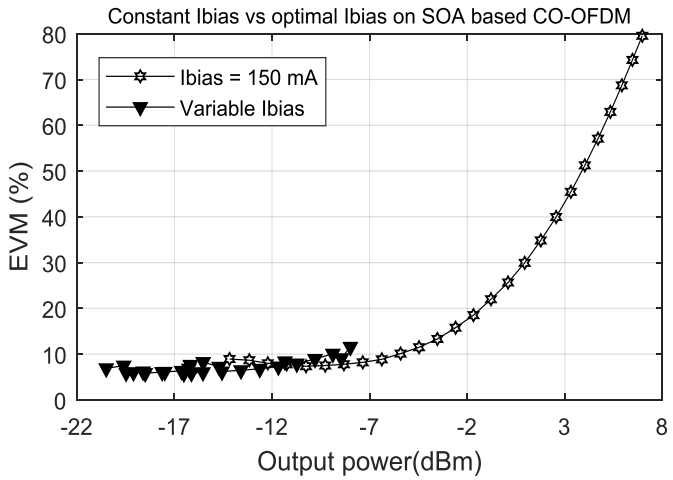

Fig. 3.7 EVM as a function of SOA output power, when SOA amplification is driven by a constant bias current (hexagram curve) and when a variable bias current is applied to SOA to obtain a minimum EVM (triangle curve) per test point. It is seen that, when variable bias current model (3-4) is applied, EVM can be minimized at the cost of keeping a low SOA output power.

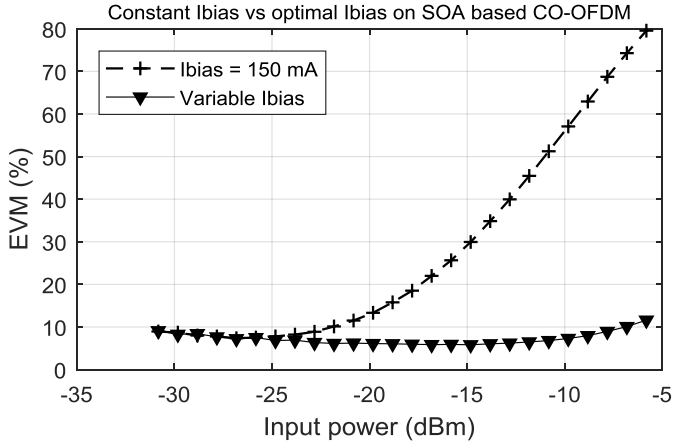

Fig. 3.8 EVM as a function of P_{in} applying a variable bias current corresponding to each power level to obtain minimum error, using model (3-4), as compared with a fixed bias current at 150 mA. It is confirmed that the second case drives the SOA based CO-OFDM system to a high EVM degradation.

how the amplifier behaves when controlling the bias current to achieve the smallest EVM depending on the input power. It is seen from Fig. 3.9 that forcing a minimal EVM by controlling I_{bias} drives the SOA to a gain depletion and output power attenuation. This situation indicates that a good profile of I_{bias} to get a sufficient gain with a certain acceptable level of distortion at the receiver (EVM) is needed.

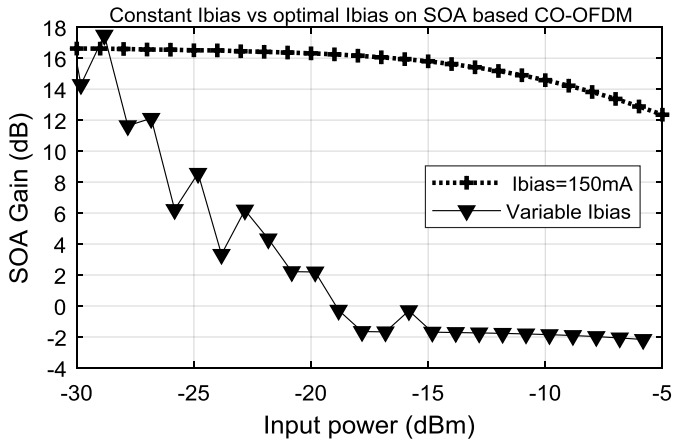

Fig. 3.9 SOA gain versus input power Pin. Gain depletion is presented by I_{bias} gradual reduction, driving the CO-OFDM system to null amplification and attenuation above Pin = –18 dBm.

3.2. Impact of Bias Current on SOA Performance

From the previous results, it is clear that it is necessary to find a good trade-off between EVM and P_{out} to have a good operational level in amplification terms. Therefore, we propose three different profile behaviors to analyze the impact of the bias current on the SOA.

The first profile is obtained under the condition of keeping the EVM at a maximum of 20%. The second profile consists of preserving a constant P_{out} equal to −7 dBm. The third profile corresponds to a constant gain of 17 dB over the whole P_{in} range.

We search in the results obtained in Section 3.1 (EVM, P_{out}, SOA gain) for the specific values of I_{bias}, for each value of P_{in}, that fit the conditions of each of the aforementioned profiles. From these values, we develop a linear regression model to get I_{bias} as a function of P_{in}, to control de SOA amplification according to the three desired profiles.

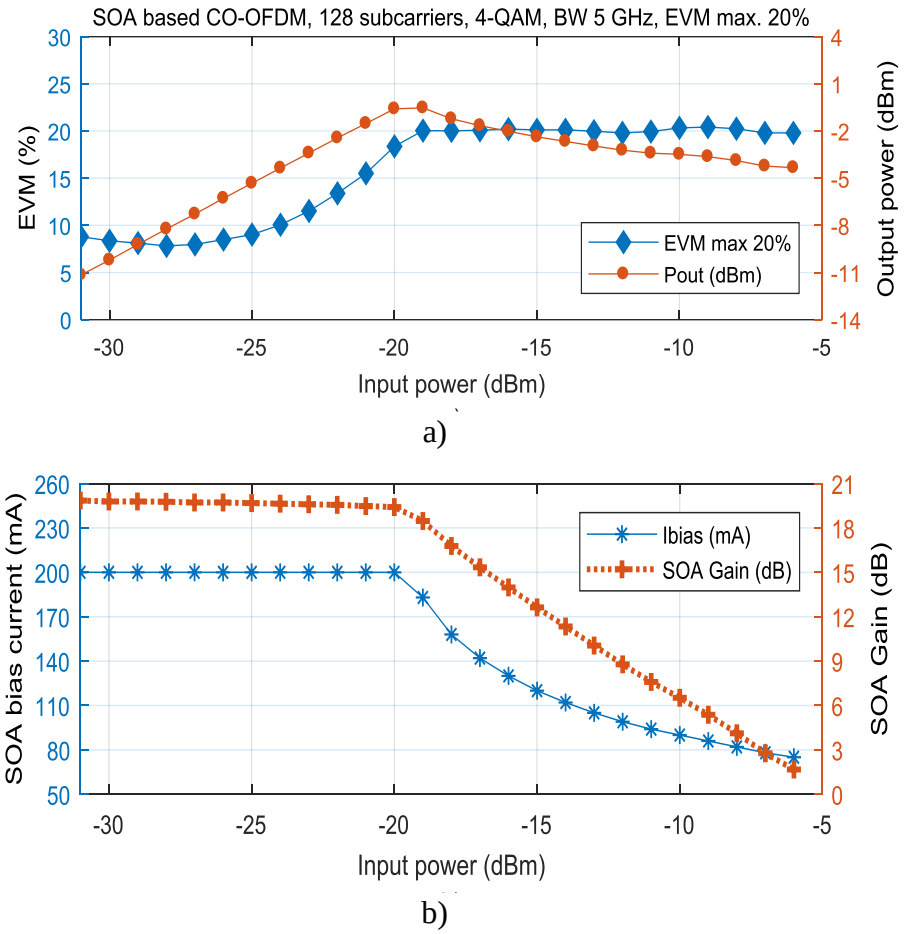

Fig. 3.10 Analysis of first approach to control I_{bias} injection on SOA for EVM < 20%, varying input power: a) EVM and P_{out}, b) I_{bias} and SOA gain.

3.2.1 Maximum EVM equal to 20%

According to the results shown in Fig. 3.1, for EVM as a function of I_{bias} and P_{in}, we observe that EVM is relatively low, EVM < 20%, in the region $P_{in} < -19$ dBm. We define an I_{bias} equal to 200 mA to obtain a SOA gain of 20 dB with low EVM. On the other hand, for high input power, $P_{in} > -19$ dBm, which is the SOA nonlinear region, we define an EVM threshold of 20%, gradually decreasing I_{bias} to keep the EVM equal to 20% for -19 dBm < $P_{in} < -6$ dBm.

The results are shown in Fig. 3.10. We observe that P_{out} decreases as a consequence of I_{bias} reduction. Also, we can observe the SOA gain attenuation in accordance with the I_{bias} decrease.

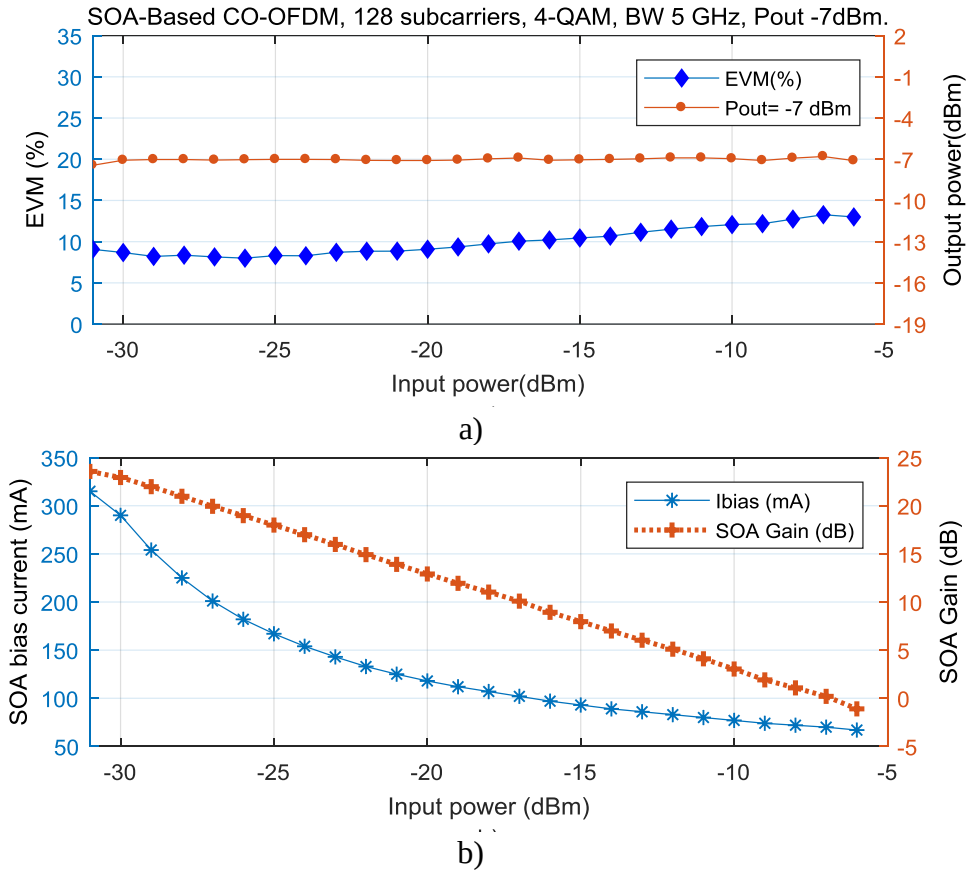

Fig. 3.11 Analysis of second approach to control I_{bias} for P_{out} = –7 dBm: a) EVM and P_{out} keep quasi-linear and almost constant, b) I_{bias} and SOA gain, with nonlinear and linear decrement, respectively.

Moreover, SOA gain decreases linearly as we increase input power, while I_{bias} decreases nonlinearly.

We compute from the I_{bias} current points a linear regression to get an I_{bias} model. Given the complexity of the I_{bias} behavior, we use a rational function model, obtaining:

$$I_{bias} = \frac{-2.8P_{in}^{5} - 145.8P_{in}^{4} - 1282P_{in}^{3} + 5.7\times10^{4}P_{in}^{2} + 1.4\times10^{6}P_{in} + 9.6\times10^{6}}{P_{in}^{4} + 77.2P_{in}^{3} + 2297P_{in}^{2} - 3.1\times10^{4}P_{in} + 1.6\times10^{5}} \quad (3\text{-}5)$$

3.2.2 Output Power set up to –7 dBm

Based on the results shown in Fig. 3.2, for P_{out} as a function of I_{bias} and P_{in}, we search for the bias current values to get P_{out} equal to –7 dBm all along the P_{in} range (from –31 dBm to –6

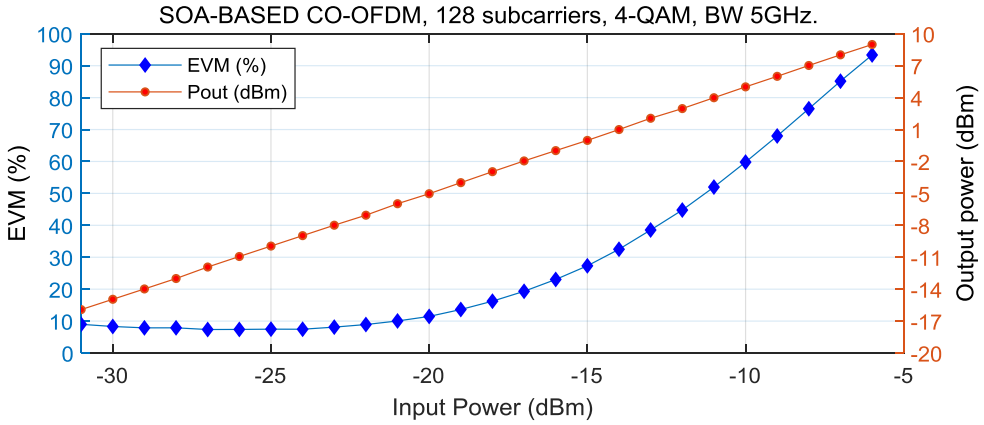

a)

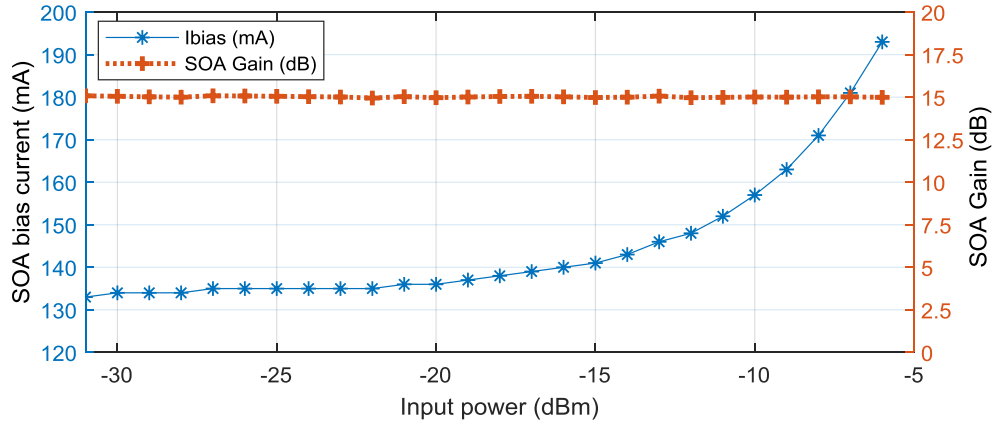

b)

Fig. 3.12 Analysis of third approach, keeping SOA gain of 15 dB: a) EVM and P_{out} as a function of P_{in}; b) bias current for a constant SOA gain of 15 dB across the SOA input power range.

dBm). The results are shown in Fig. 3.11a, where we can observe that EVM has values below 15%, even in high P_{in} values. Both EVM and P_{out} show a quasi-linear response. In addition, Fig. 3.11b shows that SOA gain has a linear decrement with input power; this effect reduces SOA gain saturation and, therefore, EVM is low. This condition could be a drawback in the case where we need to have a high gain for a P_{in} above −19 dBm.

The resultant I_{bias} behavior is modeled by the following 4th order polynomial:

$$I_{bias} = 5.6\times10^{-4}P_{in}^{\ 4} + 53.5\times10^{-3}P_{in}^{\ 3} + 1.9P_{in}^{\ 2} + 29.5P_{in} + 312.5 \qquad (3\text{-}6)$$

3.2.3 Constant SOA Gain of 15 dB

In this scenario, we search in the results shown in Fig. 3.3, for gain as a function of I_{bias} and P_{in}, in order to get the I_{bias} values needed to keep the SOA gain at 15 dB across the P_{in} range. The corresponding results are shown in Fig. 3.12. This I_{bias} profile shows a clear inconvenient when the P_{in} is higher than −20 dBm: the EVM increases exponentially (see Fig. 3.12a). This is due to the distortion caused by the SOA at such output region above −15 dBm at 30% EVM.

These results can be modelled by the following 6th order polynomial function:

$$I_{bias} = 2\times10^{-6}P_{in}{}^{5} + 1.5\times10^{-3}P_{in}{}^{4} + 73\times10^{-3}P_{in}{}^{3} + 1.4P_{in}{}^{2} + 9.5P_{in} + 87.3 \qquad (3\text{-}7)$$

3.3. Conclusions

The characterization of a SOA used as a booster amplifier in a CO-OFDM system has been presented. We investigated how the bias current and the input power affects the SOA performance in terms of EVM, output power, and gain. We demonstrated that a trade-off to obtain a good behavior is needed, depending on three different scenarios of operating conditions. We analyzed these performance profiles and developed models to compute the bias current that fits each of the three scenarios: maximum EVM equal to 20%, constant output power equal to −7 dBm, and constant SOA gain equal to 15 dB. These closed form models would allow to dynamically control the bias current to obtain the best results within each operating scenario.

4. SOA Linearization by Envelope Tracking Method for Multicarrier CO-OFDM Signal

Linear amplification and power consumption are important features in the new communication systems that use an OFDM modulation scheme, such as 4G and LTE. The present Chapter aims to present the main characteristics of envelope based methods for power management and linearization in radiofrequency power amplifiers in order to adapt them for the optical transmission case, especially on the amplification process performed by a SOA. Also, this Chapter aims at evaluating the benefits of the ET technique for advanced modulation formats like CO-OFDM. Then, an Envelope Tracking system for a SOA based CO-OFDM transmitter is proposed. Moreover, a numerical assessment to the proposed ET system is shown. Likewise, a more detailed evaluation of the filtering effects in the ET branch is proposed and the interest of combining a PAPR reduction with ET is outlined.

4.1. Envelope Based Power Management Methods for Radiofrequency Power Amplifiers

As mentioned in previous Chapters, OFDM presents high peaks of power, measured as peak to power average ratio (PAPR), which could drive a power amplifier (PA) to a low efficiency operation region, in terms of power consumption and nonlinear distortions in the output signal. Many power management methods have been deployed in the RF domain [Raab-96] [Kim-14] to enhance the power efficiency and linearity in RF PA, such as envelope elimination and restoration (EE&R), and envelope tracking (ET).

There are two main methods to manage the power in an RF power amplifier. Both are based on the envelope of the RF signal: envelope elimination and restoration (EE&R) and envelope tracking (ET). The envelope is the shape in which the RF signal varies; it is the function that describes the way the amplitude of the RF signal changes in time.

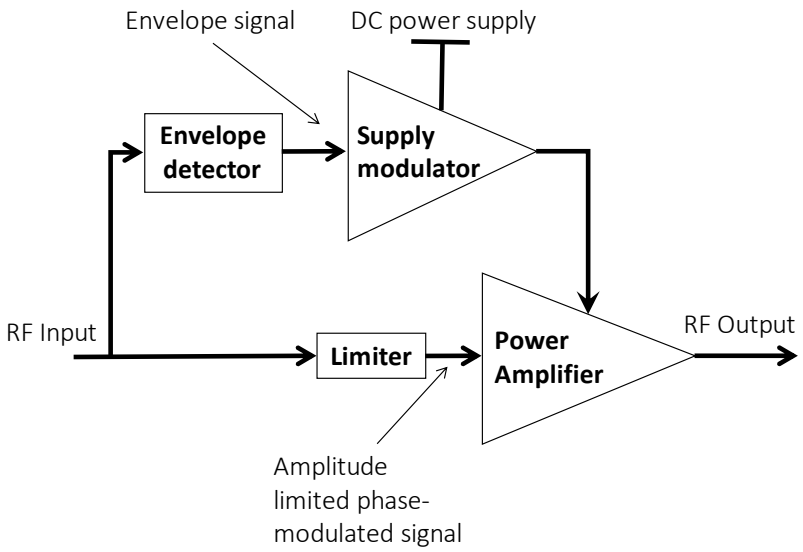

Fig. 4.1 Basic envelope elimination and restoration (EE&R) block diagram.

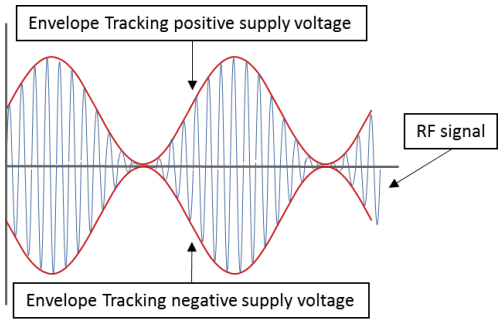

Fig. 4.2 Envelope tracking (ET) modulate the power supply according to the RF envelope reducing heat dissipation and power wasted..

4.1.1 Envelope Elimination and Restoration (EE&R)

In an EE&R process the RF signal is split in two different signals, as shown in Fig. 4.1: an envelope-signal is obtained by the envelope detector and an amplitude limited phase modulated signal is produced by the limiter, resulting in a phase-only modulated signal. The supply modulator modifies the operating power of the RF amplifier proportionally to the envelope signal by following the amplitude modulation of the limited signal [Wang-14]. This reproduces the OFDM signal present at the amplifier's input, but power amplified. EE&R is a modulation process that restores the previously clipped signal envelope and results in a high-power replica of the input signal being produced at the output.

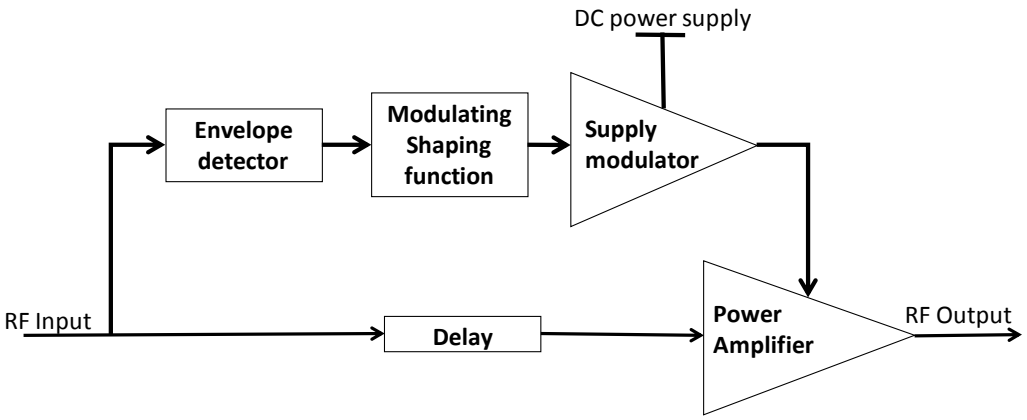

Fig. 4.3 Basic ET block diagram with modulating shaping function generator.

4.1.2 Envelope Tracking (ET)

ET enhances the power efficiency of an RF amplifier by modulating its supply voltage in such a way that it only supplies the power that is needed. The variation of the supply voltage is made according to the envelope of the RF signal [Wang-15], as shown in Fig. 4.2.

An envelope tracking system is composed of an envelope detector, a modulating shaping function generator, a power supply modulator, a delay block, and a power amplifier, as shown in Fig. 4.3.

a) Envelope detector. In this block, the envelope signal is extracted from the RF baseband signal $x(t)$. The resulting envelope signal $x_{env}(t)$ is the magnitude of the RF baseband complex input signal [Wang-14],

$$x_{env}(t) = |x(t)| = \left(I(x(t))^2 + Q(x(t))^2\right)^{\frac{1}{2}} \tag{4-1}$$

where I and Q are the corresponding in-phase and quadrature components, respectively.

b) Modulating shaping function generator. Here a signal related to the envelope is produced with the final objective to either amplify the OFDM signal efficiently or decrease non-linearities of the amplifier, or both of them. The modulating shaping function is also known as envelope shaping function.

c) Supply modulator. It is the main step on the ET process. Here, the supply voltage of the RF PA is regulated according to the envelope shaping function. In an RF ET system, there

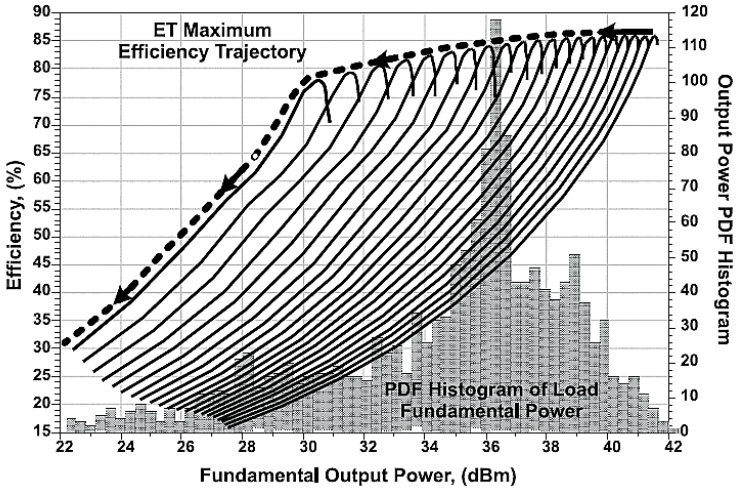

Fig. 4.4 RF PA efficiency response curves at different supply voltages. Figure taken from [Wang-14].

are three kinds of supply modulators: analog, discrete, and hybrids schemes [Kim-14].

d) Delay. This block is necessary to compensate the time mismatch introduced by the ET process [Kim-14].

4.2. ET Power Efficiency and Linearity

As mentioned before, improve linearity and efficiency in an RF PA is an important issue into the design process of an ET system. To obtain a good tradeoff between linearity and efficiency, it is necessary to have a good understanding of the dynamic power response, gain compression, and their relationship with other components in the ET system, such as the supply modulator and the power amplifier.

4.2.1 ET power efficiency

In order to understand the way that an ET system improves the power efficiency in an RF power amplifier, it is necessary to analyze the way that the efficiency and the power output vary as a function of the power supply, as illustrated in Fig. 4.4. Here, the maximum efficiency and maximum output power are well identified, corresponding to a point near to the saturation region. The clue is changing dynamically the power supply voltage as the power input changes. It is seen

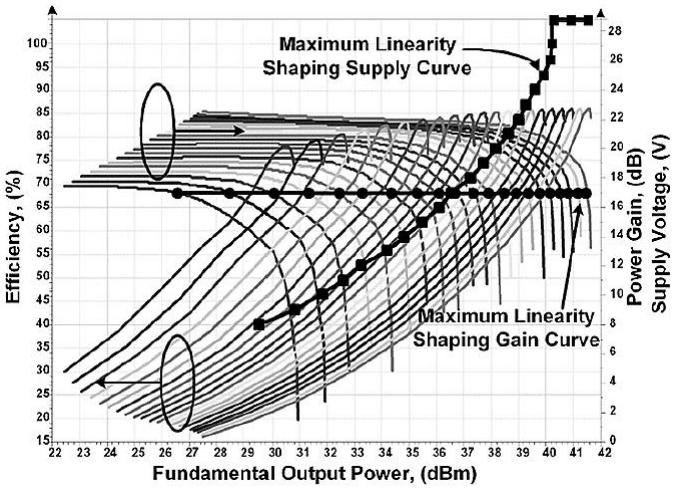

Fig. 4.5 Efficiency and gain trajectories versus output power across various supply voltages achieve efficiency and linearity ET strategy. Figure taken from [Wang-14].

that the ET system could deliver high efficiency over a wide range of output power [Wang-14].

4.2.2 ET Linearity

As mentioned before, the goal of ET is to vary the PA supply dynamically to enhance performance for either efficiency or linearity. One consequence of changing supply voltage as a function of the envelope signal is the varying gain at ET PA output. This dynamical behavior introduces an AM-AM and AM-PM distortion. AM-AM and AM-PM distortions introduce an intermodulation distortion to the amplified RF signal. One way to reduce this nonlinear behavior is to change the characteristics of the envelope signal, to produce a modulating shaping function able to transform the non-linear amplification function into a linearized operation of the RF PA [Wang-14], as shown in Fig. 4.5. Here, the curves corresponding to the power gain, related to the output power for different supply voltages have been added to the efficiency curves. The modulating shaping function must change the supply voltage as the input power changes, in such a way that it obtains the maximum linearity performance for such a supply voltage.

4.3. Envelope shaping function

As mentioned before, the modulating or envelope shaping function generator changes the

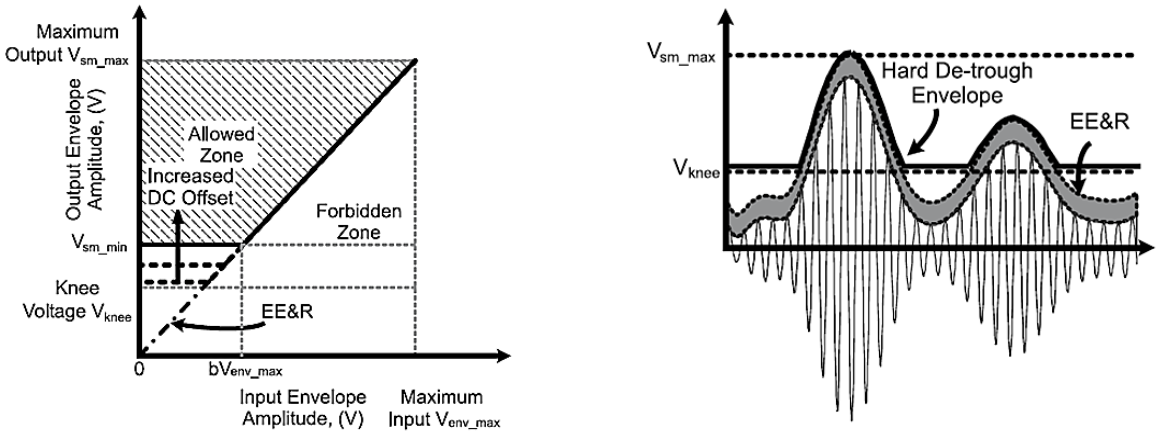

a) b)

Fig. 4.6 Hard detrough transform: a) profile, b) time signals. Figure taken from [Wang-14].

envelope signal to set up the supply modulator operation. The shaping function helps the ET system to keep the constant gain for linearity. The envelope shaping reduces the nonlinearity for a low supply voltage range, so that the ET PA works more linearly than the one without envelope shaping.

The shaping function has three basic purposes in an ET system for an RF power amplifier:

a) Amplification stability by removing near cross-zero region tracking voltage, because RF PA tends to shut down while draining the voltage to zero.

b) Reduce the bandwidth of the envelope signal, thus bandwidth requirements of the supply modulator. To achieve this, it is necessary to reduce the amplitude fast changes in the envelope signal.

c) Avoid as much as possible the risk to present time mismatch between envelope signal and RF signal before amplification.

The shaping function generator modifies the envelope signal through an operation called detrough [Wang-15]. There are three methods: hard detrough, soft detrough, and linear detrough.

4.3.1 Hard Detrough

Hard detrough applies a clipping to the envelope signal, to avoid ET working at lower voltages than the amplifier's knee voltage, as a minimum threshold [Wang-14], as shown in Fig. 4.6. This abrupt curve expands the bandwidth of the envelope signal and impacts the AM-AM

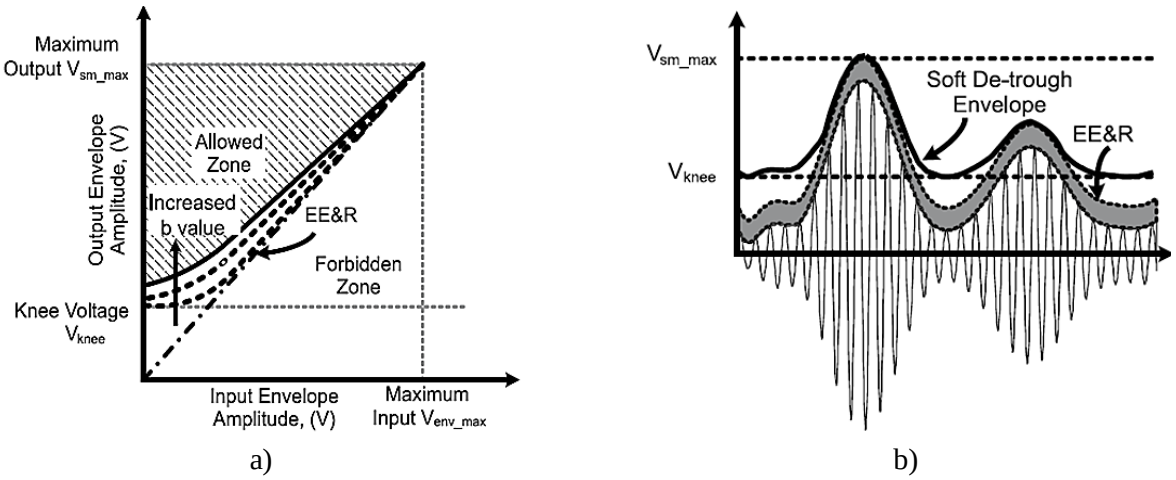

Fig. 4.7 Soft detrough transform: a) profile, b) time signals. Figure taken from [Wang-14]

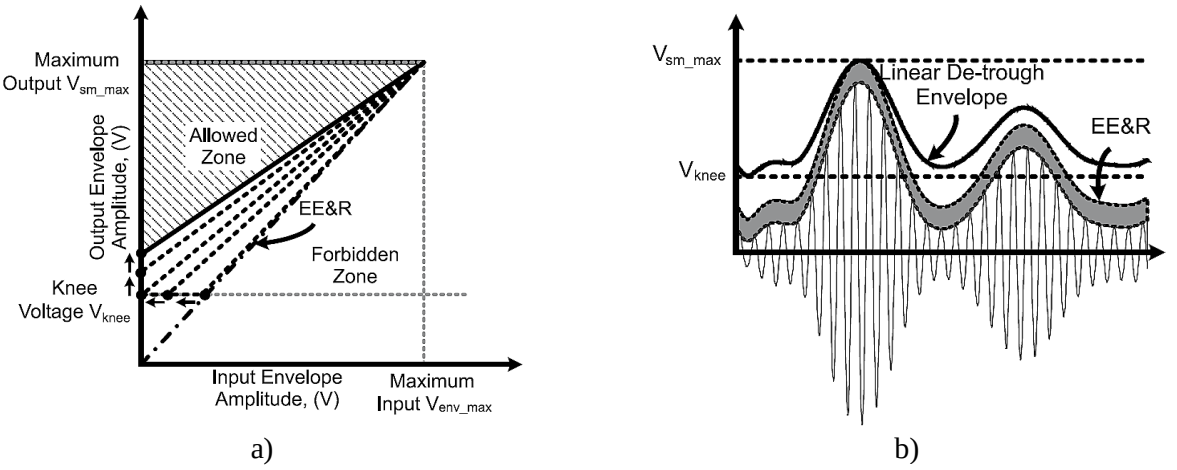

Fig. 4.8 Linear detrough transform: a) profile, b) time signals. Figure taken from [Wang-14].

characteristic of the PA.

4.3.2 Soft Detrough

Soft detrough uses a nonlinear transformation to shape the envelope signal, as shown in Fig. 4.7. The transformation operates above the knee voltage [Wang-14]. The output signal has a lower bandwidth than the original, because the high frequency components of the original envelope signal have been removed. Another advantage to smoothing the envelope signal is to reduce the sensitivity to time mismatch on the ET system.

4.3.3 Linear Detrough

For better linearity and design for the linear AM-AM and AM-PM characteristics, the envelope shaping transformer can change the envelope supply linearly [Wang-14]. Therefore, to compensate the power reduction due to the knee voltage, a linear detrough shaping function can be achieved by moving the transition point leftward to compromise linearity at the expense of efficiency, as shown in Fig. 4.8.

4.4. Mixed Methods for ET Linearity

The next subsection shows two cases of the shaping function transform in combination with other predistortion techniques to enhance linearity in the ET system, such as, clipping method and digital predistortion, respectively.

4.4.1 Shaping Function Optimized

In [Kim-11], two envelope shaping functions are presented. The first one is named as an offset shaping function. The second function is an optimized envelope shaping function based on the sweet spot tracking method. The sweet spots are local minima of intermodulation distortion (IMD). Fig. 4.9 shows both transfer profiles. Sweet spot tracking and offset shaping transfer profiles have similar responses. Hence, the optimized envelope shaping function for this case is given by

$$V_{env} = k \cdot V_{in} + V_{knee} \tag{4-2}$$

and

$$k = \frac{\mathrm{V}_{\mathrm{env.max}} - V_{offset}}{\mathrm{V}_{\mathrm{env.max}}} \tag{4-3}$$

where k is a scaling factor, V_{in} is the scaled input envelope voltage, V_{offset} is the knee voltage of the RF PA and $V_{\mathrm{env.max}}$ is the maximum envelope collector voltage. The linear detrough shaping function is combined with PAPR reduction techniques to clip the large amplitude values of the envelope signal. The clipped signal has lower PAPR. ET PA is applied to WCDMA/LTE signals, showing efficiencies of 48.8/42.2% at the peak power of 31.5/28.9 (dBm), respectively.

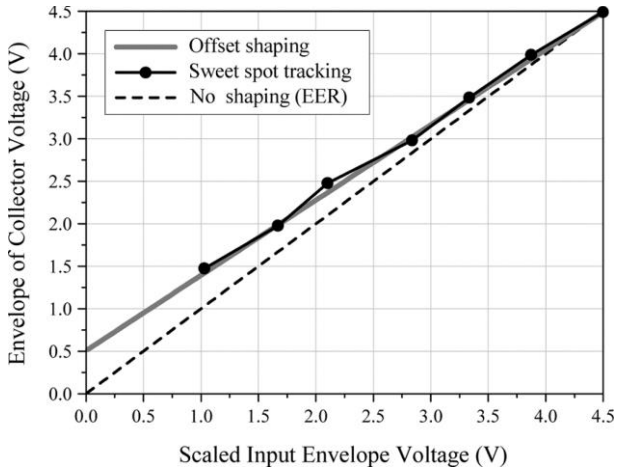

Fig. 4.9 Efficiency and gain trajectories versus output power across various supply voltages achieve efficiency and linearity ET strategy. Figure taken from [Kim-11].

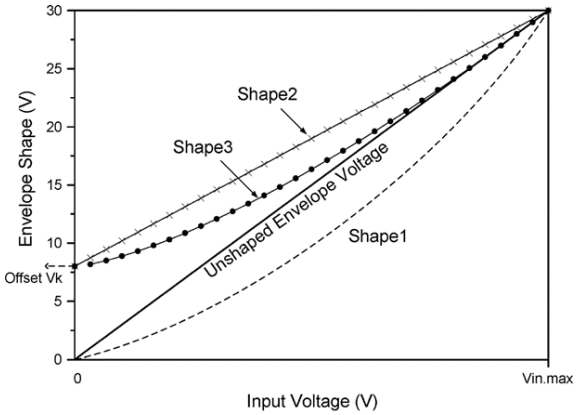

Fig. 4.10 Three different envelope shaping function profiles. Shape 1: nonlinear shaping function. Shape 2: linear detrough. Shape3: soft detrough. Figure taken from [Kim-13].

4.4.2 Envelope Shaping with Digital Predistortion

Another approach to design an ET system is presented in [J.Kim-13], where 3 different envelope shaping functions are proposed for an ET system applied to an LTE wireless system.

Shape 1 is a nonlinear transformation,

$$V_{env1} = V_{\max} \cdot V_{norm.in}^{N} \tag{4-4}$$

where V_{max} is the maximum output amplitude, $V_{norm.in}$ is the normalized input amplitude, N symbolize the curve shaping factor.

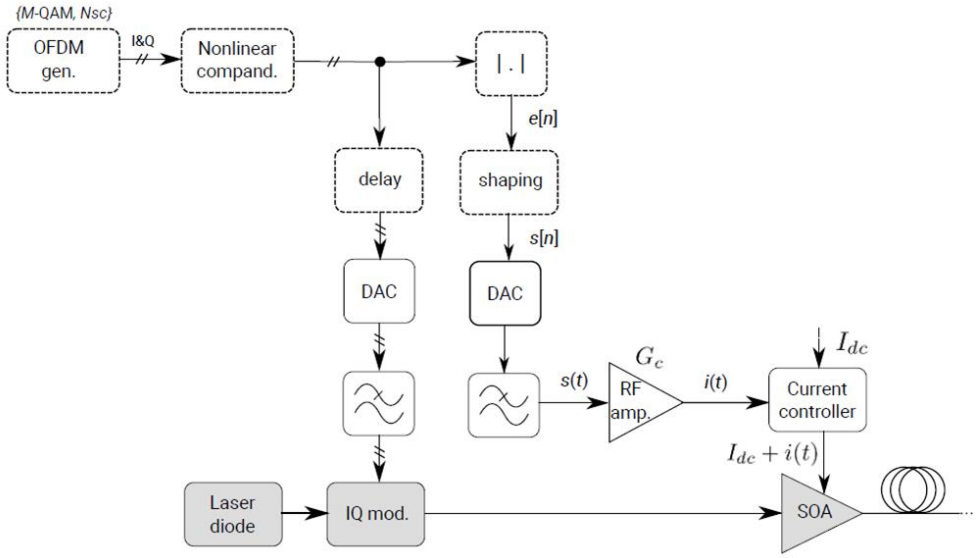

Fig. 4.11 CO-OFDM transmitter including an envelope-tracking branch for current control and a nonlinear companding block for PAPR reduction.

Shape 2 is a simple linear detrough with an offset,

$$V_{env2} = (V_{\max} - V_k) \cdot V_{norm.in} + V_k \tag{4-5}$$

where V_k is the envelope offset.

Shape 3 corresponds to a soft detrough,

$$V_{env3} = (V_{\max} - V_k) \cdot V_{norm.in}^{N} + V_k \tag{4-6}$$

The soft detrough shaping function has more flexibility of operation, because parameters N and V_k control de transformation of the envelope signal. The three transform profiles are shown in Fig. 4.10.

In addition, digital predistortion technique DPD is combined with ET system to achieve linearization. This pre-distorted signal compensates the phase distortion and maintains the high efficiency of the PA.

4.5. An Envelope Tracking Method for SOA Amplification of Multicarrier Signals

A wide variety of linearization techniques are discussed in the literature for reducing the nonlinear effects associated to optical communication systems [Zhang-14]. The ET technique has been identified as a promising scheme for improving the power efficiency of broadband wireless

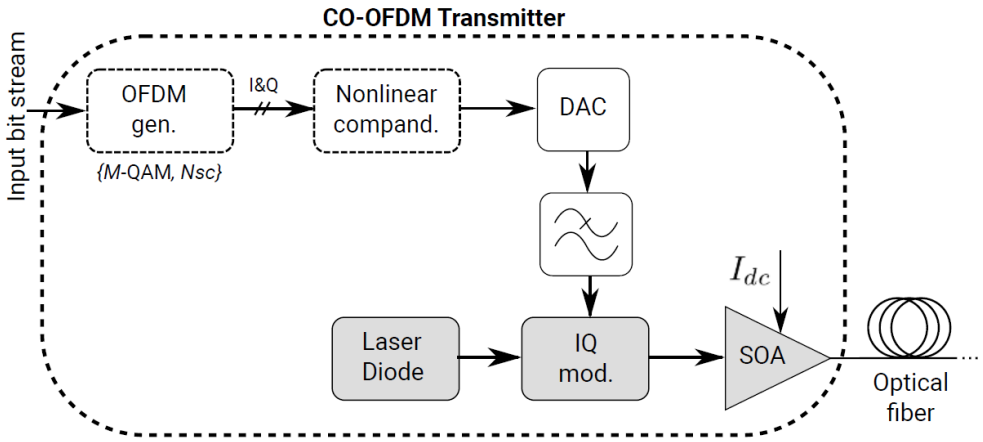

Fig. 4.12 CO-OFDM transmitter with SOA amplification.

systems [B.Kim-13] by modulating the supply voltage of the power amplifier according to the input envelope variations. The linearization capability of such technique for a SOA-based system has also been pointed out in [Saleh-88], where the amplifier has its bias current controlled by the photo-detected input signal envelope. By using some theoretical developments, authors in [Saleh-88] shown that the current translate into a constant carrier density within the active region and an increased saturation power of the amplifier. The practical feasibility of the scheme has been demonstrated by a two-tone experiment. Throughout the next sections the an envelope tracking (ET) approach is studied here for improving linearity in the SOA-based CO-OFDM transmitter, with an eventual use of crest factor reduction via μ-law companding (see Fig. 4.11).

4.5.1 ET-SOA System Model

Our implementation relies on a self-developed SOA model presented in section 1.6.1.3, which has been fitted to simulate a commercially available bulk 750 μm long SOA (INPHENIX-IPSAD1501), so that it yields a very good matching between simulated and experimental results. The overall structured of the transmitter is illustrated in Fig. 4.12; it is a classical layout featuring an optional PAPR reduction block via nonlinear companding to adjust the statistics and the peak power of the M-QAM OFDM signal (with N_{sc} subcarriers) to be amplified. For its simplicity, with only one parameter of the companding function, the μ-law technique [Chen-13] will be adopted here. The Mach-Zehnder IQ modulator has a half-wave voltage v of 6 V and a 1540 nm continuous

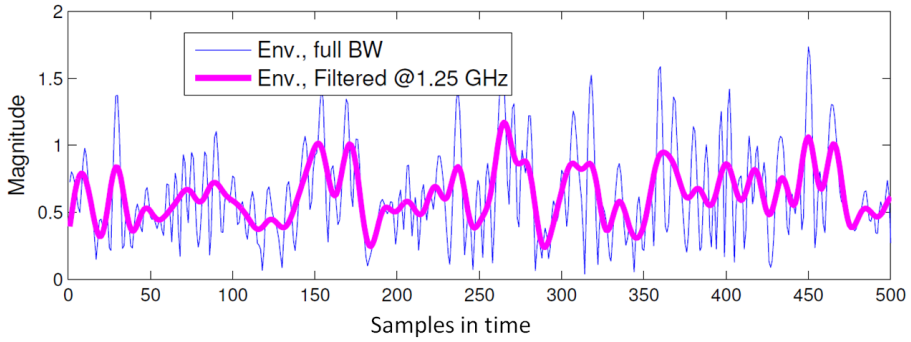

a)

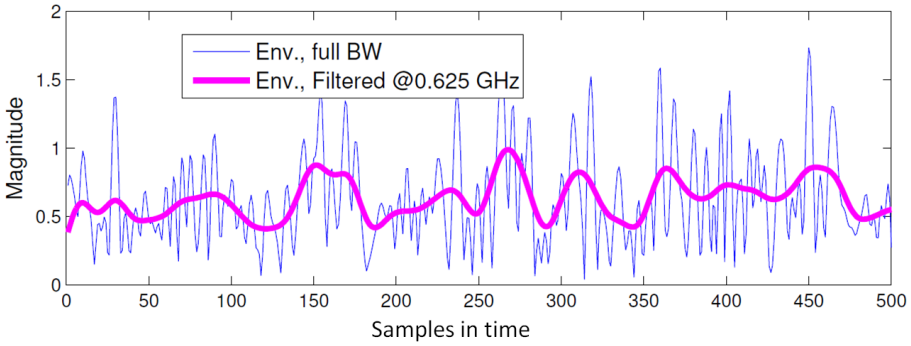

b)

Fig. 4.13 Original envelope and reduced bandwidth envelope: a) 1.25 GHz bandwidth b) 625 MHz bandwidth. Filtering reduce the ET system capacity to follow the rapid changes in the original envelope signal.

wave light applied at its input.

The receiver, not illustrated, then performs a coherent detection, followed by various operations including time synchronization, nonlinear decompanding, equalization, and digital demodulation. In the remaining of the study, a back to back performance evaluation will be considered, with the assumption of a perfect coherent detection and by neglecting the analog-to-digital converted (ADC) effects. The case of a 5 GHz electrical bandwidth 4-QAM CO-OFDM transmission spread over 128 N_{sc} will be considered, with an oversampling factor of 4.

As mentioned before, SOA nonlinear impairments may produce significant distortions, impacting the transmission link quality, and resulting in an increased BER. In the following section, the SOA nonlinear characteristic are briefly reviewed, and an ET scheme is proposed to achieve its linearization.

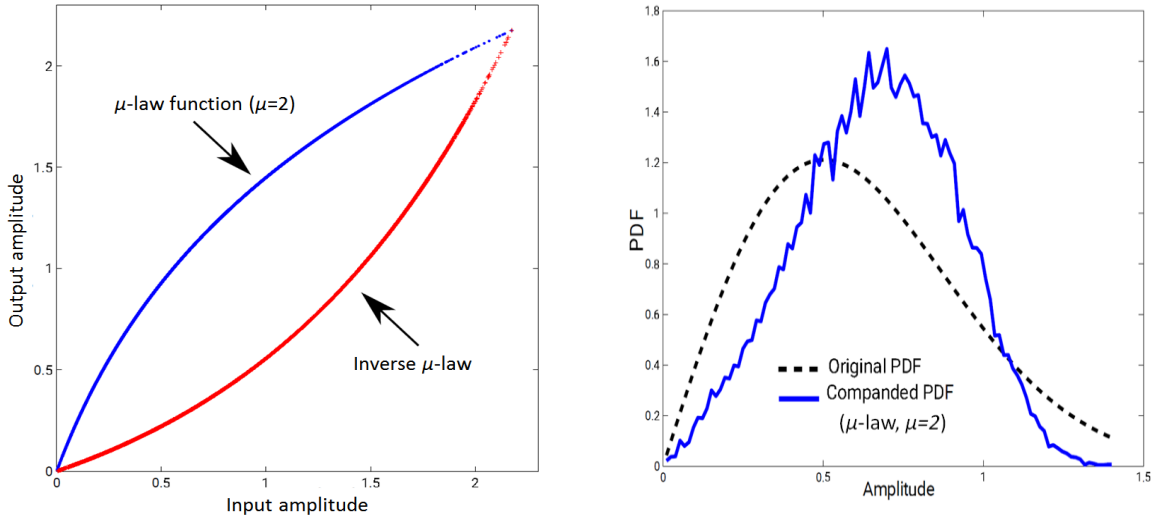

a) b)

Fig. 4.14 *Companding* function (μ-law) used in joint with ET; μ-law attempts to boost the medium amplitudes: a) μ-law transforming profile and its inverse for μ = 2, b) companded PDF and original PDF.

4.5.2 General Approach to SOA Linearization via Envelope Tracking

The general idea behind the envelope tracking is to dynamically adjust the power supply signal to track the input envelope fluctuations. The dynamic supply involves an envelope amplifier (EA) with gain Gc aiming at delivering the desired supply signal in a synchronous manner and in real time, which can be challenging in presence of multicarrier signals with large PAPR, occurring an envelope bandwidth far larger than that one of the original baseband complex signal. Hence, shaping schemes are usually required for adapting the envelope dynamics to the application objectives (linearization, power efficiency, isogain, etc.) [B.Kim-13]. Our ET-based CO-OFDM transmitter setup is depicted in Fig. 4.11.

As the SOA operates as a booster, the time-alignment, and the envelope signal generation together with the envelope shaping can directly be processed in digital domain with no need of a photo-detector, as would be the case for an inline amplifier. Theoretically, the amplifier can be perfectly linearized by adjusting the biasing current proportionally to the squared optical field envelope [Saleh-88]. The resulting control signal may have frequency components over a few tens of GHz, but due to the specific carrier density dynamics of the SOA (of the order of 0.3 ns) a

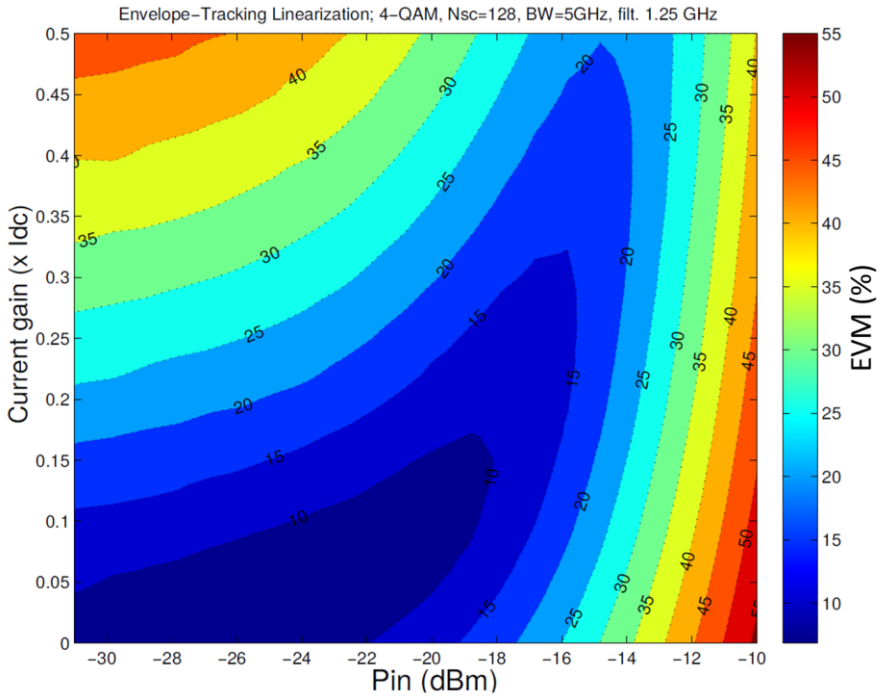

Fig. 4.15 EVM versus current gain (α) and SOA input power for a bandwidth reduced at 1.25 GHz. Current gain change becomes useless to reduce the EVM for SOA high input power level above −14dBm.

bandwidth limited to a few GHz may be sufficient for achieving linearization. The practical feasibility of the concept has been shown in [Saleh-88] for a two-tone system only, with a 2 GHz bandwidth baseband amplifier in the ET branch. In the present study, we investigate the effects of a 128 subcarriers OFDM envelope signal with a bandwidth reduced up to a lower limit of 625 MHz (Fig. 4.13), with the view to simplify as much as possible the implementation of the current control. Considering that the original OFDM signal has a 5 GHz bandwidth, this corresponds to a severe filtering effect. Thus, the shaped signal is expressed as $s[n] = h[n]*e[n]$, where $e[n]$ denotes the OFDM signal envelope and $h[n]$ is the low pass filter impulse response (a 48-th order FIR filter being chosen in the sequel); the resulting signal is then normalized in amplitude before its digital to analog conversion. The corresponding analog signal $s(t)$ is then adjusted in amplitude with a gain $G_c = \alpha I_{dc}$ depending of the amount of additional current required, where $\alpha << 1$ and I_{dc} denotes the bias current DC value. The resulting signal $i(t) = G_c s(t)$ will then be used to dynamically adjust the biasing current value. Throughout the sequel, a perfect synchronization will be assumed between the optical signal entering the SOA and the control signal $i(t)$.

In addition to the ET scheme, aiming at linearizing the optical amplifier, a companding

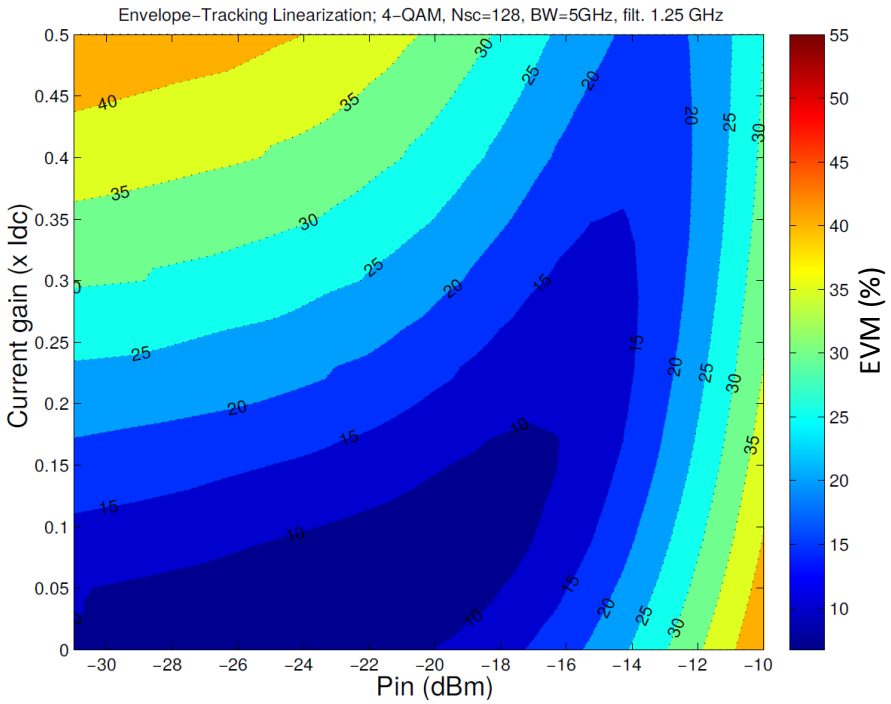

Fig. 4.16 EVM versus current gain (α) and SOA input power for a bandwidth reduced at 1.25 GHz with joint companding/ET. Low EVM values could be obtained by the combination of companding with ET.

transform is eventually applied for reducing the PAPR of the signal to be amplified. According to this approach, the original signal samples x_n have their amplitude modified by a nonlinear function f, the resulting signal $y_n = f(x_n)$ is then converted into an analog waveform. At the receiver side, the noisy signal $r_n = y_n + v_n$ is then transformed by the de-companding function to recover original signal (plus noise): $x_n = f^{-1}(r_n) \approx x_n + f^{-1}(v_n)$. For its simplicity, the following μ-law function is adopted:

$$f(x_n) = A\,\mathrm{sgn}(x_n)\frac{\log\left(1+\mu\frac{x_n}{A}\right)}{\log(1+\mu)} \tag{4-7}$$

where sign stands for the signum function and $\mu = 1, 2, 3\ldots$ denotes the key parameter for shaping the resulting PDF. Increasing μ tends to boost the amount of medium amplitudes while compressing small and large amplitudes.

The companding function together with the corresponding PDF are depicted in Fig. 4.14, for $\mu = 2$ which will be adopted in the sequel.

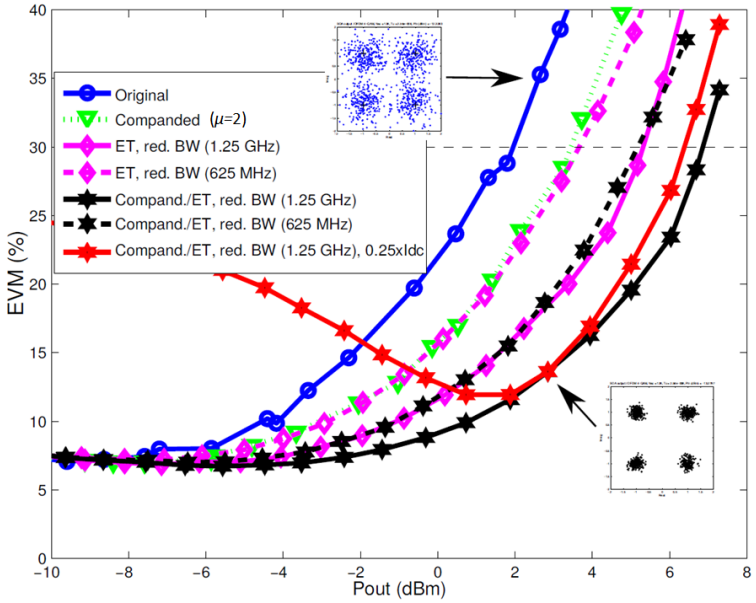

Fig. 4.17 Performance evaluation for different simulations. EVM versus SOA output power.

4.5.3 Numerical Results

The performance on the ET-based CO-OFDM transmitter is evaluated in this section for a 5 GHz bandwidth 4-QAM transmission spread 128 N_{sc} subcarriers (resulting in a data rate around 9 Gb/s). The scenario of an envelope low-pass filtered at 1.25 GHz in absence of companding has been first examined, over a wide range of SOA input power P_{in} and for a current gain G_c going up to $0.5I_{dc}$, with I_{dc} = 150 mA. For evaluating the performance, the classical criterion of (EVM) [Schmogrow-12] has been calculated for each couple (P_{in}, G_c) in a back to back configuration (receiver placed at SOA output). Due to the large computation time required for exploring the two-dimensional (2D) space, a short sequence made of 2^9 4-QAM symbols has been used for this purpose (with a PAPR going up to 10.3 dB). The results are given in Fig. 4.15, where it can be clearly observed that low EVM values are achieved via current control over a wide range of P_{in}.

For example, if an EVM limit of 30% is set (corresponding to a Bit-Error-Rate of 10^{-3}), P_{in} can be increased up to −12 dBm. It is also noticed that as more power is injected, a larger gain G_c is required for compensating the nonlinear effects, particularly above −20 dBm. An acceptable EVM value can eventually be ensured at high saturation (P_{in} > −12 dBm), but with very large

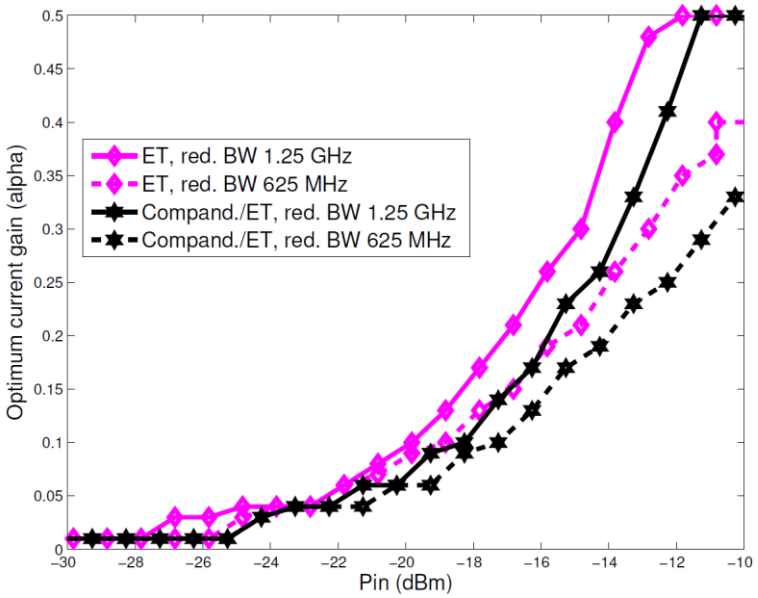

Fig. 4.18 Optimum current gain versus SOA input power. Envelope filtering effect is observed by reducing the optimal current gain.

current gain.

In a similar way, EVM has been evaluated for each couple (P_{in}, G_c) when the envelope signal undergoes a bandwidth reduction at 1.25 GHz and when a μ-law companding is jointly used with the reduced bandwidth (BW) ET technique. From Fig. 4.16, it can be observed that this scheme significantly enlarges the power range over which an acceptable EVM value can be satisfied, while alleviating the current gain G_c. The same approach has been followed with a much narrower filter bandwidth (625 MHz), with and without companding. For all the different schemes, we estimated a performance bound corresponding to the current gain G_c yielding the minimum EVM for a given input power. The results are shown in Fig. 4.17, where we can first observe a quick rise in EVM if no companding nor linearization is adopted, as we move towards the saturated region; the considered EVM limit value being reached at $P_{out} \approx 2$ dBm. If the ET technique is used with a reduced BW of 1.25 GHz, an improvement of around 3 dB is achieved at 30% of EVM. For a better linearization, the joint use of PAPR reduction (with μ-law companding here) and envelope tracking is an effective solution, as can be clearly seen also in Fig. 4.17. An additional improvement close to 2 dB is achieved in this way in the SOA saturation region, with respect to the use of ET scheme alone. It can also be observed that this approach is far more effective than the use of μ-law companding only, which just reduces the amount of nonlinear distortions by

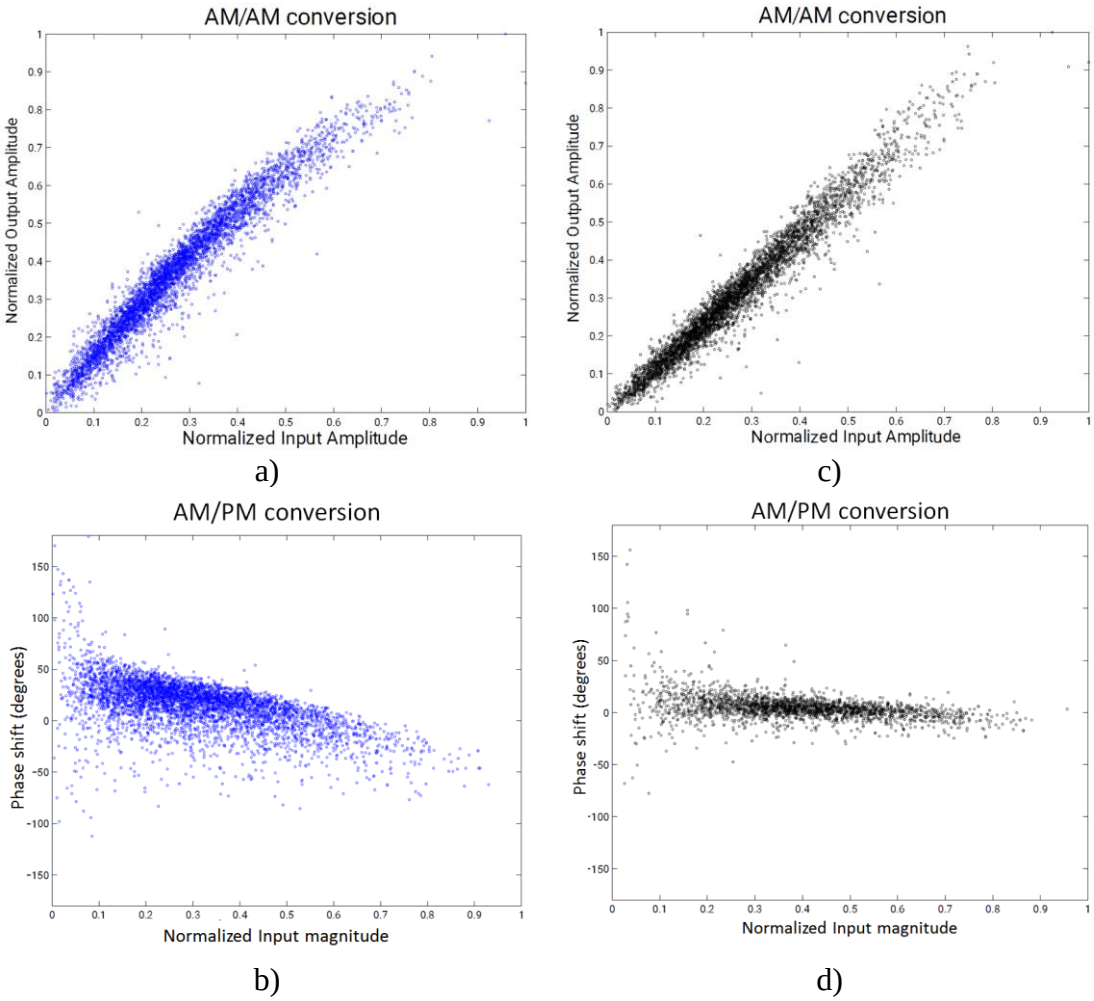

Fig. 4.19 AM/AM and AM/PM distortions for a SOA output power of 3 dBm corresponding to: a) and b) original signal; c) and d) after ET with reduced BW.

reshaping the statistics of the signal to be amplified. Notice that larger values of μ could significantly decrease the EVM at high power, but at the price of less performance at low or medium power. Inserted constellations for an output power P_{out} of 3dBm indicate a huge improvement of around 25% thanks to companding/ET as compared to the original system. If a more severe filtering is applied (bandwidth of 625 GHz), a 1 dB penalty is measured for the ET scheme at 30% of EVM, with more degradation below this limit (the penalty going up to 2 dB); the overall results are actually very close to those obtained with the μ-law PAPR reduction alone. If the latter is combined with ET, it achieves a performance close to the ET scheme with a bandwidth reduced at 1.25 GHz. Hence, despite the relatively low bandwidth of the current control signal, an effective linearization is accomplished.

The optimum gain value against input power is plotted in Fig. 4.18 for the two ET scheme

investigated (ET with reduced BW and μ-law based ET with reduced BW), with BW values of 1.25 GHz and 625 MHz. Slowing down the envelope signal variation has an obvious effect on the current control, with lowered gain. It can also be observed that the usage of PAPR reduction significantly reduces the amount of additional current $i(t)$ required while achieving a better quality for the amplified signal if the optimum gain is chosen. The case of a current control with fixed gain $G_c = 0.25I_{dc}$ is illustrated in Fig. 4.17, when companding and reduced BW ET are employed (1.25 GHz case). In such conditions, the optimum bound is reached at $P_{out} \approx 3$ dBm and the performance is still very good above this threshold, but a quick degradation is noticed as the operating point moves towards a linear region (lowering power and decreasing signal to noise ratio). These observations reveal that a self-calibrating ET technique should be designed so that the performance remains close to the optimum while the operating conditions (input power, modulation format, etc.) change.

Finally, the dynamic AM/AM and AM/PM characteristics are depicted in Fig. 4.19 for the original system (subplots a, b) and for the companding/ET-based system (subplots c, d) with a reduced bandwidth at 1.25 GHz. The static nonlinearities together with memory effects can be clearly observed for the original system, whereas the proposed system exhibit a far better linearity. However, it is evident from Fig. 4.19 (c, d) that the amplified signal is still affected by memory effects (spread along straight lines).

4.6. Conclusions

The main characteristics of power efficiency and linearity methods in an RF power amplifier have been studied. EE&R and ET functionalities were compared, finding that ET is a better solution to achieve a good tradeoff between linearity and efficiency in an amplification process. In an ET system, the envelope transformation plays a key role. Three main types of functions allow some degree of freedom in the design of the system: hard detrough, soft detrough and linear detrough. The use of predistortion schemes, such as PAPR reduction and DPD technique, could help to achieve linearization. ET approach could be adapted to semiconductor optical amplifiers to improve their linearity and reduce nonlinear distortion.

The benefits of envelope tracking have been investigated in this chapter for mitigating the nonlinear effects in a coherent optical OFDM transmitter using a SOA as a power booster. To the

best of our knowledge, only Saleh et al. [Saleh-88] have pointed out the effectiveness of the ET technique for linearizing a SOA, but by considering only a two-tone scenario. Despite of the good results exposed here; it is suitable to optimize the ET SOA system using more parameters. In the following chapters, this challenge will be addressed.

5. An improvement of ET-SOA for CO-ODFM system

In Chapter 4, ET for SOA-based CO-OFDM was successfully applied, but the study was rather restrictive as only one parameter was tuned for enhancing the linearity. The present Chapter examines a more general problem, with the identification of various optimal system parameters for improving the performance of an ET-SOA based CO-OFDM transmitter. To achieve this goal, we use the same CO-OFDM system setup as in [Ortiz-Cornejo-17], with the use of a precise SOA physical model (see section 1.6). Through the rest of this chapter the SOA typical characteristics are summarized, and an ET scheme is presented for linearizing a CO-OFDM transmitter. Then, the ET block optimization via particle swarm optimization (PSO) is studied and numerical results are developed.

5.1. SOA Linearization Math Model Via Envelope Tracking

As mentioned before, SOA nonlinear impairments may produce significant distortions, impacting the transmission link quality and yielding an increased BER. In this section, the SOA nonlinear characteristic are briefly reviewed, and an ET scheme is proposed for linearization.

An SOA is a component that amplifies an optical signal with a gain $G = P_{out}/P_{in}$, where P_{in} and P_{out} stand for the power of the input and output signals, respectively. The gain can be expressed as a function of the carrier density N after integration over the SOA length L, and by neglecting the internal losses for the sake of simplicity, as:

$$G = \exp\left(\Gamma a\left(N - N_t\right)L\right) \tag{5-1}$$

where Γ is the confinement factor, a is the differential gain and N_t is the carrier density at transparency [Bonk-11]. We present here the theoretical principle of how carrier density fluctuations can be highly attenuated by a simplified analysis that gives qualitative trends. Considering only one calculus section in an SOA, with a constant carrier density along the propagation direction, we consider the following classical rate equation for the carrier density N:

$$\frac{dN}{dt} = \frac{I}{qV} - \frac{N}{\tau} - \frac{(G-1)P_{in}}{h\nu V} \tag{5-2}$$

where I is the injected electrical current, q the elementary charge and V the active zone volume, h is Planck's constant, ν the frequency in hertz, and τ is the carrier lifetime. We also make some assumptions that allows us to separate the static (X_0) and dynamic behaviors ($x(t)$):

$$N = N_0 + n(t) \tag{5-3}$$

$$I = I_0 + i(t) \tag{5-4}$$

$$P_{in} = P_0 + p(t) \tag{5-5}$$

$$G = G_0 + g(t) \tag{5-6}$$

For instance, we separate (5-3) in two equations: static and dynamic. The static equation gives the operating point governed by the carrier density N_0, imposed by the bias current and the input optical power:

$$0 = \frac{I_0}{qV} - \frac{N_0}{\tau} - \frac{(G_0-1)P_0}{h\nu V} \tag{5-7}$$

The dynamic equation is obtained by neglecting the second order term gp in the last term of:

$$\frac{dn}{dt} = \frac{i}{qV} - \frac{n}{\tau} - \frac{(G_0-1)p + gP_0}{h\nu V} \tag{5-8}$$

where g can be expressed using (5-1) as $g = \Gamma\alpha L G_0 n$, and α is the linewidth enhancement factor. If we now manage to impose a dynamic current such that $i/qV=(G_0\text{-}1)p/h\nu V$, (5-8) becomes

$$\frac{dn}{dt} = -\frac{n}{\tau} - \frac{\Gamma\alpha L G_0 P_0}{h\nu V} = -\frac{n}{\tau} - \frac{G_0 P_0 n}{\tau\, P_{sat}} \tag{5-9}$$

where P_{sat} is the material saturation power.

Notice that (5-9) is a first order homogeneous equation, tending to zero after some relaxation time. Its general solution takes the form

$$n(t) \sim \exp\left(-\frac{t}{\tau}\left(1 + \frac{G_0 P_0}{P_{sat}}\right)\right) \tag{5-10}$$

This important result means that, provided small-signal fluctuations and regardless of the dynamic operating condition of an SOA, as soon as one can induce an appropriate dynamic bias

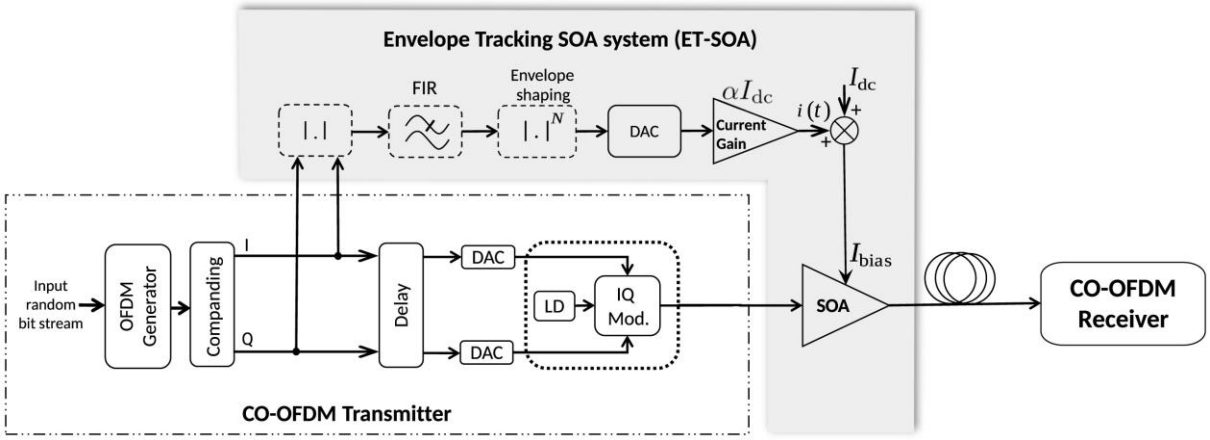

Fig. 5.1 The considered CO-OFDM transmitter scheme, embedding an ET-SOA for boosting the signal power.

current, the carrier density tends to be constant, hence, any dynamic fluctuation of the carrier density vanishes. Since we made several simplifying assumptions, of course a complete annihilation of the dynamic variation of the carrier density only based on a linear transform of the injected power is very hard if not impossible to obtain. Firstly, we neglected the second order term *gp*, which would induce nonzero time variations. Secondly, we considered a single calculus section in the SOA which of course is not the case in reality: the carrier density is not constant along the propagation axis. Thirdly, we used the rate equation as if all terms (such as gain and carrier lifetime, for example) were independent of the instantaneous input power (small signal analysis), which is not the case. There are several ways that can be thought of to ensure the expressed condition. Here, as the SOA is used as a booster amplifier, the emitted signal is already known in the electrical domain and can be applied to the SOA electrode for linearizing the device characteristics.

5.2. An SOA-Based CO-OFDM Transmitter Employing ET

ET has been originally proposed for enhancing the power efficiency and linearity of RF amplifiers by modulating the voltage supply. In an equivalent way, ET may be used for SOA linearization by dynamically adjusting bias current according to the input optical signal variations. This approach has been successfully used in [Ortiz-Cornejo-17] and exposed here in Section in 4.5, jointly with a μ-law companding method for PAPR reduction [Wang-99]. As stated before,

our proposal is a generalization of the technique in [Ortiz-Cornejo-17] exploiting more degrees of freedom to get a better linearity and consequently an improved BER performance. In the ET-SOA path (see Fig. 5.1), the envelope $e[n] = |y[n]|$ of the RF baseband complex signal is first low pass filtered using a FIR filter so as to alleviate the implementation complexity for the following DAC. A nonlinear shaping function (NLSF) of the form $|e_f[n]|^N$ is then applied to the filtered envelope $e_f[n]$ with the view to take advantage of the degree of freedom *N* for improving the linearization efficiency. For $N > 1$ the NLSF compresses the low amplitudes and increases the highest ones, leading to a larger bias current when SOA needs to increase the carrier density to counteract the carrier density depletion. Note that from the analysis given in previous subsection, $N = 2$ is expected to give the best performance, as also pointed out in other references [Saleh-88].

The shaped envelope signal $e_s(t)$obtained from the DAC is scaled so that the bias current is adapted as

is then used to control the SOA with bias current expressed as

$$I_{bias} = i(t) + I_{dc} \tag{5-11}$$

and

$$i(t) \cong \alpha \cdot I_{dc} |e_f(t)|^N \tag{5-12}$$

where α denotes the gain used for scaling the dynamic part of the current and $e_f(t)$ is the bandwidth limited envelope corresponding to the baseband signal *y*[*n*]. For $N > 1$ the NLSF compresses the low amplitudes and increases the highest ones, leading to a larger bias current when SOA needs to increase the carrier density to counteract the carrier density depletion. Note that from the analysis given in previous subsection, $N = 2$ is expected to provide the best performance, as also pointed out in other references [Saleh-88]. In [Ortiz-Cornejo-17], was pointed out the usefulness of the joint use of a μ-law companding method [Wang-99] with ET for an effective SOA linearization. So, we keep this combination in this chapter with a companding block working just before the ET branch, according to the nonlinear function

$$f(x(n)) = \text{sgn}(x(n)) \cdot \frac{A}{\ln(1+\mu)} \ln\left(1 + \frac{\mu}{A}|x(n)|\right) \tag{5-13}$$

where $\text{sgn}(.)$ stands for the complex signum function, A is the maximum amplitude of the baseband

signal $x[n]$, $\mu > 0$ is the companding parameter and $|x[n]|$ denotes the amplitude of $x[n]$. PAPR reduction via nonlinear companding generally offers a good tradeoff between complexity and BER performance, with transparency to modulation format and no requirement of side information [Jiang-08]. With a single parameter to be tuned, the μ-law scheme is attractive in comparison with other nonlinear companding methods [Azou-15].

5.3. ET SOA System Performance Evaluation

In our previous work [Ortiz-Cornejo-17] the optimum operating conditions, in the sense of EVM performance, were found by an exhaustive search of the current gain (parameter α) with fixed values of all other parameters involved in the ET process (N = 1, I_{dc} = 150 mA, and μ = 2). Obviously, such an approach is no longer effective for many degrees of freedom, as it is the case in this work. Thus, a global optimization is reported here based on PSO, by considering different scenarios depending on the parameters to be calibrated in the ET branch.

5.3.1 Analyzed Scenarios

We analyzed three different scenarios to evaluate the performance of the proposed ET-SOA system:

a) No companding and ET. In this first scenario, only the ET block is subject to optimization with variable parameters $\{I_{dc}, \alpha, N\}$, and no companding is performed.

b) Fixed μ-law companding and ET. In this second scenario, the optimization is conducted with the same degrees of freedom in the ET branch (I_{dc}, α, N) and a joint use of μ-law companding with μ = 2 (the same value used in [Ortiz-Cornejo-17]).

c) μ-law companding and ET with fixed shaping function. Here, the objective is to identify the best values for the ET parameters $\{I_{dc}, \alpha\}$ jointly with μ parameter. A fixed value of N is adopted according to the results obtained in the previous two scenarios.

5.3.2 Optimization Method

The optimization problem consists in searching the best parameters values, corresponding

to a minimized EVM while keeping the SOA gain at a predefined constant value. Then, the objective function to be minimized can be formulated as

$$J(\boldsymbol{p}) = \phi\left|G(\boldsymbol{p}) - G^*\right| + EVM(\boldsymbol{p}), \quad \boldsymbol{p} \in \mathcal{D} \tag{5-14}$$

where $\boldsymbol{p}$ stands for the vector of parameters, $G(\boldsymbol{p})$ is the evaluated SOA gain in steady state, G^* is the target gain, and ϕ represents a weighting factor. For this study G^* is fixed at 15 dB. Note that the parameters vector $\boldsymbol{p}$ and the search space change depending on the considered scenario, as follows:

- *First and second scenarios:* $\boldsymbol{p} = [\alpha, I_{dc}, N]$ and $\mathcal{D} = \{0.01 < \alpha < 2,\ 80\text{ mA} < I_{dc} < 200\text{ mA}\ 0.8 < N < 3\}$;
- *Third scenario:* $\boldsymbol{p} = [\alpha, I_{dc}, \mu]$ and $\mathcal{D} = \{0.01 < \alpha < 2,\ 80\text{ mA} < I_{dc} < 200\text{ mA},\ N = 2,\ 1 < \mu < 255\}$.

In each case, a PSO[4] algorithm is used to find the best setting parameters $\boldsymbol{p}^*$. PSO is an evolutionary algorithm which uses a stochastic searching method to find global optimal solutions [Kennedy-95] by emulating the swarm behavior, where one group of individuals follows one of the members through a space looking for the best location.

5.4. Numerical Results

In this section we describe the simulation and optimization results for a back-to-back CO-OFDM transmission with 2^{11} 4-QAM symbols allocated over 128 subcarriers, corresponding to a total BW of 5 GHz. In the ET path, the FIR filter reduces the envelope BW to 1.25 GHz. We compare the performance of the three ET-SOA schemes presented before (Section 5.3, after an initial step of optimization via PSO at a given SOA input optical power and with a target gain G^* = 15 dB. Also, we examine the solutions from the optimization process to draw some conclusions regarding the influence of various parameters on the considered optical transmitter.

5.4.1 ET-SOA Based CO-OFDM Transmitter Performance

[4] Function particleswarmoptimization.m embedded in Global Optimization toolbox under Matlab 2017 (The MathWorks, Inc.).

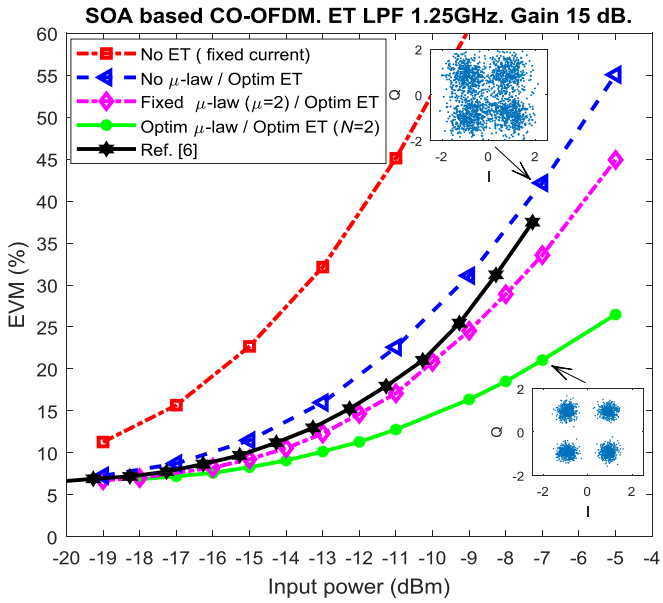

Fig. 5.3 EVM performance against SOA input optical power for the various SOA linearization methods, compared to the conventional system.

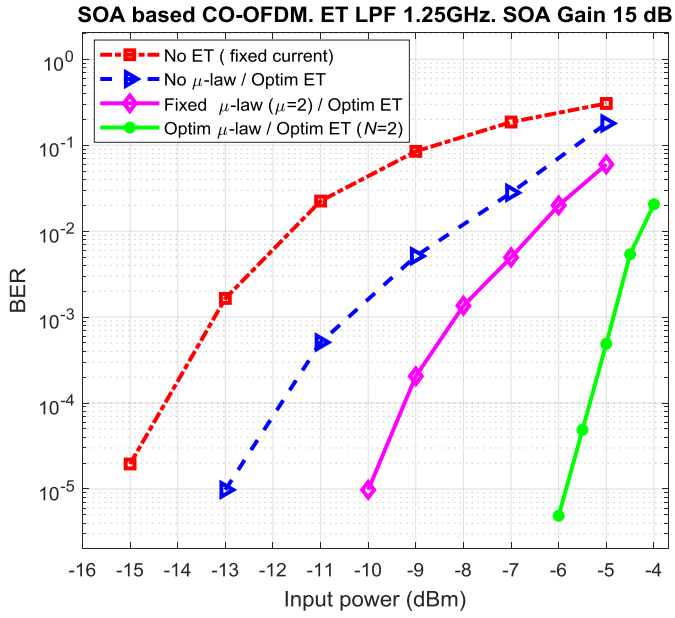

Fig. 5.2 BER performance versus SOA input optical power. An 8 dB improvement is reached at a target BER = 10^{-3} over a traditional transmitter with no ET.

The CO-OFDM system performance is evaluated based on EVM and BER metrics. Fig. 5.3 shows the results among a wide range of input power for each of the three scenarios, in addition to the results reported in [Ortiz-Cornejo-17] for comparison purposes. A clear EVM improvement can be noticed for the three schemes studied, the third one outperforming the other two. By observing

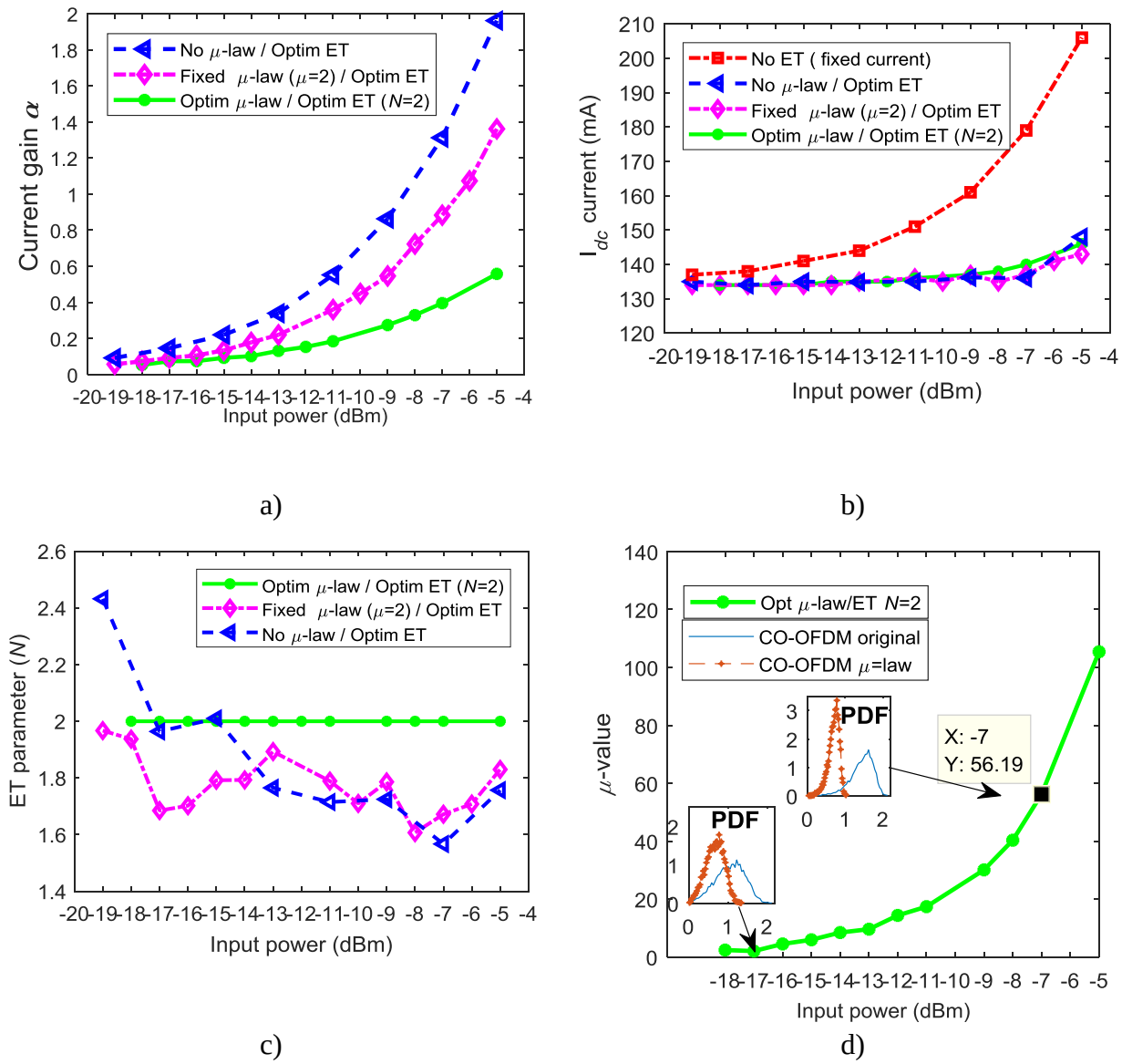

Fig. 5.4 Optimization results as a function of SOA input power: a) optimal values of the current gain α versus SOA input power; b) direct current I_{dc} for each scenario; c) comparison of parameter N for each performance scenario; d) nonlinear companding parameter μ.

that the optimum setting for the parameter N is close to 2 over a wide operating range (as will be illustrated in the sequel), this fixed value has been adopted for the third scenario. This choice is also motivated by the fact that a square transform is realized by a photodetector device, required if the SOA is used as an inline amplifier. Likewise, linearization effect is observed in the insets showing received QAM constellations. Moreover, Fig. 5.2 shows the BER performance versus SOA input optical power P_{in}; an 8 dB improvement has been reached at a target BER of 10^{-3}, as compared to

the conventional transmitter not using ET or nonlinear companding.

5.4.2 Optimal Nonlinear Companding and ET-SOA Parameters

In Fig. 5.4 shows the optimization results as a function of SOA input power. Fig. 5.4a depicts the optimal current gain for all scenarios. It can be clearly seen that α has a quick rise when the P_{in} goes towards the SOA saturated region (above −11 dBm). Fig. 5.4b shows the resulting optimal I_{dc}; it is quasi constant for all scenarios with a slight increase up to 145 mA for high P_{in}. Fig. 5.4c shows the optimal N settings which are close to N = 2 for first and second scenario. Finally, Fig. 5.4d shows the optimal μ-law setting where the optimal μ parameter applies a high signal compression for high P_{in} to reduce high signal peaks (see insets PDF).

5.5. Conclusions

The main objective of this chapter was to improve both the performance and flexibility of the ET technique reported in [Ortiz-Cornejo-17] for linearizing an SOA-based CO-OFDM transmitter. Three different ET-SOA settings have been examined in this report, with successful results. The third scheme, jointly using an optimized μ-law nonlinear companding together with an optimized ET processing, offers the best BER performance gain with reduced current injection. An 8 dB power margin has been attained at a target BER of 10^{-3} in comparison with the conventional SOA-based CO-OFDM transmitter not using linearization. In the following chapter a more extensively numerical assessment is made, to prove the robustness of the ET-SOA under different conditions.

6. A Numerical Assessment of An Effective Envelope Tracking Semiconductor Optical Amplifier Design for Coherent-Optical OFDM Transmission

In this chapter, ET-SOA for CO-OFDM system [Ortiz-Cornejo-18] is investigated to test it, under different operational conditions. An optimized design of the ET subsystem is performed under various scenarios, with the eventual joint use of PAPR reduction either via hard-clipping [Rahmatallah-13] or nonlinear companding [Wang-99]. A thorough carrier density analysis is performed in the amplifier, for various target gain values, so as to assess the effectiveness of the proposed scheme. Moreover, we investigate the robustness of the proposed approach against some parameters variation, both inside the ET path (DAC characteristics and bandwidth limited envelope generation). Extensive simulations performed with a precise SOA model show that up to 8 dB (resp. 7 dB) BER improvement can be achieved via the proposed scheme in the case of 4-QAM/OFDM (resp. 16-QAM/OFDM), as compared to the conventional system with no linearization, and that even an envelope quantized with 2 bits still enables a significant performance increase.

6.1. Introduction to Carrier Density and Dynamic Bias Current on ET-SOA

And as mentioned in chapter 3 SOA is a multipurpose device that can not only compensate for fiber losses but also enable the all-optical implementation of many functions (such as regeneration, switching or wavelength conversion) required in modern optical networks [Connelly-02]. If the inherent device nonlinearity is very useful in the latter case, it turns out to be a significant drawback when it comes to handling the power budget with non-constant envelope signals. Nevertheless, it has been pointed out in several studies that SOAs may be a pertinent choice for amplifying advanced modulation formats [Koenig-14]. For OFDM signals, use of some linearization schemes have been recommended so as to cope with the large PAPR typical of such format [Diouf-17].

SOA gain saturation is actually likely to introduce signal distortions translating into transmission quality degradation. To alleviate these distortions a high saturation output power is required. SOA's optical gain is defined as a function of the carrier density *N* in (5-1) The gain results from the effect of population inversion inside the active region, under the influence of the set bias current. The population inversion may be reduced in situations where the injected optical signal exhibits occasional high peaks; then, a carrier density depletion may occur near the output section, as a result of large photon density, which translates into nonlinear impairments. Thus, SOA's optical gain is mainly controlled by the carrier density generation. We consider the classical rate equation (5-2) for the carrier density *N*, with only one SOA section. In the small-signal regime, and neglecting the second-order terms, it can be shown that the following model holds for the carrier density dynamics in a single section SOA [Ortiz-Cornejo-18], if a non-uniform bias current is adopted

$$n(t) \sim \exp\left(-\frac{t}{\tau}\left(1+\frac{G_0 P_0}{P_{sat}}\right)\right) \tag{6-1}$$

where G_0 and P_0 are SOA gain and input power, respectively, and P_{sat} corresponds to the material saturation power.

The above expression means that if a proper dynamic bias current is applied to the device, $\lim_{t\to\infty} n(t) = 0$ and the carrier density tends to be constant, meaning a linear behavior of the SOA. In the following subsection, we describe a setup based on an envelope tracking scheme with the view to maintain a constant carrier density in an SOA used for boosting the power of multicarrier signals at the transmitter.

6.1.1 Envelope Tracking SOA System Model

As mentioned in section 5.1 Envelope tracking consists in dynamically adjusting the SOA bias current proportionally to the incoming optical signal's envelope with the view to maintain the carrier density at a constant value. In the present chapter, extended results are derived with respect to our previous contributions [Ortiz-Cornejo-17], [Ortiz-Cornejo-18] which considered a similar setup. The ET-SOA system under study in this chapter is explained in Section 5.2, depicted in Fig. 5.1, corresponds to a CO-OFDM transmitter embedding an SOA as a power booster. The baseband multicarrier signal is generated according to a standard CP-OFDM format and a companding

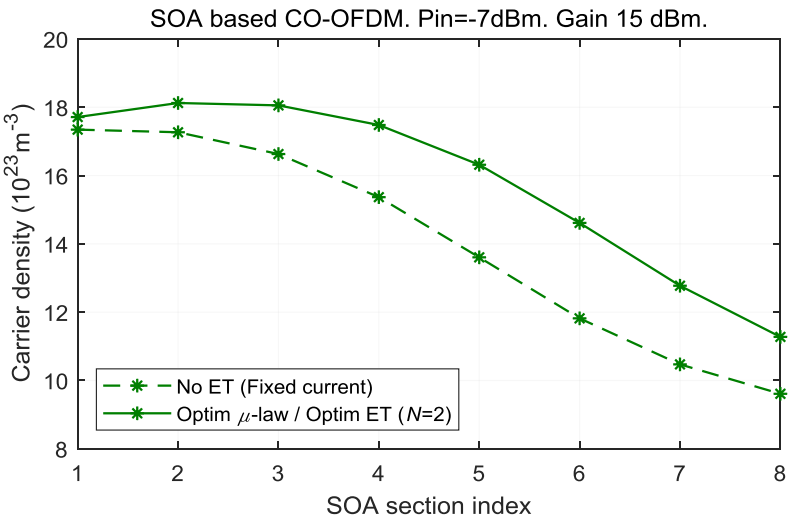

Fig. 6.1 Carrier density variation for one signal sample passing through the SOA active region, for a conventional CO-OFDM transmitter employing SOA as a booster with constant bias current and for an envelope tracking-based transmitter.

transform is then eventually applied so as to reduce the PAPR [Rahmatallah-13]. Nonlinear companding aims at changing the amplitude statistics via a function (.) which has to be inverted at the receiver side for recovering the original signal plus noise. In this chapter, we consider again the μ-law scheme (5-13), as in Section 5.2.In addition to this technique, a hard-clipping scheme will also be considered for comparison purposes. Despite its simplicity and the induced in-band and out-of-band distortions, it has been pointed out that this approach may lead to favorable performance tradeoff [Amiralizadeh-15]. The obtained optical signal is finally boosted by an SOA which operates under envelope tracking regime and the performance is evaluated in a back-to-back configuration (the amplified signal is directly sent to the receiver). At the receiver side, no frequency equalization is performed. In this section, the simulation platform presented in Section 1.6, is considered.

6.2. Carrier Density Analysis Under Envelope Tracking Regime

As mentioned in the previous section, carrier density governs the SOA gain. In this section the carrier density through SOA active region is investigated, and the benefits of envelope tracking for carrier density depletion reduction is shown for an optimal tuning of the ET block (in the case

where the shaping function uses $N = 2$) combined with μ-law companding.

6.2.1 Numerical Simulation

To carry out the numerical simulations, SOA active region has been divided into 8 sections to compute the carrier population inversion which is responsible for the optical amplification process. Simulations were conducted for a frame made of 2^{11} 4-QAM symbols with 128 subcarriers, occupying a bandwidth of 5 GHz to be consistent with our previous studies [Ortiz-Cornejo-17], [Ortiz-Cornejo-18]. Later in the article, a larger bandwidth of 20 GHz will be considered while keeping the same subcarrier spacing (use of 512 subcarriers). Note also that throughout this study the QAM symbols are mapped onto the whole set of subcarriers.

Each performed simulation results in a matrix $N = \left[N_{lm}\right] \in \Re^{L \times M}$ reflecting the carrier density variation along the SOA's M sections for the lth injected signal sample (l = 1, 2, ..., L). A fine analysis of the carrier density dynamics can then be conducted in presence of multicarrier signals, and the effectiveness of some linearization schemes can then be assessed from the device inherent properties.

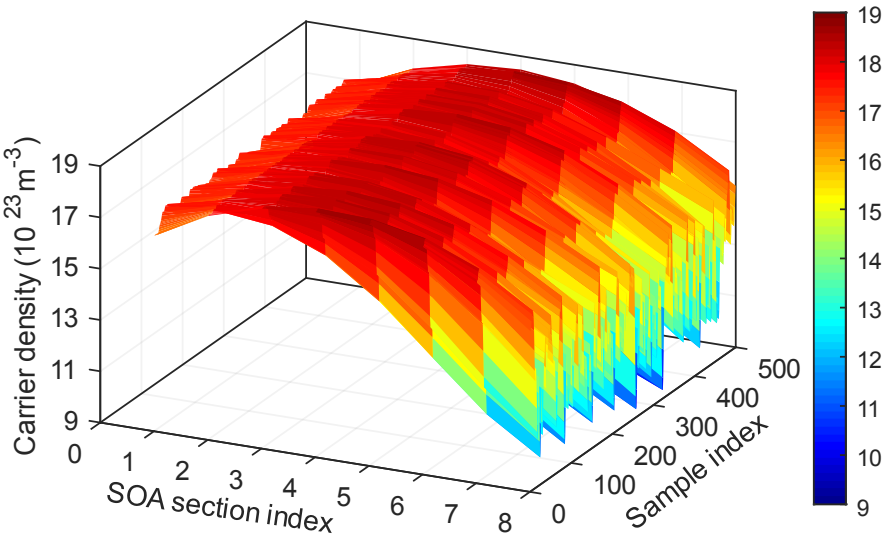

a)

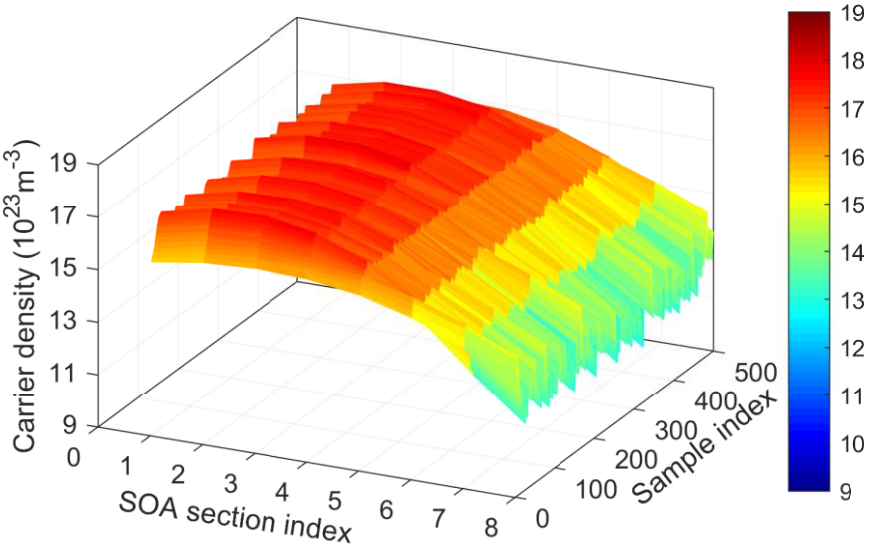

b)

Fig. 6.2 Carrier density variation in the SOA for a CO-OFDM signal made of 500 samples; a) constant bias current, b) non uniform biasing via envelope tracking.

Two cases have been considered for an SOA operating in saturation with an injected optical power of −7 dBm and 15 dB of gain: the first one corresponds to a classical CO-OFDM transmission, with no linearization nor PAPR reduction, yielding an EVM performance[5] of 78 %. In a second case an optimal tuning of the ET-SOA system is adopted with joint use of μ-law

[5] Throughout the manuscript, a normalization by the average constellation power is used for computing the EVM.

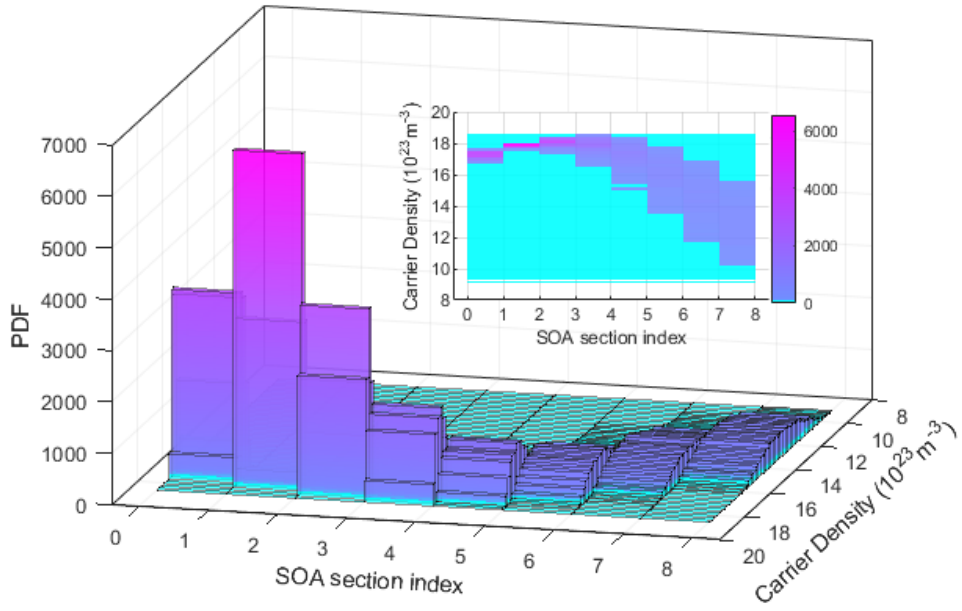

a)

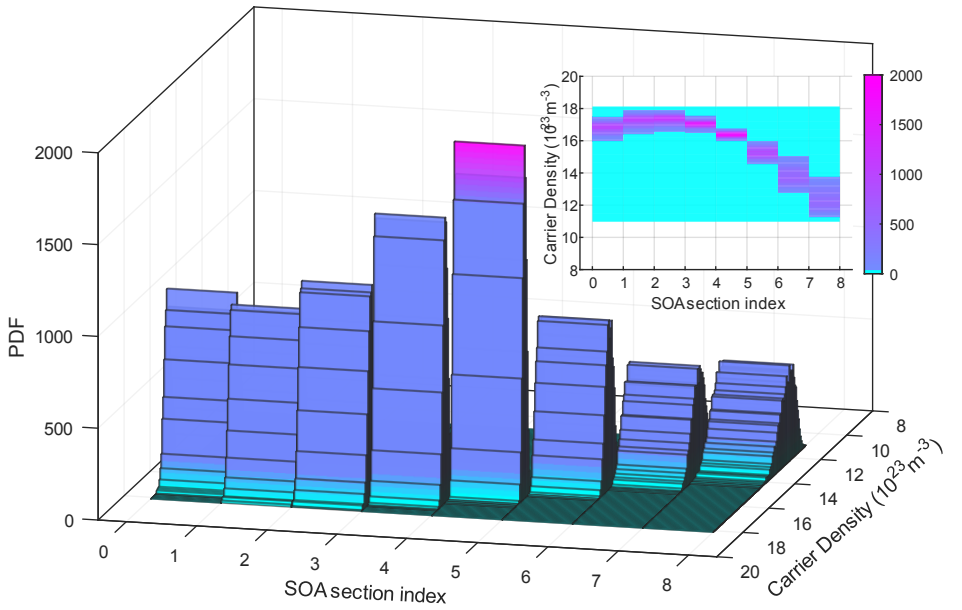

b)

Fig. 6.3 Sample distribution of carrier density against the SOA section. a) constant bias current, b) non uniform biasing via envelope tracking.

companding, resulting in a far better performance with 20% EVM.

The Fig. 6.1 illustrates the carrier density change when one CO-OFDM sample is passing through the SOA active region. If the SOA is driven by a constant bias current, a large decrease of the carrier density can be observed, especially from the third SOA section. This effect is because a signal with higher power will interact with a larger number of excited electrons in the conduction

band, thus resulting in depletion of carrier density and SOA gain. In contrast, a non-uniform bias current via envelope tracking enables a significant reduction of this issue.

Likewise, Fig. 6.2 shows the carrier density variation along the device, as a surface response for 500 CO-OFDM samples injected. The first subplot a) corresponds to the classical implementation using a fixed bias current. A similar behavior as before can be observed, with an almost constant carrier density around $17{,}1.10^{23}\,m^{-3}$ at the input, followed by a slight increase up to $18{,}61.10^{23}\,m^{-3}$ over the next two sections and finally a large carrier depletion beyond the fourth section with a density falling around $9{,}32.10^{23}\,m^{-3}$. In the second subplot b), an optimally tuned ET-SOA implementation is adopted. It can be clearly seen that the device exhibits a totally different behavior, with less spread of the carrier density together with less imbalance between the input ($15{,}59.10^{23}\,m^{-3}$) and output ($11{,}08.10^{23}\,m^{-3}$) values.

A complementary comparative illustration is given in Fig. 6.3, with the sample distributions of the carrier density along the SOA active region, for a CO-OFDM frame of 2^{15} 4-QAM samples. A strong carrier depletion is revealed by subplot a) corresponding to a constant bias current, whereas a more stable carrier density can be observed in the case of an ET-SOA scheme (subplot b).

6.2.2 Gain Influence in an ET-SOA

We now consider the influence of increasing the SOA gain on the carrier density while achieving a non-constant bias current via envelope tracking with a target gain in the range of 15 up to 21 dB. As before, the ET subsystem still operates at its optimum tuning and with $N = 2$. For an injected optical power going from −19 dBm up to −5 dBm, we evaluated the minimum and the maximum carrier density in the active region. The results are depicted in Fig. 6.4. The first subplot shows the minimum value of the carrier density, which is observed at the output of the active

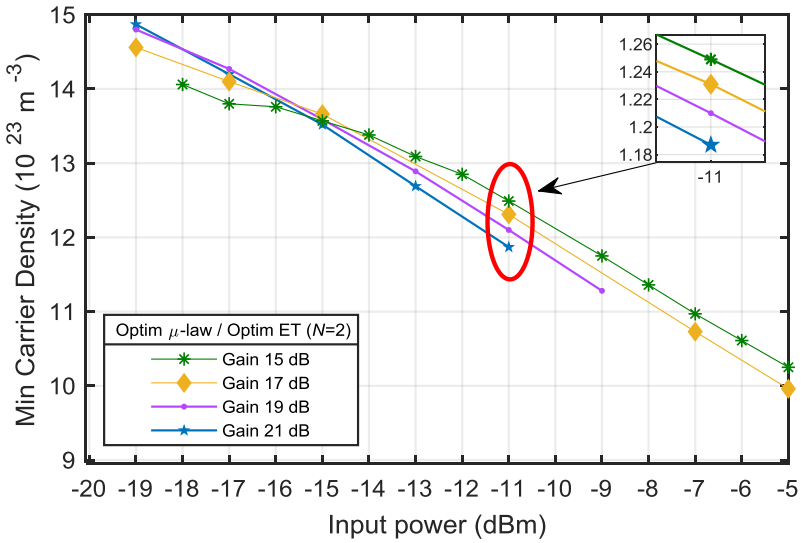

a)

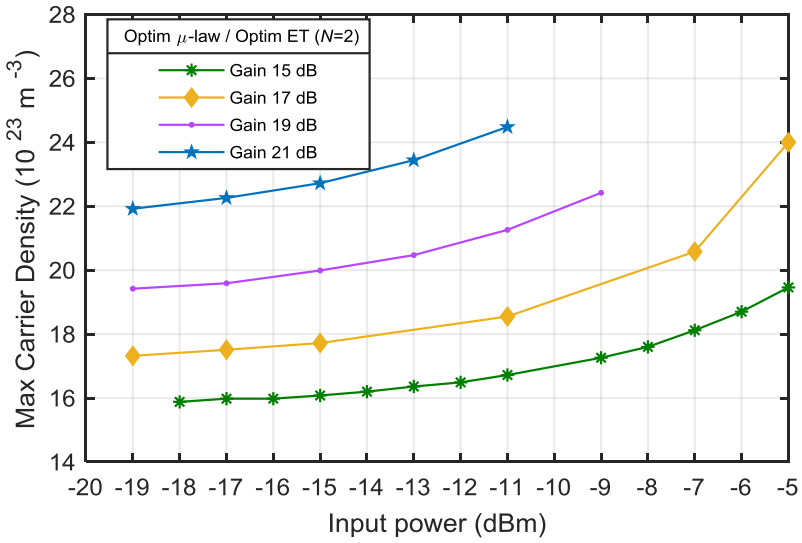

b)

Fig. 6.4 Range of the carrier density in the SOA active region under envelope tracking optimal regime, for different target gain values and 2^{12} CO-OFDM signal samples. a) Minimal carrier density, b) maximal carrier density.

region. It is first seen that going towards high input power translates into accentuated carrier depletion, as a result of more pronounced nonlinear effects. However, an interesting feature of the ET-SOA is that rather close values of the minimum carrier density are obtained despite an increased target gain. The next subplot illustrates the maximum carrier density recorded over the whole active region. Clearly, combating strong nonlinearities tends to require a higher bias current, which turns into a higher maximum carrier density value. Also, a neat difference can be noted

between the curves revealing that boosting the gain translate into a huge increase of the peak carrier density. All these values were obtained by using an optimal design of ET-SOA system following the same optimization algorithm than in [Ortiz-Cornejo-18], but reoptimizing for new target gain values (in our previous work only the value 15 dB has been considered).

6.3. Optimization of the ET-SOA-Based CO-OFDM Transmitter

This section describes the optimization of the envelope tracking subsystem by eventually jointly using a clipping scheme for handling the PAPR, with the view to get the best EVM performance for the CO-OFDM system in a back-to-back setup. The same cost function $J(\boldsymbol{p})$ presented in [Ortiz-Cornejo-18] is adopted, with extended scenarios and investigations,

$$J(\boldsymbol{p}) = \varepsilon\left|G(\boldsymbol{p}) - G^*\right| + EVM(\boldsymbol{p}), \quad \boldsymbol{p} \in \mathcal{D} \tag{6-2}$$

where $\boldsymbol{p} \in \mathcal{D}$ stands for the vector of parameters in the domain $\mathcal{D}$, $G(\boldsymbol{p})$ is the observed SOA gain in steady state, G^* denotes the target gain, $EVM(\boldsymbol{p})$ is the error vector magnitude and ε represents a weighting factor.

Note that the parameters and the corresponding search space may depend on the considered scenario. In the present study, the following four cases have been investigated.

1) ET optimization with no PAPR reduction,

   $\boldsymbol{p} = [\alpha, I_{dc}, N]$,

   $\mathcal{D} = \{0.01 < \alpha < 2,\ 80\ \text{mA} < I_{dc} < 200\ \text{mA}\ 0.8 < N < 3\}$.

2) ET optimization with fixed μ-law nonlinear companding ($\mu = 2$),

   $\boldsymbol{p} = [\alpha, I_{dc}, N]$,

   $\mathcal{D} = \{0.01 < \alpha < 2,\ 80\ \text{mA} < I_{dc} < 200\ \text{mA}\ 0.8 < N < 3\}$.

3) Joint optimization of ET and μ-law nonlinear companding, with fixed envelope shaping ($N = 2$),

   $\boldsymbol{p} = [\alpha, I_{dc}, \mu]$,

   $\mathcal{D} = \{0.01 < \alpha < 2,\ 80\ \text{mA} < I_{dc} < 200\ \text{mA}\ 1 < \mu < 255\}$.

4) Joint optimization of ET and hard-clipping, with fixed envelope shaping ($N = 2$),

   $\boldsymbol{p} = [\alpha, I_{dc}, \gamma]$,

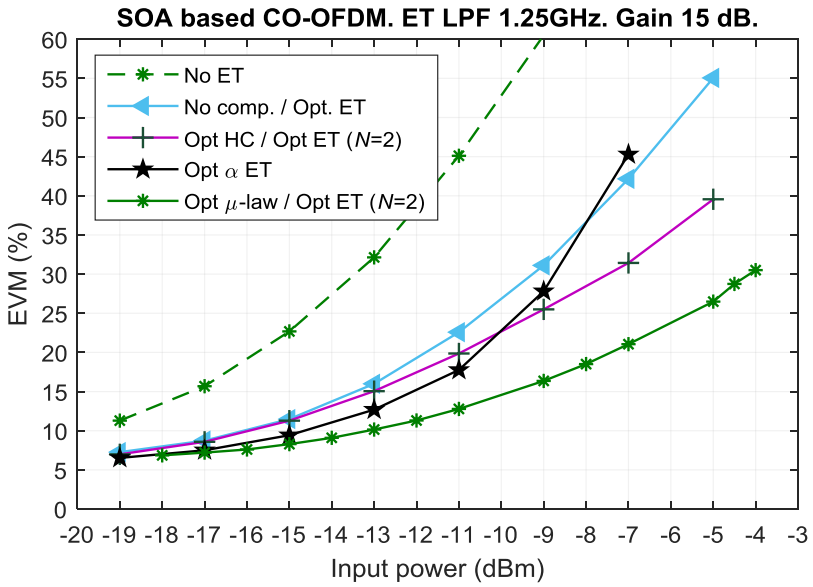

Fig. 6.5 EVM as a function of input optical power for various system setups.

$$\mathcal{D} = \{0.01 < \alpha < 2,\ 80\ \text{mA} < I_{dc} < 200\ \text{mA}\ 1\ \text{dB} < \gamma < 12\ \text{dB}\}.$$

where $\gamma = A'/E\{|x[n]|\}$ stands for the clipping ratio of the baseband OFDM signal $x[n]$, expressed in dB, and A' being the clipping threshold.

Heuristic optimization methods appear to be well suited to solving this nonlinear optimization problem, for their ability to perform derivative free global optimization in presence of many parameters and constraints. In particular, we consider a Particle Swarm Optimization (PSO) scheme, which has proved to be highly effective in many engineering problems while being simple to implement [Rios-13]. The approach, first introduced in [Kennedy-95], consists in emulating a swarm behavior, where one group of individuals follows one of the members through a space looking for the best location. PSO algorithm produces an initial random population of particles where the cost function is evaluated. Then, the particles iteratively move towards the best location by adapting their speed and location until a stopping criterion is reached. In our study, the algorithm was set up with a swarm size of 80, and a stopping criterion of 20 stall generations or a minimum change of 10^{-3} for the objective function. The optimization is performed over the nonsaturated and saturated regions of the SOA, with an input optical power ranging from −19 dBm up to −5 dBm.

As reported in our previous work [Ortiz-Cornejo-18], the third optimization scenario offers the best SOA linearization performance with a huge transmission quality improvement, as far as 8

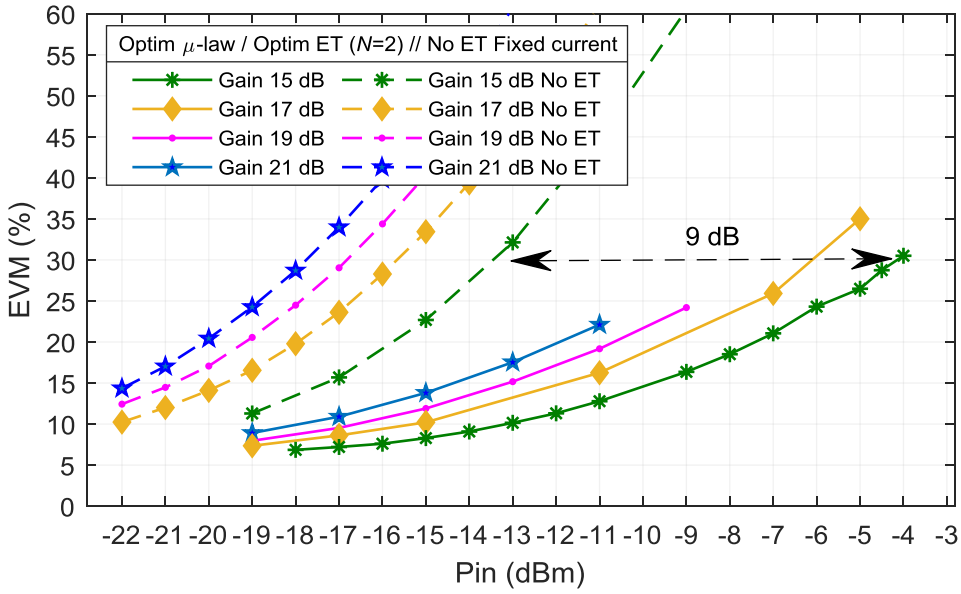

Fig. 6.6 EVM as a function of input optical power using an optimized ET path (scenario #3), for different SOA gain values.

dB power margin at a target BER of 10^{-3} compared to the conventional system implementation (4-QAM/OFDM with no ET nor PAPR reduction), when the SOA operates at a gain of 15 dB. The optimization results are reported in Fig. 6.5, in terms of EVM with respect to input optical power. As can be observed, a large improvement is brought by the nonlinear companding, as for scenario #1 a power penalty of around 5 dB is observed at 30% EVM, in comparison with scenario #3. On this plot we also report the complementary results for the fourth scenario including hard-clipping optimization. A significant EVM improvement can be seen in this case with respect to the conventional system, especially at high input power (enhancement of 2 dB at 30% EVM). We also consider on the same plot the approach described in [Ortiz-Cornejo-17] revisited with an SOA target gain of 15 dB; in this approach, a simple processing is achieved in the ET subsystem with use of the scaling gain α only, and a joint use of a μ-law companding in baseband with $\mu = 2$. If this scheme copes with slight nonlinear impairments, with performance very close to implementation #3 up to a power of −15 dBm, its effectiveness is rapidly decreasing as the operating point moves towards SOA saturation regime.

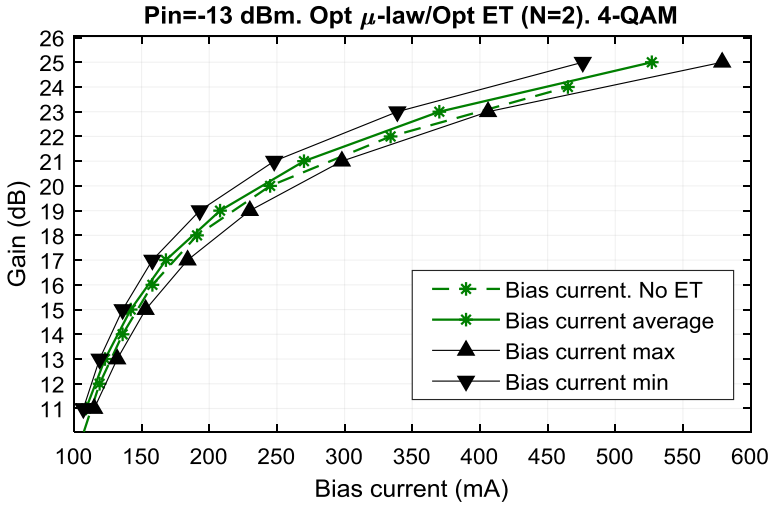

a)

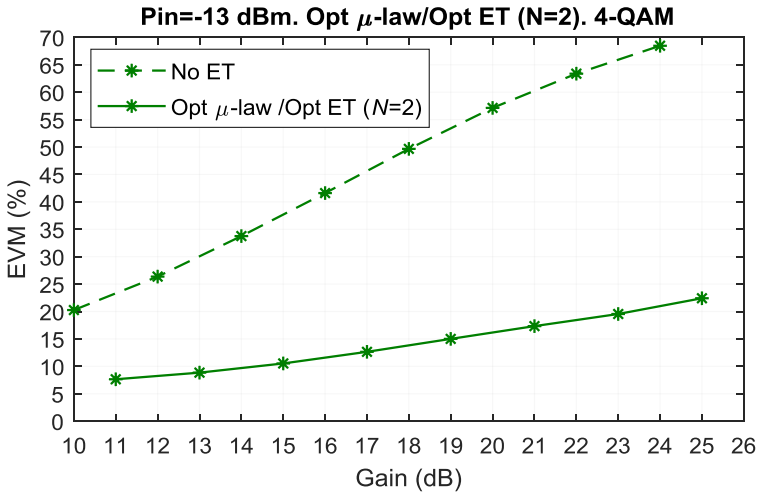

b)

Fig. 6.7 Analysis of optimal ET-SOA in comparison with conventional SOA for an input optical power of −13 dBm. a) Gain as a function of I_{dc} ; b) EVM performance as a function of target gain.

6.3.1 ET-SOA Optimization for Various SOA Target Gains

As shown by the previous simulations, the scheme #3 outperforms other implementations if the SOA operates at a gain of 15 dB. We now investigate the influence of the SOA target gain by considering larger values (17 dB, 19 dB, 21 dB), and therefore higher nonlinearities. For each input optical power and SOA gain, parameters (α, I_{dc}) in the ET block have been reoptimized (with

a fixed envelope shaping, i.e. $N = 2$) jointly with the μ parameter of the nonlinear companding. The obtained results are depicted in Fig. 6.6, in comparison with the standard system operating with constant bias current. The proposed scheme offers a neat EVM improvement and even at a SOA gain of 21 dB the system still operates with a large performance advantage.

Likewise, the same optimization process has been conducted for a fixed input power of −13 dBm while increasing the SOA gain, still in comparison with standard implementation. As displayed by Fig. 6.7a, investigating the relation between the gain and the required bias current, use of the proposed scheme tends to decrease the bias current on average. The second subplot (Fig. 6.7b) exhibits a growing EVM enhancement thanks to optimized ET-SOA scheme as we move towards large SOA gain. The proposed technique still succeeds in linearizing the SOA at a gain of 25 dB, with an EVM less than 25%.

6.3.2 ET-SOA Optimization for 16-QAM/OFDM Format

Until now, only the 4-QAM/OFDM format has been considered in our work. Due to the SOA nonlinear effects, use of a higher modulation order makes the transmission more challenging while meeting a given quality of service. To extend our investigations we now examine the performance of our ET-SOA-based system in presence of 16-QAM/OFDM modulation format, still with the optimization setup #3 which appeared to be the best option in our previous analysis. The results are sketched in Fig. 6.8, in comparison with the 4-QAM/OFDM case. The EVM performance is reported in the first subplot. In absence of linearization, the 16-QAM/OFDM system has poor EVM performance. The theoretical limit of 13% EVM, which should not be exceeded if a 10^{-3} BER is desired [Schmogrow-12], only allows to operate up to −19 dBm. By adopting the optimum ET-SOA tuning (scenario #3), it can be seen that a huge EVM improvement is gained with the possibility to operate up to a power of −12 dBm. The second subplot is devoted to the BER performance. Considering a target BER of 10^{-3}, an increase of around 7 dB of power at the SOA input can be achieved thanks to envelope tracking in the case of 16-QAM/OFDM format.

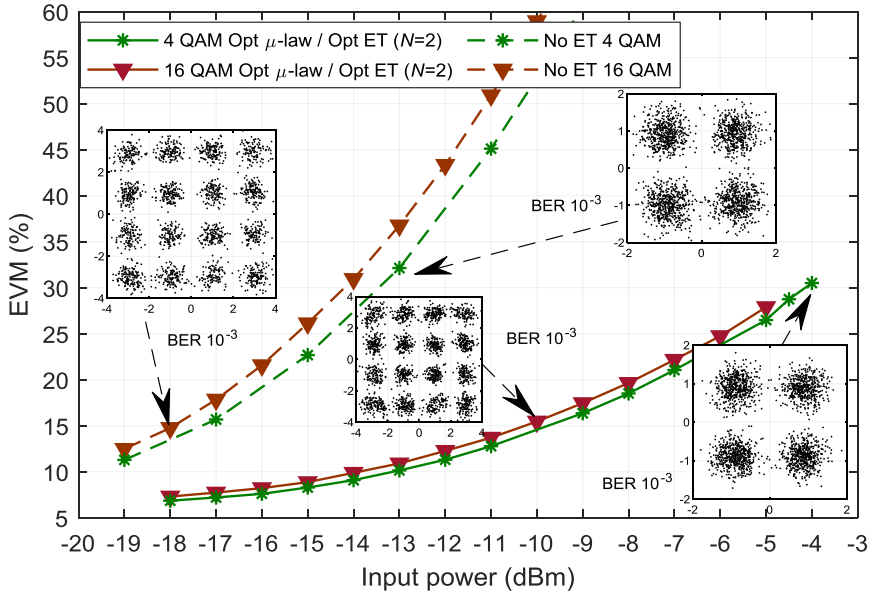

a)

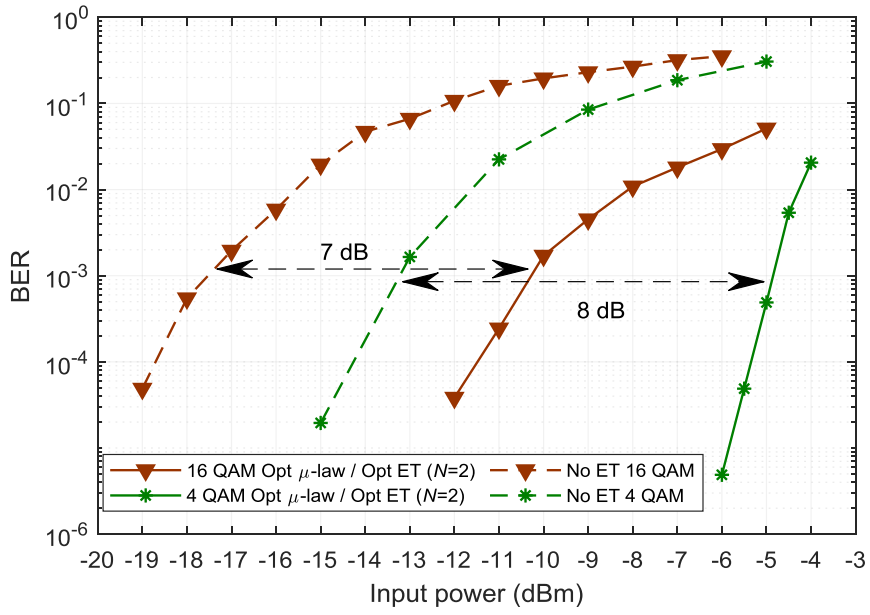

b)

Fig. 6.8 ET-SOA-based transmitter optimal performance with 4-QAM/OFDM and 16-QAM/OFDM modulation formats (use of optimization setup #3). a) EVM performance, b) BER performance

The system behavior is investigated in the frequency domain in Fig. 6.9. The first subplot reveals no significant distortion induced by the amplifier, which is controlled by its ET block. In the second subplot, it can be observed that the average EVM per subcarrier has a relatively low spreading (it should be remembered that there is no use of frequency equalizer here).

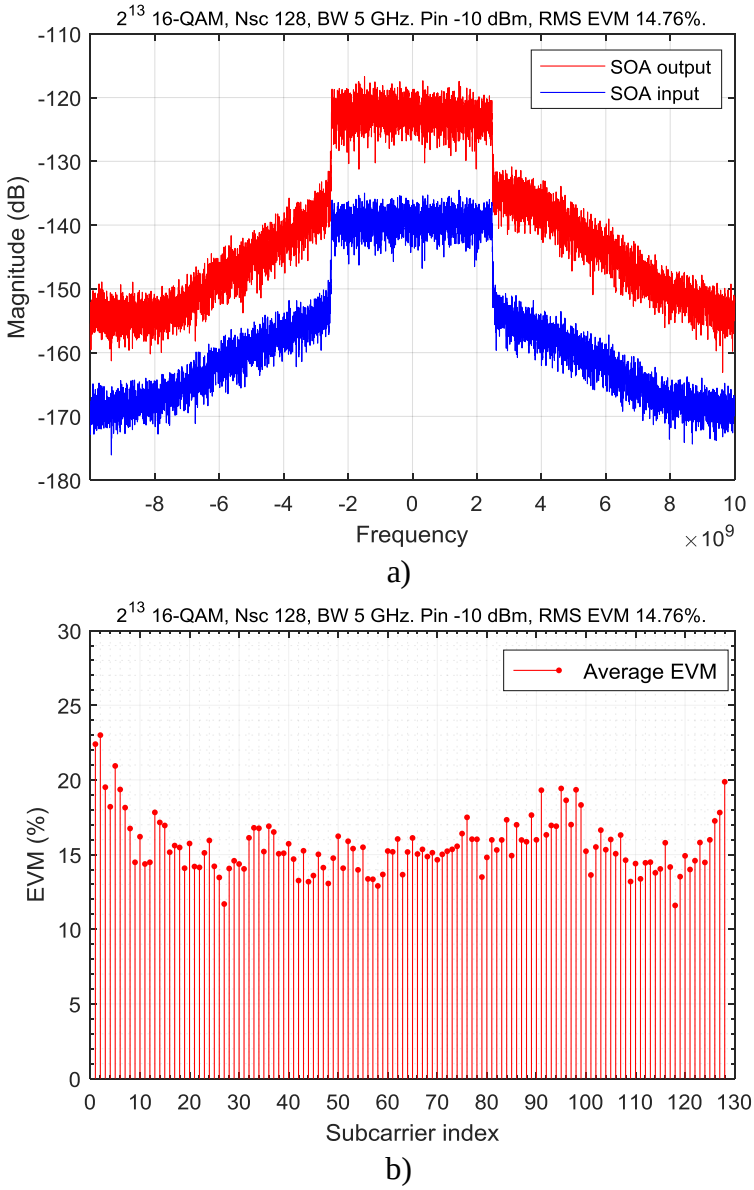

Fig. 6.9 Analysis of optimal ET-SOA in comparison with conventional SOA for an input optical power of −13 dBm. a) Gain as a function of I_{dc} ; b) EVM performance as a function of target gain.

6.4. Robustness Analysis

Keeping the same tuning of the envelope tracking block while operating with different system settings is highly desirable in practice. In this section, we focus first on the influence of the lowpass filter cutoff frequency together with the DAC sampling rate and resolution while

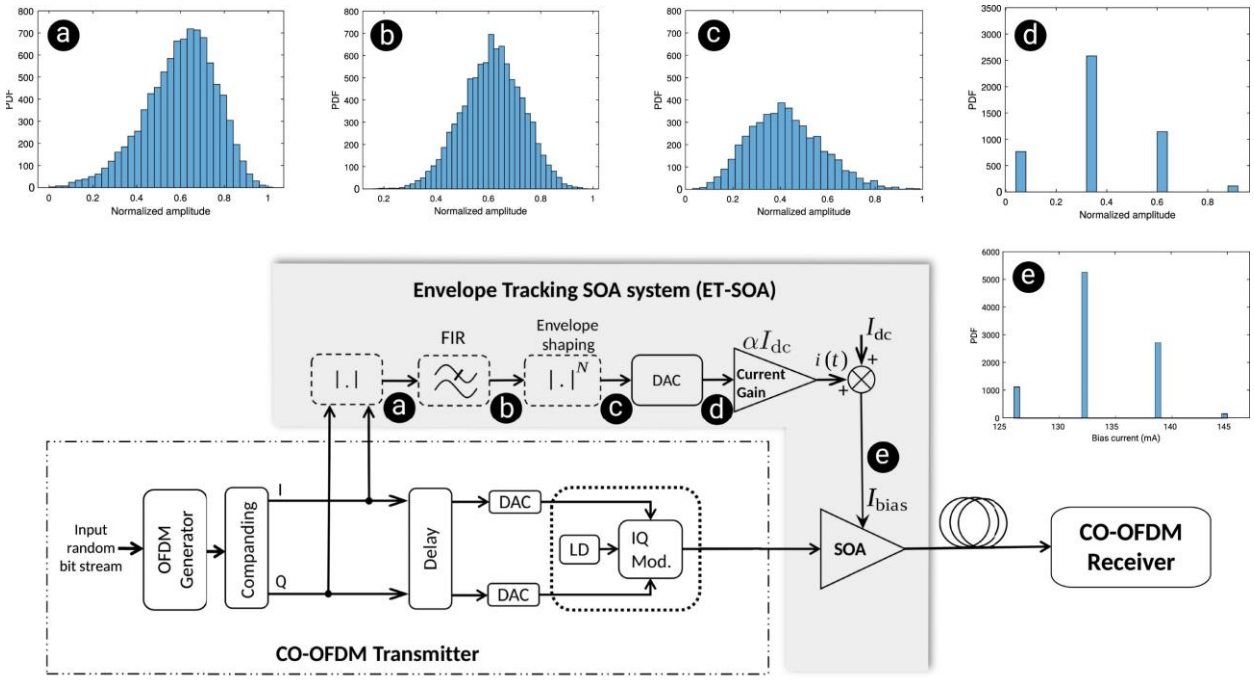

Fig. 6.10 Block-diagram of the Envelope Tracking SOA-based CO-OFDM transmitter with an envelope filtered at 1.25 GHz and using a 2 bits digital-to-analog Converter (the original 4-QAM/OFDM signal has a bandwidth of 5 GHz and 128 subcarriers). The distribution of the signal amplitude is illustrated in various points of the ET block: a) OFDM signal, being eventually companded, b) Bandwidth limited envelope, c) Nonlinearly shaped envelope (N = 2), d) Quantized envelope (2 bits DAC), e) Non-uniform bias current.

preserving the optimum settings of the ET-SOA subsystem (still with scenario #3); then we pursue by investigating the impact of any laser wavelength shift and finally the effect of increasing the bandwidth of the CO-OFDM signal is examined.

6.4.1 Filtering and Digital-to-Analog Converter influence

The results reported so far have been obtained using an infinite precision DAC. But for practical application, a low complexity of implementation must be assessed while maintaining an acceptable quality of service. So, the effectiveness of the ET-SOA scheme designed previously is now evaluated for various DAC sampling rates and resolutions while keeping the same optimal parameters as before (α, I_{dc}, μ, N). The considered DAC is based on a uniform quantization scheme, with input range corresponding to the maximum/minimum signal amplitudes. In this study, the cutoff frequency of the lowpass filter used prior to the conversion will be also changed.

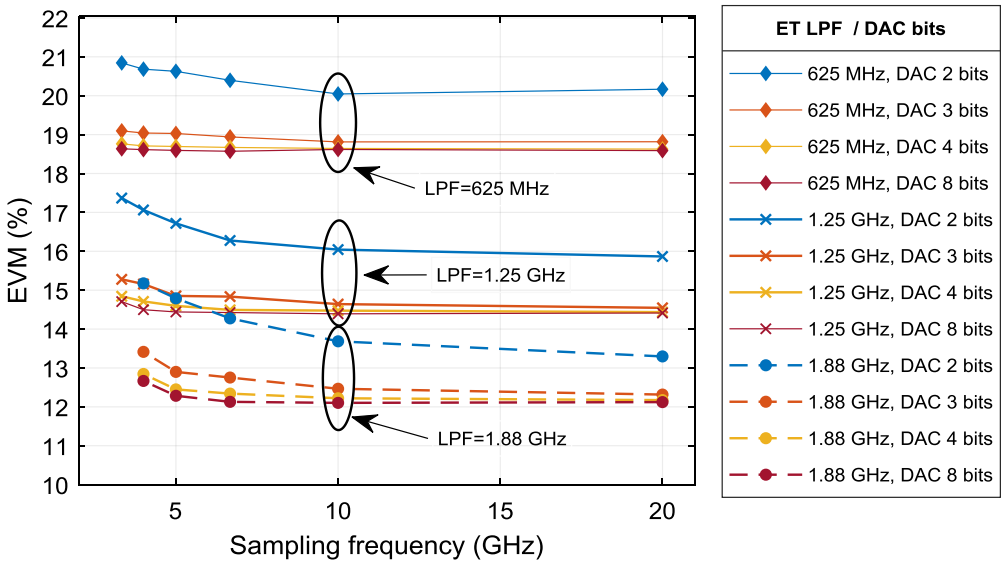

a)

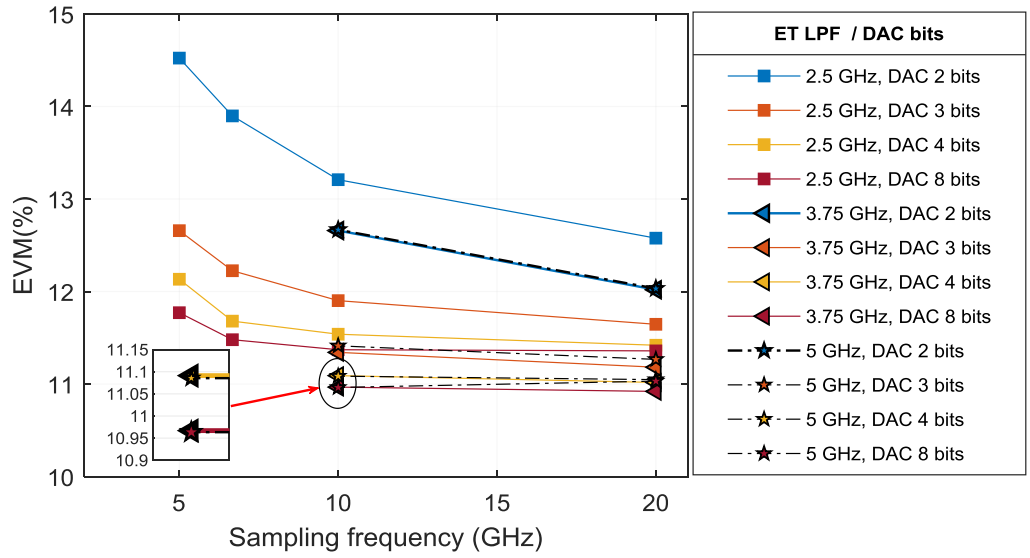

b)

Fig. 6.11 Influence of some ET block parameters (lowpass filter cutoff frequency, DAC sampling rate and resolution) on the proposed ET-SOA-based CO-OFDM transmitter, operating with fixed $\{\alpha, Idc, \mu, N\}$ specification resulting from PSO optimization (scenario #3).

As illustrated in Fig. 6.10 the lowpass filter and the DAC strongly contribute to the envelope signal dynamics modification, specially in the considered example where a 2 bits DAC is used.

The EVM performance of the proposed ET-SOA-based CO-OFDM transmitter (tuned according to scenario #3 described in Section 5.3.1, with 4-QAM/OFDM signal occupying a

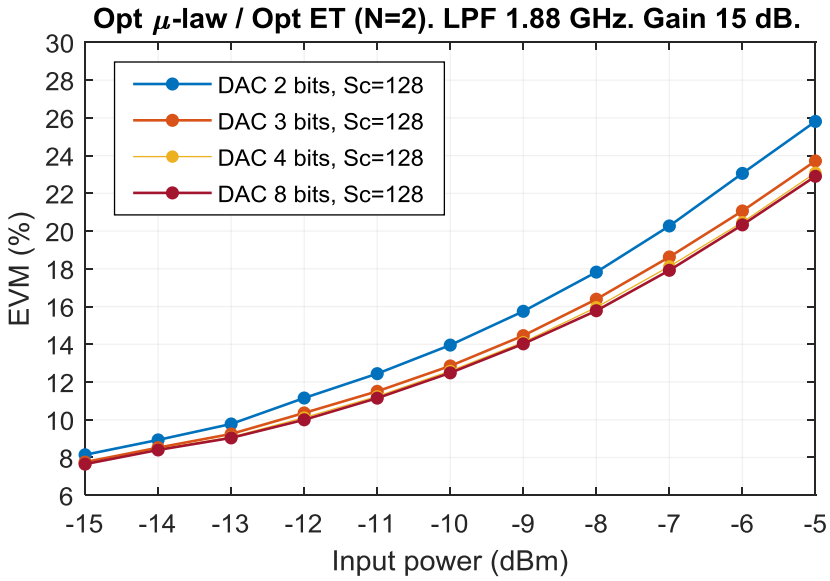

Fig. 6.12 Influence of the DAC resolution (with 10 GHz cutoff frequency and a sampling rate of 1.88 GS/s) on the proposed ET-SOA-based CO-OFDM transmitter EVM performance, as a function of input optical power. The system operates with fixed $\{\alpha, Idc, \mu, N\}$ specification resulting from PSO optimization (scenario #3). The SOA operates at a gain of 15 dB, with an input optical power of –10 dBm.

bandwidth of 5 GHz with 128 subcarriers) in presence of filter cutoff frequency, DAC sampling rate and resolution changes is studied in Fig. 6.11.

Overall the system exhibits a good robustness to the parameters changes, but it is clear that a very slow envelope, resulting from a filtering at 625 MHz, does not lead to suitable EVM performance. For the lowest complexity implementation (filter cutoff frequency at 625 MHz, sampling frequency of 1.25 GHz and 2 bits DAC), an EVM of 21% is obtained. Increasing the sampling rate and the number of bits tends to lower EVM (as it is the case for all the filter bandwidth values) but the too slow envelope cannot fulfill the objective of a constant carrier density in the SOA active region. A decent performance is observed once the filter bandwidth is above 1.25 GHz, provided that the DAC has at least 3 bits. Among the various combinations, a good complexity/performance tradeoff may be achieved for 1.88 GHz filter cutoff frequency. Fig. 6.12 gives a complementary insight into this setup, for a 10 GS/s sampling rate, with the variation of EVM against SOA input optical power, for various DAC resolutions.

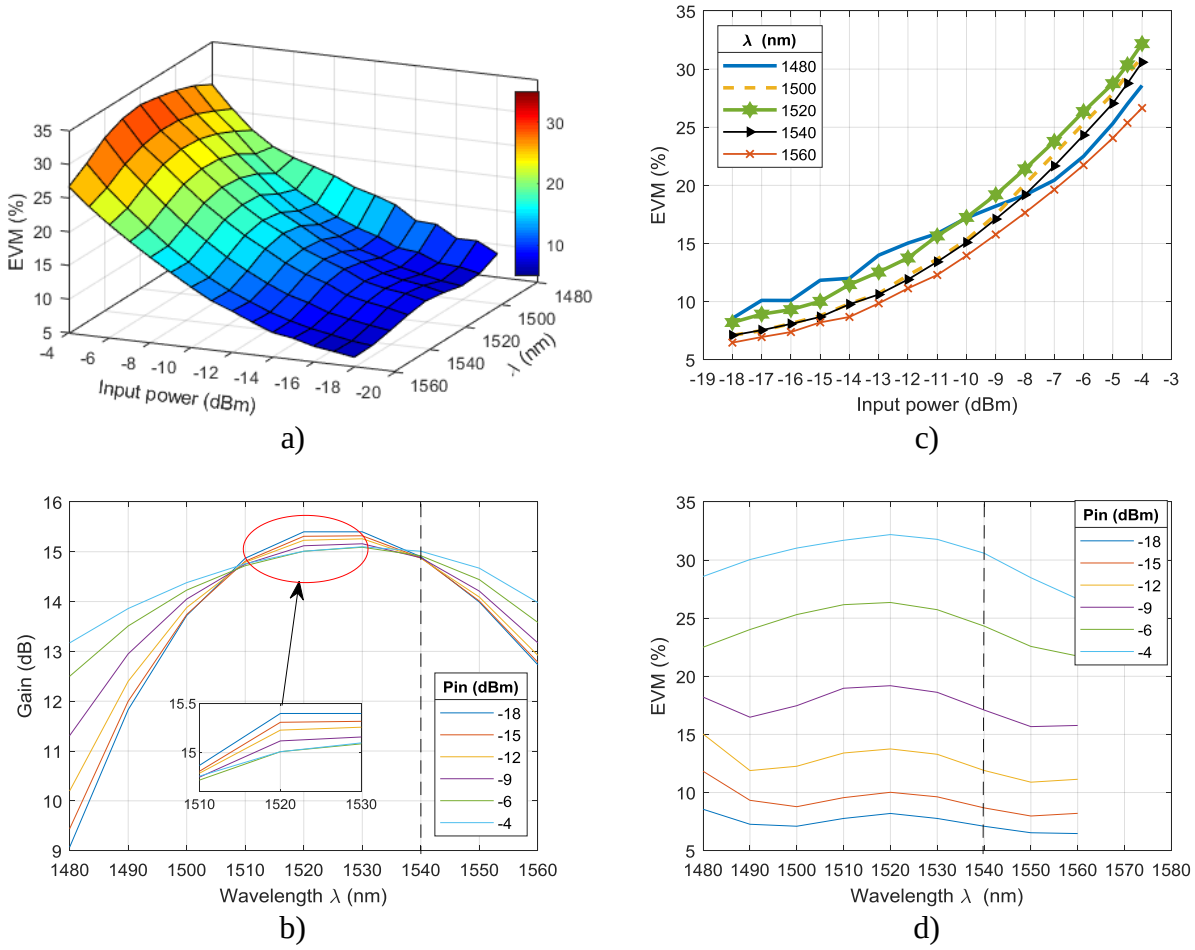

Fig. 6.13 Wavelength shift influence on the μ-law/ET-SOA system optimized at 1540 nm. a) EVM surface against injected input power and laser wavelength λ, b) EVM as a function of input power for different laser wavelength λ. c) EVM as a function of . λ for different input powers. d) SOA gain against wavelength for different input power levels.

6.4.2 Laser Wavelength Shift Influence

We now investigate the impact of a laser wavelength shift on the proposed μ-law/ET-SOA-based CO-OFDM transmitter while keeping the previous optimal settings calculated at the wavelength of 1540 nm with a target gain of 15 dB. As a result of the wavelength shifting, in the interval [1480, 1560] nm, the SOA gain will no longer meet the initial constraint imposed for the optimization when the input optical power is changed from – 18 dBm up to – 4 dBm. The obtained results are reported in Fig. 6.13. In the first subplot a), the EVM performance can be observed as

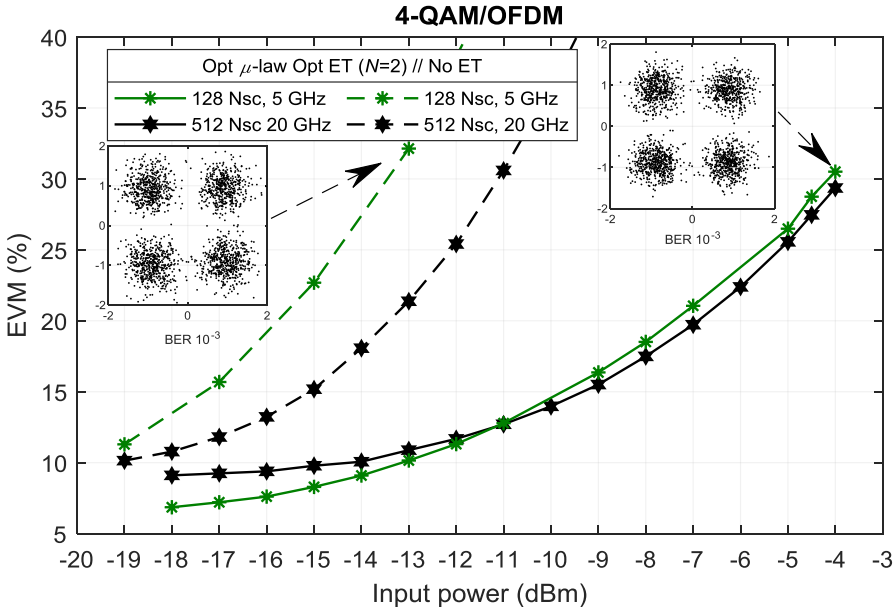

a)

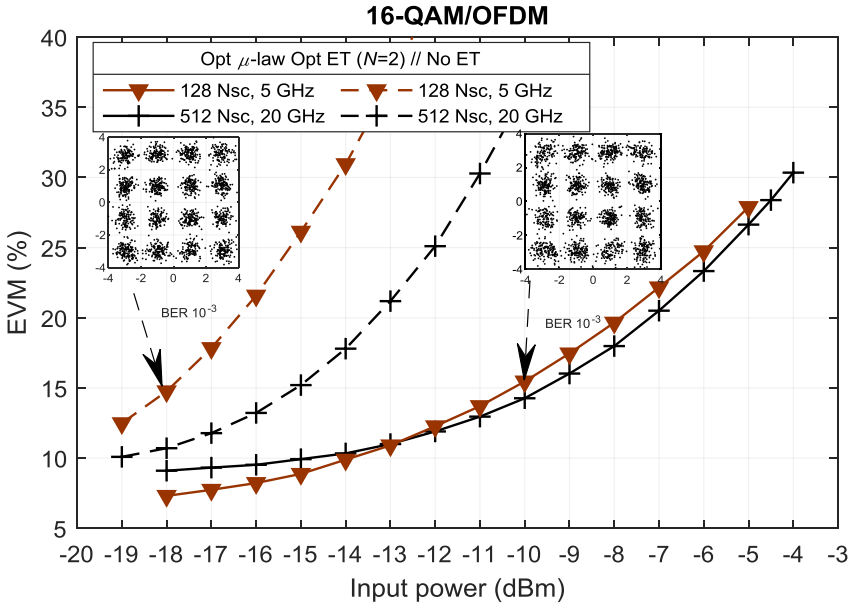

b)

Fig. 6.14 Influence of an increased OFDM signal bandwidth (20 GHz bandwidth, the ET-SOA subsystem being optimized at 5 GHz). a) 4-QAM transmission, b) 16-QAM transmission.

a surface against wavelength λ and SOA input optical power. For a better perception the two following subplots (b, c) give bidimensional representations, revealing a good robustness against the wavelength variation. Over the considered range of input power, it can be seen that the EVM increase remains below 5%, compared to the original system optimized at 1540 nm. A slight EVM

improvement can possibly be obtained depending on the SOA gain which both depends on the wavelength and the SOA input power. The EVM variation against the wavelength shift tends to become more pronounced as we move towards high input optical power. What can be also observed in a last subplot, showing the SOA gain versus wavelength for various input power values, is that a relatively symmetrical behavior occurs for the gain around 1520 nm, which yields the gain peak of the amplifier. In addition, it can be seen that the gain values around this wavelength value are close to the target of 15 dB initially considered for tuning the ET sub-system.

6.4.3 OFDM Signal Bandwidth Influence

5-GHz bandwidth may be too narrow for some coherent applications, so we conducted additional simulations at a larger bandwidth of 20 GHz for the OFDM signal to be transmitted, while keeping the same subcarrier spacing. This translates into a higher transmission speed, going up to 71 Gb/s for the 16-QAM case. As can be clearly seen in Fig. 6.14, the ET-SOA subsystem still offers interesting performance with no need of reoptimizing the system parameters when the electrical bandwidth is changed.

6.5. Conclusions

In this chapter is devoted to the optimization of the ET sub-system for OFDM signals. Moreover, the joint use of a PAPR reduction via hard-clipping or μ-law soft-clipping is considered. Extensive simulations performed with a precise SOA model revealed that the proposed μ-law/ET scheme reduces the carrier density variation inside the SOA, which translates into a large performance increase compared to the standard system using no linearization nor PAPR reduction: up to 8 dB (resp. 7 dB) BER improvement can be achieved via the proposed scheme in the case of 4-QAM/OFDM (resp. 16-QAM/OFDM). The envelope tracking block has also shown to be robust against a wavelength shifting or some parameter changes (lowpass filter cutoff frequency, DAC characteristics or OFDM signal bandwidth) in the ET block. In particular, it was shown that even an envelope quantized with 2 bits still enables favorable performance. Hence, ET is an attractive solution for SOA linearization with interesting complexity/performance tradeoff and some flexibility.

General Conclusions

Due to the highly increment in requirements for high data-rates in communication systems, orthogonal frequency division multiplexing (OFDM) has been exhaustively researched over the last decade, and also has pointed out as a good candidate for the next generation of optical communications systems. Hence, it is attractive to search for novel techniques that increase performance, reduce PAPR, and thus prevent nonlinearities in optical power amplifiers such as SOA's. Through this doctoral dissertation an optimal tuned envelope tracking system has been developed and demonstrated, through numerical assessment, for coping with nonlinear impairments due to an SOA, as a power booster, in a CO-OFDM transmitter.

In Chapter 1, an introduction of OFDM system has been presented. The most important steps in digital signal processing to generate the OFDM signal has been described. Also, main drawbacks in OFDM signals such as PAPR, has been discussed. Associated to PAPR reduction techniques, the nonlinear companding methods are shown as more suitable due to their low computational complexity to be implemented.

Also, in Chapter 1, a SOA based CO-OFDM simulation platform was described. The proposed simulation platform allows to customize their features to test different companding and linearization methods thanks to the flexibility given by Matlab coding. This simulation platform was used through all the simulation presented in this dissertation for the numerical assessment of different techniques to improve system's performance.

Chapter 2 presented an overview of the companding methods including the most recent nonlinear companding methods such as Wang's nonlinear companding transform WNCT [Wang-13]. A nonlinear regression function for each WNCT optimized parameter was proposed. The EVM curves were obtained by simulations showing slight improvements in the SOA-based CO-OFDM. Given these results, the search of optional linearization methods was conducted and the results were addressed in the following chapters.

In order to understood how SOA's performance is affected by the multicarrier signals, the Chapter 3 reveals how the bias current and the input power affects the SOA performance in terms of EVM, output power, and gain. Also, different scenarios of operating conditions were presented

as well as some closed form models are proposed. These models would allow to dynamically control the bias current to obtain the best results within each operating scenario to achieve linearization on SOA based CO-OFDM system.

Linearization of optical amplifier is a critical issue to enhance the performance on a CO-OFDM transmitter. Envelope based methods are a well-known technique to solve power management and linearization of power amplifiers in radiofrequency OFDM systems. In chapter 4 the main characteristics of power efficiency and linearity methods in an RF power amplifier have been studied. It is proposed that the ET approach could be adapted to SOA amplifiers to improve their linearity and reduce nonlinear distortion. Then, a first approach of envelope tracking have been studied for mitigating the transmission impairments.

Chapter 5 is devoted to enhancing the performance and flexibility of the ET technique reported in [Ortiz-Cornejo-17] for linearizing an SOA-based CO-OFDM transmitter. An evolutionary optimization algorithm has been used to reach the optimal ET-SOA in joint with μ-law nonlinear companding. Objective function and optimization setup has been exposed. Three different ET-SOA settings have been examined in this chapter, with successful results. The third scheme, optimized μ-law/ET-SOA, offers the best BER performance gain with reduced current injection. Despite of that an extensively numerical assessment is necessary to ensure the system robustness.

Finally, in chapter 6 several simulations were performed with the proposed ET-SOA system. This scheme reduces the carrier density variation inside the SOA, which translates into a large performance increase compared to the standard system. BER improvement via the optimal tuned ET/SOA scheme in the case of 4-QAM/OFDM (resp. 16-QAM/OFDM), was illustrated. Also, ET-SOA has shown to be robust against a wavelength shifting or some parameter changes (lowpass filter cutoff frequency, DAC characteristics or OFDM signal bandwidth) in the ET block.

In this doctoral dissertation, a classical OFDM format with cyclic prefix (CP-OFDM), has been adopted, but these results may be beneficial for other researchers interested in more recent multicarrier waveforms or any other non-constant envelope waveforms. The proposed approach is not limited to use nonlinear companding transforms; any other PAPR reduction method may be adopted for meeting the specific application constraints.

As possible future work, it is suggested to develop the ET-SOA system as an in-line amplifier. In this case, a photodetector would be necessary to generate the electrical envelope

signal. This approach would give more insights about the channel impairments and the effects induced by the photodetector and the optical fiber

Another possibility of extended work is to use a digital predistortion technique to alleviate the memory effects on SOA, emulating the receiver and the channel under more realistic conditions.

Regarding the optimization of the proposed approach ET-SOA, is highly convenient to develop a real time optimization algorithm to evolve the system toward to an active learning system, which permits continuous auto-tuned ET-SOA parameters, reaching the optimal operation point in a few tens of iterations.

Finally, the ET-SOA hardware implementation for proof of concepts experimentation should be conducted to ensure the reliability of the model as a prototype under real conditions.

Conclusiones Generales

Debido al alto incremento en las necesidades de alta velocidad de intercambio de datos en los sistemas de comunicaciones, la modulación de OFDM ha sido exhaustivamente estudiada durante la última década, también ha sido señalada como una buena candidata para la siguiente generación de sistemas de comunicaciones ópticas. Siendo así, es atractivo llevar a cabo la búsqueda de técnicas novedosas para incrementar el desempeño, reducir el PAPR, y por lo tanto prevenir no linealidades en los amplificadores de potencia ópticos como el SOA. A través de esta disertación doctoral un sistema optimizado de rastreo de envolvente ha sido desarrollado y demostrado, usando métodos de evaluación numéricos, para lidiar con las distorsiones no lineales inducidos por el SOA, en su función como amplificador de potencia, en un transmisor CO-OFDM.

El Capítulo 1, presenta una introducción al sistema OFDM. También se describen los pasos más importantes en el procesamiento digital para generar la señal OFDM. Igualmente, las principales desventajas en las señales OFDM como el PAPR se han discutido. Asociado a las técnicas de reducción de PAPR, se muestran los métodos de compensación no lineal como los más adecuados debido a su baja complejidad de implementación a nivel computacional.

En el mismo Capítulo 1 se ha descrito la plataforma de simulación del sistema CO-OFDM basado en SOA como amplificador de potencia, la cual ha sido usada en todas las simulaciones presentadas en esta tesis para la evaluación numérica de todas las técnicas para mejorar el comportamiento del sistema.

En el Capítulo 2 se presentó un compendio de los métodos de compensación, enfatizando en los más recientes métodos de compensación no lineal como la transformada de compensación no lineal de Wang WNCT [Wang-13]. Una función de regresión no lineal para cada parámetro optimizado de la WNCT ha sido propuesta. Las curvas de EVM fueron obtenidas por simulaciones, mostrando pequeñas mejoras en sistema CO-OFDM amplificado por SOA. Dados los resultados anteriores se buscaron métodos de linealización alternativos y serán mostrados en los próximos capítulos.

Con el fin de entender cómo el comportamiento del SOA es afectado por las señales multi portadora, en el Capítulo 3 se mostró cómo la corriente de bias y la potencia de entrada afectan el rendimiento del SOA en término del EVM, potencia de salida, y ganancia. Además, diferentes

escenarios de operación fueron presentados y algunos modelos de forma cerrada fueron propuestos. Estos modelos permiten controlar de forma dinámica la corriente de bias en función de la potencia de entrada para obtener el mejor resultado dentro de cada escenario de operación, buscando alcanzar la linealización del sistema CO-OFDM basado en SOA.

La linealización del amplificador óptico es un asunto crítico para elevar el rendimiento en un transmisor CO-OFDM basado en SOA. Los métodos basados en envolvente son una técnica muy bien conocida para resolver el manejo de potencia y linealización de amplificadores de potencia en sistemas de radiofrecuencia modulados por OFDM. En el Capítulo 4 se estudiaron las principales características de los métodos de eficiencia de potencia y linealización en amplificadores de potencia en RF. Se encontró que el método de ET puede ser adaptado para amplificadores SOA para mejorar su linealidad y por ende reducir sus distorsiones no lineales. Es por eso que se propuso un primer enfoque de aplicación de ET para mitigar los errores en la transmisión del sistema.

El Capítulo 5 se enfocó en mejorar el comportamiento y la flexibilidad de la técnica de ET propuesta en [Ortiz-Cornejo-17] para linealización del sistema CO-OFDM basado en SOA. Se expuso un algoritmo de optimización para alcanzar el punto óptimo de operación del sistema ET-SOA in conjunto con la función de compensación no lineal μ-law. Tres diferentes configuraciones de ET-SOA se examinaron en este capítulo, con resultados satisfactorios. La tercera configuración, optimización de μ-law/ET-SOA, ofreció el mejor rendimiento de la ganancia de BER con reducción de inyección de corriente de bias. A pesar de eso, una extensa evaluación numérica es necesaria para asegurar la robustez del sistema.

Finalmente, en el Capítulo 6 múltiples simulaciones fueron realizadas con el sistema ET-SOA propuesto. Este esquema reduce la variación en la densidad de portadores dentro del SOA, lo cual se traduce en el incremento del rendimiento comparado con el sistema tradicional. También se mostraron las mejoras en la reducción del BER cuando se utilizó el sistema óptimo ET-SOA en el caso de 4-QAM/OFDM (16 QAM/OFDM respectivamente). Así mismo se mostró la robustez del sistema ET-SOA optimizado contra el desplazamiento de la longitud de onda de la señal, o al cambio de otros parámetros (frecuencia de corte del filtro pasa bajas, características del DAC o ancho de banda de la señal OFDM) en el bloque del sistema ET.

En esta disertación doctoral un formato clásico de OFDM con prefijo cíclico (CP-OFDM), ha sido adoptado, pero estos resultados pueden ser benéficos para otros investigadores interesados

en formas de onda multiportadora más recientes o en alguna otra forma de onda de envolvente no constante. El método propuesto no está limitado para el uso de transformadas de compensación no lineales; cualquier otro método de reducción de PAPR puede ser adoptado para ajustarse a especificaciones específicas de restricción.

Como posible trabajo a futuro, se sugiere analizar el sistema ET-SOA como amplificador en línea. En este caso se vuelve necesario usar un fotodetector para detectar y generar la señal eléctrica de la envolvente de la señal transmitida. Este nuevo escenario daría una visión sobre los efectos del canal de transmisión inducidos por el fotodetector y la fibra óptica. Otra posibilidad es usar técnicas de predistortion digital para reducir efector de memoria en el SOA, y considerar extender el presente trabajo emulando el receptor y el canal de transmisión bajo condiciones más realistas.

En relación a la optimización del sistema propuesto ET-SOA, es muy conveniente diseñar un algoritmo de optimización en tiempo real, lo cual permita evolucionar el sistema hacia un sistema de aprendizaje activo, que favorezca la auto sintonización continua de los parámetros del ET-SOA, alcanzando así la operación optima en unas cuantas decenas de iteraciones.

Finalmente, se vuelve necesario la implementación en hardware del ET-SOA, de manera que pueda realizarse la experimentación necesaria para asegurar la confiabilidad del modelo como prototipo bajo condiciones más reales.

.

Appendix

A. LIST OF INTERNAL RESEARCH REPORTS

1) J. C. Ortiz, J. A. Pardiñas-Mir, and S. Azou, "An introduction to peak to average power ratio in orthogonal frequency division multiplexing," Internal Report *PhDEngScITESO-15-10-R*, ITESO, Tlaquepaque, Mexico, Aug. 2015.
2) J. C. Ortiz, J. A. Pardiñas-Mir, and S. Azou, "Power management methods for radiofrequency power amplifiers," Internal Report *PhDEngScITESO-16-24-R*, ITESO, Tlaquepaque, Mexico, Dec. 2016.
3) J. C. Ortiz, J. A. Pardiñas-Mir, and S. Azou, "Companding techniques to reduce nonlinearities in orthogonal frequency division multiplexing systems," Internal Report *PhDEngScITESO-17-14-R*, ITESO, Tlaquepaque, Mexico, May. 2017.
4) J. C. Ortiz, J. A. Pardiñas-Mir, and S. Azou, "On nonlinear companding optimization over a SOA-based CO-OFDM system," Internal Report *PhDEngScITESO-17-33-R*, ITESO, Tlaquepaque, Mexico, Nov. 2017.
5) J. C. Ortiz, J. A. Pardiñas-Mir, and S. Azou, "On envelope tracking for SOA amplification of multicarrier signals," Internal Report *PhDEngScITESO-18-20-R*, ITESO, Tlaquepaque, Mexico, Jun. 2018.
6) J. C. Ortiz, J. A. Pardiñas-Mir, and S. Azou, "An improved envelope tracking SOA amplifier for CO-OFDM transmission," Internal Report *PhDEngScITESO-18-24-R*, ITESO, Tlaquepaque, Mexico, Aug. 2018.
7) J. C. Ortiz, J. A. Pardiñas-Mir, and S. Azou, "Characterization of the bias current behavior in a SOA for linearizing amplification in a CO-OFDM system," Internal Report *PhDEngScITESO-18-32-R*, ITESO, Tlaquepaque, Mexico, Dec. 2018.
8) J. C. Ortiz, J. A. Pardiñas-Mir, and S. Azou, "A numerical assessment of an effective envelope-tracking semiconductor optical amplifier design for coherent-optical OFDM transmission," Internal Report *PhDEngScITESO-19-15-R*, ITESO, Tlaquepaque, Mexico, Sep. 2019.
9) J. C. Ortiz, J. A. Pardiñas-Mir, and S. Azou, "Simulation platform for a semiconductor optical amplifier (SOA) based coherent optical orthogonal frequency division multiplexing (CO-OFDM) system," Internal Report *PhDEngScITESO-19-17-R*, ITESO, Tlaquepaque, Mexico, Oct. 2019.

B. LIST OF PUBLICATIONS

B.1. JOURNAL PAPER

1) J. C. Ortiz-Cornejo, P. Morel, S. Azou, and J. A. Pardiñas-Mir, "A numerical assessment of an effective envelope tracking semiconductor optical amplifier design for coherent-optical OFDM transmission," *Opt. Commun.*, vol. 454, pp. 1-11, Jan. 2020. (published online: 29 August 2019).

B.2. CONFERENCE PAPERS

1) J. C. Ortiz-Cornejo, S. Bejan, S. Azou, J. A. Pardiñas-Mir, and P. Morel, "On envelope tracking for SOA amplification of multicarrier signals," in *IEEE Int. Symp. Circuits Systems (ISCAS 2017)*, Baltimore, MD, May 2017, pp. 1-4. (ISSN: 2379-447X; ISBN: 978-1-5090-1427-9; e-ISBN: 978-1-4673-6853-7; INSPEC: 17208281; DOI: 10.1109/ISCAS.2017.8050451).
2) J. C. Ortiz-Cornejo, S. Azou, J. A. Pardiñas-Mir and P. Morel, "An improved envelope tracking SOA amplifier for CO-OFDM transmission by using PSO," in *IEEE Latin-American Conf. on Communications (LATINCOM-2018)*, Guadalajara, Mexico, Nov. 2018, pp. 1-5. (ISSN: 2330-989X; p-ISBN: 978-1-5386-6755-2; e-ISBN: 978-1-5386-6754-5; INSPEC: 18419648; DOI: 10.1109/LATINCOM.2018.8613235).
3) J. C. Ortiz-Cornejo, and J. A. Pardiñas-Mir, "Characterization of the Bias Current Behavior in a SOA for Linearizing Amplification in a CO-OFDM System," in *Proceedings of the 16th International Joint Conference on e-Business and Telecommunications (ICETE 2019)*, Prague, Czech Republic, Jul. 2019,pp 243-248. (ISBN 978-989-758-378-0, pages. DOI: 10.5220/0007931502430248)

Bibliography

[Agrell-16] E. Agrell, et al., "Roadmap of optical communications," *Journal of Optics*, vol. 18, no. 6, pp. 1- 40, May 2016.

[Akiyama-07] T. Akiyama, M. Sugawara, and Y. Arakawa, " Quantum-dot semiconductor optical amplifiers," *Proc. IEEE*, vol. 95, no. 9, pp. 1757-1766, Sept. 2007.

[Amari-17] A. Amari, O. A. Dobre, R. Venkatesan, O. S. S. Kumar, P. Ciblat, and Y. Jaouën, "A survey on fiber nonlinearity compensation for 400 Gb/s and beyond optical communication systems," *IEEE Commun. Surveys Tuts.*, vol. 19, no. 4, pp. 3097-3113, Fourth Quarter 2017.

[Amiralizadeh-15] S. Amiralizadeh, A. T. Nguyen, and L. A. Rusch, "Modeling and compensation of transmitter nonlinearity in coherent optical OFDM," *Optics Express*, vol. 23, no. 20, pp. 26192-26207, Oct. 2015.

[Armstrong-09] J. Armstrong, "OFDM for optical communications," *J. Lightw. Technol.*, vol. 27, no. 3, pp. 189-204, Feb. 1, 2009.

[Azou-15] S. Azou, S. Bejan, P. Morel, and A. Sharaiha, "Performance improvement of a SOA-based coherent optical-OFDM transmission system via nonlinear companding transforms," *Optics Communications*, vol. 336, pp. 177-183, Feb. 2015.

[Barry-90] J. R. Barry and E. A. Lee, " Performance of coherent optical receivers," in *Proceedings of the IEEE*, vol. 78, no. 8, pp. 1369-1394, Aug. 1990.

[Bejan-15] S. Bejan, A. Azou, P. Morel, C. Diouf, M. Telescu, N. Tanguy, and A. Sharaiha, "A joint linearization/companding approach for improving a CO-OFDM transmitter," *IEEE Photon. Technol. Lett.*, vol. 27, no. 20, pp. 2162-2165, Jul. 2015.

[Bendimerad-17] D. F. Bendimerad, and Y. Frignac, "Numerical investigation of SOA nonlinear impairments for coherent transmission systems based on SOA amplification," *IEEE J. Lightw. Technol.*, vol. 35, no. 24, pp. 5286-5295, Nov. 2017.

[Bohémond-11] C. Bohémond, P. Morel, A. Sharaiha, T. Rampone, and B. Pucel, "Experimental and simulation analysis of the third-order input interception point in an all-optical RF mixer based on a semiconductor optical amplifier," *IEEE J. Lightw. Technol*., vol. 29, no. 1, pp. 91-96, Jan. 2011.

[Bonk-11] R. Bonk et al., "The input power dynamic range of a semiconductor optical amplifier and its relevance for access network applications," *IEEE Photon. J.*, vol. 3, no. 6, pp. 1039-1053, Dec. 2011.

[Chen-13] H. Chen, J. Yu, J. Xiao, Z. Cao, F. Li, and L. Chen, "Nonlinear effect mitigation based on PAPR reduction using electronic pre-distortion technique in direct-detection optical OFDM system," *Optical Fiber Technology*, vol. 19, no. 5, pp. 387–391, Oct. 2013.

[Connelly-02] M. J. Connelly, *Semiconductor Optical Amplifiers*. Boston, USA: Kluwer, 2002.

[Connelly-98] M. J. Connelly, "Semiconductor optical amplifiers and their applications," in *Conf. Design of Circuits and Integrated Systems*, Madrid, Spain, Nov. 1998.

[Cvijetic-12] N. Cvijetic, "OFDM for next-generation optical access networks," *IEEE J. Lightw. Technol.*, vol. 30, no. 4, pp. 384-398, Feb. 2012.

[Dar-17] R. Dar, and P. J. Winzer, "Nonlinear interference mitigation: methods and potential gain," *IEEE J. Lightw. Technol.*, vol. 35, no. 4, pp. 903-930, Jan. 2017.

[Deb-01] K. Deb, *Multi-Objective Optimization Using Evolutionary Algorithms*. West Sussex, UK: Wiley, 2001.

[Del Marco-14] S. P. Del Marco, "General closed-form family of companders for PAPR reduction in OFDM signals using amplitude distribution modification," *IEEE Trans. Broadcast.*, vol. 60, no. 1, pp. 102-109, Mar. 2014.

[Diouf-17] C. Diouf, M. Younes, A. Noaja, S. Azou, M. Telescu, P. Morel, and N. Tanguy, "Robustness analysis of a parallel two-box digital polynomial predistorter for an SOA-based CO-OFDM system," *Opt. Commun.*, vol. 402, pp. 442-452, Nov. 2017.

[Fitz-07] M. Fitz, *Fundamentals of Communications Systems.* New York: McGraw-Hill, 2007.

[Fujiwara-07] M. Fujiwara and R. Koma, "Long-reach and high-splitting-ratio WDM/TDM-PON systems using burst-mode automatic gain controlled SOAs," *IEEE J. Lightw. Technol.*, vol. 34, no. 3, pp. 901-909, Sept. 2007.

[Ghazisaeidi-11] A. Ghazisaeidi and L. Rusch, "On the efficiency of digital back-propagation for mitigating SOA-induced nonlinear impairments," *IEEE J. Lightw. Technol.*, vol. 29, no. 21, pp. 3331-3339, Aug. 2011.

[Hamze-15] M. Hamze, *Study of Different SOA Structures Impact on the Transmission of IMDD OOFDM Signals*, Ph.D. Thesis, Université de Bretagne Occidentale, Brest, France, 2015, (available at: https://tel.archives-ouvertes.fr/tel-02169590/document).

[Hu-14] M. Hu, Y. Li, Y. Liu, and H. Zhang, "Parameter-adjustable piecewise exponential companding scheme for peak-to-average power ratio reduction in orthogonal frequency division multiplexing systems," *IET Commun.*, vol. 8, no. 4, pp. 530–536, Mar. 2014.

[Huang-04] X. Huang, J. Lu, J. Zheng, K. B. Letaief, and J. Gu, "Companding transform for reduction in peak-to-average power ratio of OFDM signals," *IEEE Trans. Wireless Commun..*, vol. 3, no. 6, pp. 2030–2039, Nov. 2004.

[Jeng-11] S. S. Jeng and J. M. Chen, "Efficient PAPR reduction in OFDM systems based on a companding technique with trapezium distribution," *IEEE Trans. Broadcast.*, vol. 57, no. 2, pp. 291–298, Jun. 2011.

[Jiang-05] T. Jiang, Y. Yang, and Y. Song, "Exponential companding transform for PAPR reduction in OFDM systems," *IEEE Trans. Broadcast.*, vol. 51, no. 2, pp. 244–248, Jun. 2005.

[Jiang-08] T. Jiang and Y. Wu, "An overview: peak-to-average power ratio reduction techniques for OFDM signals," *IEEE Trans. Broadcast.*, vol. 54, no. 2, pp. 257-268, Jun. 2008.

[Keiser-00] G. Keiser, *Optical Fiber Communications.* New York, NY: McGraw-Hill, 2000.

[Kennedy-95] J. Kennedy and R. Eberhart. "Particle swarm optimization," in *Proceedings of the IEEE International Conference on Neural Networks.* Perth, Australia, Nov. 1995, pp. 1942-194.

[Khaleghi-12] H. Khaleghi, *Influence of Semiconductor Optical Amplifiers (SOA) on Coherent Optical-OFDM (CO-OFDM) Transmission System*, Ph.D. Thesis, Université de Bretagne Occidentale, Brest, France, 2012.

[Khaleghi-13] H. Khaleghi, P. Morel, A. Sharaiha, and T. Rampone, "Experimental validation of numerical simulations and performance analysis of a coherent optical-OFDM transmission system employing a semiconductor optical amplifier," *IEEE J. Lightw. Technol.*, vol. 31, no. 1, pp. 161-170, Jan. 2013.

[Kim-11] D. Kim, *et al.*, "Optimization for envelope shaped operation of envelope tracking power amplifier," *IEEE Trans. Microw. Theory Techn.*, vol. 59, no. 7, pp. 1787-1795, Jul. 2011.

[B.Kim-13] B. Kim, J. Kim, D. Kim, J. Son, Y. Cho, J. Kim, and B. Park, "Push the envelope: design concepts for envelope-tracking power amplifiers," *IEEE Microwave Mag.*, vol. 14, no. 3, pp. 68-81, Mar. 2013.

[J.Kim-13] J. Kim, *et al.*, "Optimization of envelope tracking power amplifier for base-station applications," *IEEE Trans. Microw. Theory Techn.*, vol. 61, no. 4, pp. 1620-1627, Apr. 2013.

[Kim-14] J. Kim *et al*., "Analysis of envelope-tracking power amplifier using mathematical modeling," *IEEE Trans. Microwave Theory Tech.*, vol. 62, no. 6, pp. 1352-1362, June 2014.

[Koenig-14] S. Koenig, R. Bonk, H. Schmuck, W. Poehlmann, T. Pfeiffer, C. Koos, W. Freude, and J. Leuthold, "Amplification of advanced modulation formats with a semiconductor optical amplifier cascade," *Optics Express*, vol. 22, no. 15, pp. 17854–17871, Jul. 2014.

[Lange-13] S. Lange, Y. Yoshida, and K. Kitayama, "A low-complexity digital pre-compensation of SOA induced phase distortion in coherent QAM transmissions," in *Optical Fiber Communication Conference and Exposition and the National Fiber Optic Engineers Conference (OFC/NFOEC)*, Anaheim, USA, Mar. 2013, pp. 1-3.

[Li-10] X. Li and G. Li, "Joint fiber and SOA impairment compensation using digital backward propagation," *IEEE Photon. J.*, vol. 2, no. 5, pp. 753-758, Aug. 2010.

[Louët-08] Y. Louët and J. Palicot, "A classification of methods for efficient power amplification of signals," *Ann. Telecommun.*, vol. 63, Issue 7-8, pp. 351-368, May, 2008.

[Molish-11] F. Molisch, Wireless Communications. West Sussex, UK: Wiley – IEEE, 2011.

[Morel-09] P. Morel and A. Sharaiha, "Wideband time-domain transfer matrix model equivalent circuit for short pulse propagation in semiconductor optical amplifiers," *IEEE J. Quantum Electron.*, vol. 45, no. 2. pp. 103-116, Feb. 2009.

[Napoli-18] A. Napoli, et al., "Digital pre-compensation techniques enabling high-capacity bandwidth variable transponders," *Opt. Commun.*, vol. 409, pp. 52-65, Feb. 2018.

[Ng-12] W. P. Ng, A. A. E. Aziz, Z. Ghassemlooy, M. H. Aly, and R. Ngah, "Optimized non-uniform biasing technique for a highspeed optical router to achieve uniform semiconductor optical amplifier gain," *IET Commun.*, vol. 6, no. 5, pp. 484-491, Mar. 2012.

[Ó Dúill-17] S. P. Ó Dúill, P. Landais, and L. P. Barry, "Estimation of the performance improvement of pre-amplified PAM4 systems when using multi-section semiconductor optical amplifiers," *Appl. Sci.*, vol. 7, no. 9, pp. 908-921, Sept. 2017.

[Ortiz-Cornejo-17] J. C. Ortiz-Cornejo, S. Bejan, S. Azou, J. A. Pardiñas-Mir, and P. Morel, "On envelope-tracking for SOA amplification of multicarrier signals," in *IEEE Int. Symp. Circuits Systems (ISCAS 2017)*, Baltimore, MD, May 2017, pp. 1-4.

[Ortiz-Cornejo-18] J. C. Ortiz-Cornejo, S. Azou, J. A. Pardiñas-Mir and P. Morel, "An improved envelope tracking SOA amplifier for CO-OFDM transmission by using PSO," in *IEEE Latin-American Conf. on Communications (LATINCOM-2018)*, Guadalajara, Mexico, Nov. 2018, pp. 1-5.

[Ortiz-Cornejo-20] J. C. Ortiz-Cornejo, P. Morel, S. Azou, and J. A. Pardiñas-Mir, "A numerical assessment of an effective envelope-tracking semiconductor optical amplifier design for coherent-optical OFDM transmission," *Opt. Commun.*, vol. 454, pp. 1-11, Jan. 2020. (published online: 29 August 2019).

[Proakis-02] J. G. Proakis and M. Salehi, *Communications Systems Engineering.* Upper Saddle River, New Jersey: Prentice-Hall, 2002.

[Raab-96] F. H. Raab, "Intermodulation distortion in Kahn-technique transmitters," *IEEE Trans. Microwave Theory Tech.*, vol. 44, no. 12, pp. 2220–2225, Dec. 1996.

[Rahmatallah-13] Y. Rahmatallah and S. Mohan, "Peak-to-average power ratio reduction in OFDM systems: a survey and taxonomy," *IEEE Commun. Surveys Tuts.*, vol. 15, no. 4, pp. 1567-1592, Fourth Quarter 2013.

[Reixats-12] L. N. Reixats, *Performance analysis of optical OFDM transmission systems using PAPR mitigation techniques and alternative transforms*, Master Thesis, Dept. of Teoria del Senyal i Comunicacions, Universitat Politècnica de Catalunya, Barcelona, España, 2012.

[Renaudier-19] J. Renaudier and A. Ghazisaeidi, "Scaling capacity growth of fiber-optic transmission systems using 100 + nm ultra-wideband semiconductor optical amplifiers," *IEEE J. Lightw. Technol.*, vol. 37, no. 8, pp. 1831-1838, Jan. 2019.

[Rios-13] L. M. Rios and N. V. Sahinidis, "Derivative-free optimization: a review of algorithms and comparison of software implementations," *J. Global Optim.*, vol. 56, no. 3, pp. 1247-1293, Jul. 2013.

[Sahin-14] A. Sahin, I. Guvenc, and H. Arslan, "A survey on multicarrier communications: Prototype filters, lattice structures, and implementation aspects," *IEEE Commun. Surveys Tuts.*, vol. 16, no. 3, pp. 1312-1338, Third Quarter 2014.

[Saleh-88] A. A. M. Saleh, R. M. Jopson, and T. E. Darcie, "Compensation of nonlinearity in semiconductor optical amplifiers," *Electron. Lett.*, vol. 24, no. 5, pp. 950-952, Jul. 1988.

[Santa-19] M. D. Santa, C. Antony, G. Talli, and P. D. Townsend, "Variable gain SOA preamplifier for optical equalization of a 25Gb/s burst-mode PON upstream with 10G optics," in: *2019 Optical Fiber Communications Conference and Exhibition (OFC)*, San Diego, CA, USA, Mar. 2019, pp. 1-3.

[Schmogrow-12] R. Schmogrow *et al*., "Error vector magnitude as a performance measure for advanced modulation formats," *IEEE Photon. Technol. Lett.*, vol. 24, no. 1, pp. 61-63, Jan. 2012.

[Sen-11] S. Sen, R. Senguttuvan, and A. Chatterjee, "Environment-adaptive concurrent companding and bias control for efficient power-amplifier operation," *IEEE Trans. Circuits Syst. I, Reg. Papers*, vol. 58, no. 3, pp. 607-618, Mar. 2011.

[Shieh-10] W. Shieh and I. Djordjevic, *OFDM for Optical Communications*. London, UK: Elsevier, 2010.

[Tabatabai-07] F. Tabatabai and H. S. Al-Raweshidy, "Feedforward linearization technique for reducing nonlinearity in semiconductor optical amplifier," *IEEE J. Lightw. Technol.*, vol. 25, no. 9, pp. 2667-2674, Sept. 2007.

[Tiemeijer-96] L. F. Tiemeijer, G. N. van den Hoven, P. J. A. Thijs, T. van Dongen, J. J. M. Binsma, and E. J. Jansen, "1310-nm DBR-type MQW gain-clamped semiconductor optical amplifiers with AM-CATV-grade linearity," *IEEE Photon. Technol. Lett.*, vol. 8, no. 11, pp. 1453-1455, Nov. 1996.

[Wang-05] F. Wang, A. Yang, D. Kimball, L. Larson, and P. Asbeck, "Design of wide-bandwidth envelope-tracking power amplifiers for OFDM applications," *IEEE Trans. Microw. Theory Techn.*, vol. 53, no. 4, pp. 1244-1255, Apr. 2005.

[Wang-12] D. Wang, N. Zou, G. Cui, Y. Yang, Y. Namihira, and Y. Zhang, "Companding scheme for peak-to-average power ratio reduction in optical orthogonal frequency division multiplexing systems," *Optical Review*, vol. 19, no. 6, pp. 371-375, Dec. 2012.

[Wang-13] Y. Wang, J. Ge, L. Wang, J. Li, and B. Ai, "Nonlinear companding transform for reduction of peak-to-average power ratio in OFDM systems," *IEEE Trans. Broadcast.*, vol. 59, no. 2, pp. 369–375, Jun. 2013.

[Wang-14] Z. Wang, *Envelope Tracking*. London, UK: Artech House, 2014.

[Wang-15] Z. Wang, "Demystifying envelope tracking: use for high-efficiency power amplifiers for 4G and beyond," *IEEE Microw. Mag.*, vol. 16, no 3, pp. 106-129, Mar. 2015.

[Wang-99] X. Wang, T. Yjhung, and C. Ng, "Reduction of peak-to-average power ratio of OFDM system using a companding technique," *IEEE Trans. Broadcast.*, vol. 45, no. 3, pp. 303-307, Sept. 1999.

[Ware-11] C. Ware. (2011, November 30). *Optical Amplifiers* [Online]. Available: http://opti500.cian-erc.org/opti500/pdf/25 20cian_amplis_slides_handout.pdf.

[Yang-11] P. Yang and A. Hu, "Two-piecewise companding transform for PAPR reduction of OFDM signals," in *Wireless Communications and Mobile Computing Conference (IWCMC)*, Istanbul, Turkey, Jul. 2011, pp. 619-623.

[Younes-17] M. Younes, M. Telescu, N. Tanguy, C. Diouf, P. Morel, and S. Azou, "Robustness improvement of compact predistorters in a CO-OFDM system using semiconductor optical amplifiers," in *29th International Conference on Microelectronics (ICM)*, Beirut, Lebanon, Dec. 2017, pp. 1-4.

[Zhang-13] G. Zhang, M. D. Leenheer, A. Morea, and B. Mukherjee, "A survey on OFDM-based elastic core optical networking," *IEEE Commun. Surveys Tuts*., vol. 15, no. 1, pp. 65-87, Feb. 2013.

[Zhang-14] X. Zhang, R. Zhu, D. Shen, and T Liu, "Linearization technologies for broadband radio-over-fiber transmission systems," *Photonics*, vol. 1, no.4, pp. 455-472, Nov. 2014.

[Zhao-14] J. Zhao, "DFT-based offset-QAM OFDM for optical communications," *Optics Express*, vol. 22, no. 1, pp. 1114-1126, Jan. 2014.

Author Index

Subject Index

G

H

I

L

M

N

O

P

Q

R

S

T

U

W